THESIS FOR THE DEGREE OF DOCTOR OF PHILOSOPHY

# Hydrodynamics and Heat Transfer in Vertical Falling Films with Smooth and Modified Heat-Transfer Surfaces – An Experimental and Numerical Investigation

ANDERS ÅKESJÖ


Department of Chemistry and Chemical Engineering
CHALMERS UNIVERSITY OF TECHNOLOGY
Gothenburg, Sweden
2018

Hydrodynamics and Heat Transfer in Vertical Falling Films with Smooth and Modified Heat-Transfer Surfaces – An Experimental and Numerical Investigation

ANDERS ÅKESJÖ
ISBN 978-91-7597-816-1



Doktorsavhandlingar vid Chalmers tekniska högskola
Ny serie nr 4497
ISSN 0346-718X

CHALMERS UNIVERSITY OF TECHNOLOGY
Department of Chemistry and Chemical Engineering
SE-412 96 Gothenburg
Sweden
Phone: +46 (0)31-772 10 00

Cover: Photographs of the falling film on a smooth (Left) and a modified (Right) heat transfer surface in the *Atmospheric setup*. The close-ups show the temperature contour plot inside the liquid film flow obtained from the numerical framework.

Printed by Chalmers Reproservice
CHALMERS UNIVERSITY OF TECHNOLOGY
Gothenburg, Sweden
2018

# Hydrodynamics and Heat Transfer in Vertical Falling Films with Smooth and Modified Heat-Transfer Surfaces – An Experimental and Numerical Investigation

ANDERS ÅKESJÖ
Forest Products and Chemical Engineering
Department of Chemistry and Chemical Engineering
Chalmers University of Technology

## ABSTRACT

High energy utilization efficiency is important to achieve a sustainable society. By having highly efficient heat exchangers, more energy can be recovered and reused at a lower cost. One commonly used type of heat exchangers is a vertical falling film unit, which is a device where a thin liquid film is flowing down a vertical wall in the presence of a gas layer. Such units can operate with small temperature differences and have short residence times and small pressure losses. Those qualities are favourable in the food industry for the concentration of heat-sensitive fluids such as fruit juice and dairy products, or, in the pulp and paper industry for concentration of black liquor in the chemical recovery process. Since evaporation is inherently very energy-intensive and these industrial units are typically large, relatively small efficiency improvements can lead to significant reduction of operational costs.

In this thesis, the hydrodynamics and heat transfer in vertical falling films are investigated. Novel measuring procedures are developed to study the local time-varying properties of the film, such as film thickness profiles. The procedures are used to distinguish between entrance effects and statistically steady conditions, which is of importance for an industrial unit. It is shown that these steady conditions are typically achieved 1-2 meters downstream from the inlet.

Film thickness profiles, along with local heat transfer coefficients, are measured to categorize and understand the variation between different operating conditions for industrially relevant fluids. The measurements are also used to introduce and validate a numerical framework for falling films for industrially relevant conditions. The framework solves the Navier-stokes equations in two dimensions using the Volume of Fluid method. The numerical framework is used to study complex flow inside the thin liquid film and to differentiate between the convective and conductive mechanisms that govern the rate of the heat transfer. It is shown that both mechanisms are of importance for the heat transfer.

The knowledge acquired about the film flow behaviour on smooth heat-transfer surfaces used nowadays is utilized to propose a novel design of heat transfer surfaces, with millimetre-high structures, for industrial use. Both the experimental measurements and the numerical framework show that it is possible to enhance the rate of heat transfer by up to 150 %, dependent upon how sharp the new modified surfaces are constructed. The modified surfaces enhance the rate of heat transfer by initializing more bulk mixing by utilizing the time-varying behaviour of the falling film. The irregularities in the flow lead to the occurrence of time-fluctuating recirculation zones behind the surface modifications, which results in a significant increase in the convective heat transfer.

**Keywords:** heat transfer, falling film, film thickness, local heat transfer coefficient, numerical simulations, VOF, evaporation.

*To Nunne and the rest of my family*

# Appended Papers

This thesis is based on the work contained in the following papers, referred to by Roman numerals in the text:

I. **Åkesjö, Anders**; Vamling, Lennart; Sasic, Srdjan; Olausson, Lars; Innings, Fredrik; Gourdon, Mathias (2018)
On the measuring of film thickness profiles and local heat transfer coefficients in falling films.
*Experimental Thermal and Fluid Science*, 99: 287-296.

II. **Åkesjö, Anders**; Gourdon, Mathias; Vamling, Lennart; Innings, Fredrik; Sasic, Srdjan (2017)
Hydrodynamics of vertical falling films in a large-scale pilot unit – a combined experimental and numerical study.
*International Journal of Multiphase Flow*, 95: 188-198.

III. **Åkesjö, Anders**; Gourdon, Mathias; Vamling, Lennart; Innings, Fredrik; Sasic, Srdjan (2018)
Experimental and numerical study of heat transfer in a large-scale vertical falling film pilot unit.
*International Journal of Heat and Mass Transfer*, 125: 53-65.

IV. **Åkesjö, Anders**; Gourdon, Mathias; Vamling, Lennart; Innings, Fredrik; Sasic, Srdjan (2018)
Modified surfaces to enhance vertical falling film heat transfer – an experimental and numerical study.
*Revised manuscript submitted to International Journal of Heat and Mass Transfer*.

# Contribution Report

The author of this thesis has made the following contributions to the appended papers:

I. Main author. Developed the film thickness profile measurement procedure and validated the performance of the local heat transfer measurement procedure. Planned and performed the experiments, analysed and evaluated the results. Wrote the paper with the support of the co-authors.

II. Main author. Planed and performed the experiments and simulations. Analysed and evaluated the results and wrote the paper with the support of the co-authors.

III. Main author. Planed and evaluated the experiments which was conducted by two Master Thesis worker who the author supervised. Planned and performed the simulations, analysed and evaluated the results and wrote the paper, with the support of the co-authors.

IV. Main author. Planed and evaluated the experiments which was conducted by two Master Thesis worker who the author supervised. Planned and performed the simulations, analysed and evaluated the results and wrote the paper, with the support of the co-authors.

## Related work not included in this thesis

Karlsson, Erik; Broberg, Anna; **Åkesjö, Anders**; Gourdon, Mathias (2013), Dissolution rate of sodium salt scales in falling film evaporators. *Conference Proceeding, Heat Exchanger Fouling and Cleaning*, June 09-14, Budapest.

Mura, Ernesto; **Åkesjö, Anders**; Vamling, Lennart; Jongsma, Alfred; Innings, Fredrik; Gourdon, Mathias (2014), Experimental Study of the Heat Transfer in a Falling Film Evaporator: Influence of the Co-Flowing Vapor. *Proceedings of the 10th International Conference on Heat Transfer, Fluid Mechanics and Thermodynamics - HEFAT 2014,* s. 1938-1944.

**Åkesjö, Anders**; Olausson, Lars; Vamling, Lennart; Gourdon, Mathias (2015), New measurement approaches for film thickness and wall temperature in falling film heat exchangers. *Proceedings of the 11th International Conference on Heat Transfer, Fluid Mechanics and Thermodynamics - HEFAT 2015,* s. 613 -619.
(This is a conference version of Paper I)

Mura, Ernesto; **Åkesjö, Anders**; Vamling, Lennart; Jongsma, Alfred; Innings, Fredrik; Gourdon, Mathias (2016), Effect of Co-flowing Vapor during Vertical Falling-film Evaporation. *Experimental Heat Transfer*, 29 (2) s. 561-575.

Olausson, Lars; Pettersson, Krister; Apel, Martin; Gourdon, Mathias; **Åkesjö, Anders** (2018), Heat transfer tube and method for manufacturing a heat transfer tube. *Patent WO2018143880,* 2018-08-09.

# Table of Contents

# 1 Introduction

To achieve a sustainable society and reduce our carbon footprint, we need to switch to more renewable energy sources. Today we are still to a large degree dependent on fossil fuels. Since we have become accustomed to a certain living standard, it is unlikely that our energy demand will decrease in the future. On contrary, this demand will increase if the average living standard on this planet has a similar development. High reuse of energy means that less energy needs to be put into our system, creating a more sustainable society. By having highly efficient heat exchangers, more energy can be recovered and reused at a lower cost. Therefore, optimizing the performance of these units is extremely important. One commonly used type of heat exchanger for evaporation and concentration of fluids is a falling film unit.

## 1.1 Falling film evaporation

Falling liquid film is a special kind of flow where a liquid film with a distinct liquid-vapour interface flows down an inclined or vertical wall. The thin film gives this technology excellent heat and mass transport characteristics. The unit can operate with small temperature differences and have short residence times and small pressure losses. Therefore are falling film units a popular choice for a wide range of engineering and technological applications, such as condensers, fluid heaters and chillers, absorbers and evaporators. They are especially good for viscous and heat-sensitive fluids since they have relatively good resistance to fouling, due to the possibility to operate with a low thermal driving force.

Falling films are, for example, used in the food industry for the concentration of heat-sensitive fluids such as fruit juice and *Dairy products*, to produce fruit juice concentrate and dairy powder. Another area of application is the pulp and paper industry for concentration of *Black liquor* in the chemical recovery process. There, *Black liquor* needs to be concentrated to be burnt in the recovery boiler to recover energy and cocking chemicals to digest the wood into pulp.

In both fields of applications, the Dry Solids content (DS) of the fluid (product) is increased through the process of evaporation:

$$DS = \frac{m_{solids}}{m_{solids} + m_{water}}, \tag{1.1}$$

where $m_{solids}$ is the mass of the dissolved solids and $m_{water}$ is the mass of water. Steam is usually used as the energy supply. Therefore, the falling film unit ends up with having

one side where steam is condensing and another where water is evaporated, see Figure 1-1. Most of the heat transfer resistance is on the evaporative side, and thus if one wants to make improvement to the unit, the evaporative falling film is the part to study.

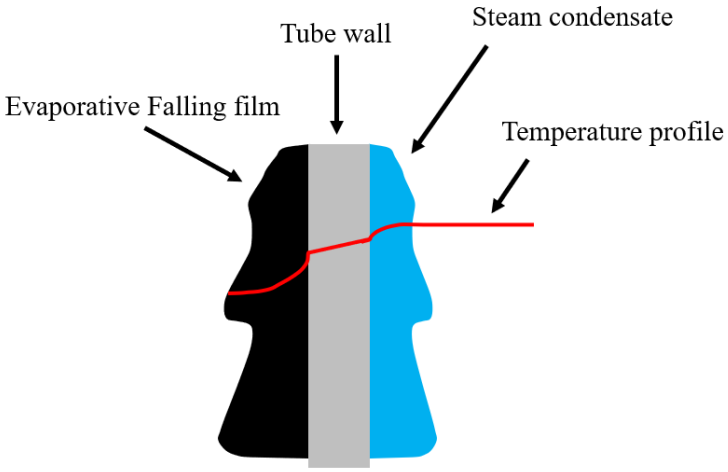


*Figure 1-1. Schematic temperature profile inside a vertical falling film unit where steam is used as the heating medium to concentrate a fluid (product) through the process of evaporation.*

The industry sectors where falling film units are utilized are numerous. Nowadays, only the process of *Black liquor* concentration in all pulp & paper mills in Sweden has an energy demand of 12 TWh/year, which corresponds to about 2-3% of Sweden's total energy demand (SEA, 2017). As the worldwide demand for biomaterials is increasing, there is a trend of building increasingly larger *Black liquor* evaporation plants. In 2005, an evaporation plant was built in Stora Enso Skoghall, capable of evaporating ~400 metric ton water per hour. In 2012, an evaporation plant was built at Eldorado's Três Lagoas in Brazil with the capacity of ~1600 metric ton water per hour. The most recent one, was constructed in APP OKI pulp and Paper Indonesia with a capacity of ~2900 metric ton water per hour (Valmet, 2018). The global dairy powder production is also expected to increase in the near future according to the Food and Agriculture Organization (OECD-FAO, 2018). Due to the increasing demand and the large scales of these processes, relatively small efficiency improvements can lead to large savings in absolute numbers.

### 1.1.1 Multistage evaporation train

To meet the high production demands, large heat-transfer surfaces are needed. The surfaces are usually of a plate lamella type with the product flow on the outside of the plates, or of a tubular type with the flow either on the inside or the outside of the tube. Having the product flow on the inside is usually less costly, but the opposite type of flow is more robust in the cases where severe fouling is expected (Gullichsen & Fogelholm, 2000). To create a large surface area, hundreds of long tubes, in the range of 12-20 meters, are usually mounted inside a shell, forming an evaporation *Stage* (Valmet, 2018).

To achieve high thermal efficiency, the *Stages* are usually connected in series into a multistage evaporation train, see Figure 1-2. Multiple stages allow evaporated vapour from one *Stage* to heat the subsequent *Stage*, which is possible because the pressure is decreased

and thus the boiling point of the product lowered in the subsequent *Stage*. The *Stages* are numbered according to the steam flow, with the first *Stage* where primary steam is introduced and the steam from the last *Stage* condensed in a condenser. If there is a shortage of steam on site, Mechanical Vapour Recompression (MVR) can be used to increase the steam temperature, allowing the steam to be reused and thereby lowering the primary steam demand. The drawback is that the MVR unit requires electricity to operate, see Figure 1-2.

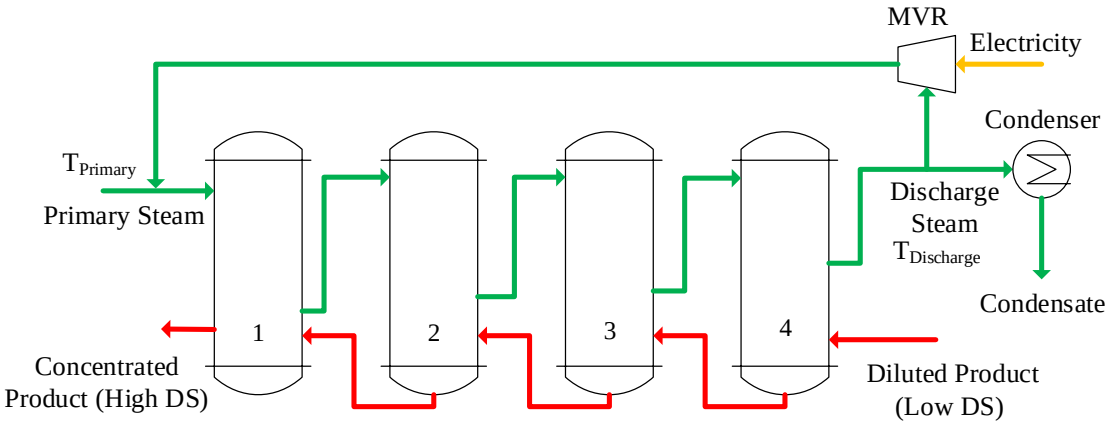


*Figure 1-2. Simplified process-flow diagram of a Multistage evaporation train with a Mechanical Vapour Recompression unit (MVR).*

Today usually 6-7 *Stages* are used in a *Black liquor* evaporation train. Due to the size of each *Stage*, there exists a techno-economical optimum. If we were able to increase the rate of heat transfer inside a *Stage*, each *Stage* could be made smaller. Smaller *Stages* would be cheaper due to less construction material needed, making it feasible to add more *Stages* to the evaporation train and thus lowering the primary steam demand.

In the business of concentrating *Dairy Product*, fewer *Stages* are usually used due to restriction on the highest allowable temperature of the product. Therefore, the temperature difference between the primary and the discharge steam limits the number of *Stages*. If the rate of heat transfer could be increased inside a *Stage* here, the thermal driving force (the temperature difference between the steam and the product) could be lowered, increasing the discharge temperature, lowering the load on the MVR unit and hence reducing the electricity usage.

### 1.1.2 Knowledge gaps

Even though vertical falling films have been extensively studied over the years, little is known about the conditions inside an industrial falling film unit and especially in regard to their typical tube length. Current literature mainly deals with very specific aspects of the falling film, generally occurring at the film flow entrance. In addition, these studies usually focus on low flow rates, as they can be assumed truly Laminar, or high flow rates as they can be approximated as fully Turbulent. However, in a falling film unit, the flow is usually more complex and in the transition region between these flow types. Due to these reasons,

there are difficulties in transferring that knowledge to what is needed for understanding the film dynamics on an industrial scale.

In addition, most heat exchanger types have some sort of general design concepts on how to construct an effective modified heat transfer surface (Webb & Kim, 2005). However, for vertical falling film units, no such general design suggestions exist (Miriam, 2007) and instead the heat transfer surfaces are made of smooth tubes.

## 1.2 Objectives

The main objective of this work is to increase our understanding of how heat is transported within a vertical liquid film. By obtaining a thorough understanding of the transport mechanisms inside the film, higher heat transfer rates could be obtained through redesigning the heat exchanger, for example by introducing modifications of the heat transfer surfaces. To obtain such knowledge, first a thorough understanding of hydrodynamics of falling films is needed as the latter is believed to strongly affect the heat transfer. Therefore, accurate measuring methods are needed to understand how the hydrodynamics varies both in time and space as the thin liquid film flows downwards, and how that affects the local heat transfer coefficients. Even with such measuring techniques, detailed measurements of the fast-changing dynamics, especially temperature profiles within the thin liquid film, are extremely complicated to carry out. Additional approaches, such as comprehensive numerical simulations, are thus needed to better understand the dynamics of falling films. However, many questions need to be addressed before such a framework can be used to represent operating conditions in a large-scale unit.

A broad range of fluid properties need to be investigated as falling film units are operated under a wide range of conditions. With such increased knowledge, the performance of an industrial vertical falling film unit can be improved by introducing the design changes.

### 1.2.1 Limitations

Only Newtonian fluids will be considered in this work, and hence the dry solids content will not exceed 45 % in our investigations. Also, it will initially be assumed that knowledge within the field of heating of falling films is transferable to evaporative conditions. This assumption will be theoretically motivated in Chapter 2.4 and experimentally addressed in Chapter 6.5.

Further, the flow is only studied on vertical tubes and no distinct consideration is made when it comes to the differences between inside and outside flow on a tube. Fouling is not considered but it has been checked that there have not been any time degradations of the heat transfer rate due to potential fouling issues.

## 1.3 Timeline of the work and the appended papers

The long-term goal of this work has always been to present experimental and theoretical foundation for the introduction of modified heat transfer surfaces for falling-film units of industrial size, with the aim of increasing the rate of heat transfer. The initial plan was to study heat transfer on modified surfaces under heating conditions and when enough knowledge had been obtained, design a heat transfer surface and then install it in a pilot falling film evaporator. Our research group has a long experience of working with large-scale measurements relevant for units of industrial scale. To connect that knowledge to the transient behaviour of the thin liquid film, two novel measuring techniques for film thickness profiles and local temperature measurements were developed and presented in a conference paper (here given as related work). However, while writing **Paper III**, it became clear that there was interest in the scientific community to better understand the mentioned techniques. As a result, the conference paper was rewritten into a journal paper, **Paper I** in the thesis. Therefore, **Paper I** was published after **Papers II** and **III** even though the techniques were developed and calibrated prior to **Papers II** and **III**.

To understand what happens within the liquid film, numerical simulations were introduced. However, it became clear that, even though much work had been done on simulating falling films, there was a knowledge gap between fine theoretical work and the information needed to explain events on an industrial scale. Therefore, considerable time in the course of this project was spent on exploring how a numerical framework should be configured in order to predict the hydrodynamics on smooth surfaces in an industrial unit, the work that resulted in **Paper II**. Afterwards, heat transfer on smooth surfaces was studied both experimentally and numerically. They gave further insights into the behaviour of the thermal entrance region, a phenomenon seldom discussed in the literature. Therefore, these entrance effects were discussed in detail in **Paper III** even though such a subject was not initially intended to be investigated.

In **Papers II** and **III** significant effort was spent on validating the numerical framework against experiments and, therefore, the discussion of more far-reaching conclusions from the simulations was somewhat limited. For that reason, a broader perspective on the numerical results will be presented in the thesis.

**Paper IV** introduced modified surfaces and could be composed relatively fast due to the knowledge accumulated from the previous papers. After studying several heat transfer surfaces under heating conditions, it became clear that there was not just one recommended design. Several designs needed to be investigated under evaporator conditions. Hence, considerable time was spent to redesign the pilot evaporator to make several changes of heat transfer surfaces considerably easier, instead of just permanently installing a new surface.

## 1.4 Outline of the thesis

The thesis will first give a theoretical background to the field of vertical falling films. State of the art will be given regarding their hydrodynamics, heating and evaporation. We will discuss how they relate and also the assumption that heating and evaporation can be rather similar under certain conditions. Different methods on how to improve the performance of a heat exchanger will be discussed in Chapter 3.

Chapter 4 will describe the experimental equipment used in this work. The new measurement procedures, developed in **Paper I**, for film thickness profiles and local temperatures will be presented along with the methodology used during the different experiments. The numerical framework established in this project will be presented in Chapter 5. Governing equations and boundary conditions will be described in detail along with the post processing of data. Actions taken to validate the proposed framework will also be discussed.

Chapter 6 starts with a summary of the main findings from **Papers II** and **III** about hydrodynamics and heat transfer of vertical falling films on smooth surfaces, followed by a detailed discussion about the mechanisms driving the heat transfer. In Chapter 6.2, the design characteristics of the heat transfer surfaces will be discussed. Chapter 6.3 will discuss the hydrodynamics and heat transfer on modified surfaces investigated in **Paper IV** and relate the results to the mechanisms discussed in Chapter 6.1. In Chapter 6.4, experimental results for evaporative conditions will be presented. Chapter 6.5 will discuss the similarities and differences between heating and evaporative results on both smooth and modified heat transfer surfaces.

Finally, the conclusions are presented in Chapter 7, whereas Chapter 8 will offer suggestions for further work.

# 2 Vertical Falling film

The flow in falling film units is often described using dimensionless numbers. The most important ones are the Kapitza number (*Ka*), the Reynolds number (*Re*), the Prandtl number (*Pr*) and the Nusselt number (*Nu*). In literature, different definitions of these numbers can be found. In this work, the following definitions are used:

$$Ka \equiv \frac{\text{surface tension forces}}{\text{inertia forces}} \equiv \frac{\sigma \cdot \rho^{1/3}}{\mu^{4/3} \cdot g^{1/3}}, \tag{2.1}$$

$$Re \equiv \frac{\text{inertial forces}}{\text{viscous forces}} \equiv \frac{\Gamma}{\mu}, \tag{2.2}$$

$$Pr \equiv \frac{\text{momentum diffusivity}}{\text{thermal diffusivity}} \equiv \frac{c_p \mu}{k}, \tag{2.3}$$

$$Nu \equiv \frac{\text{convective heat transfer}}{\text{conductive heat transfer}} \equiv \frac{hL}{k}, \tag{2.4}$$

where $\sigma$ is the surface tension, $\rho$ is the density, $\mu$ is the dynamic viscosity, $g$ is the gravitational acceleration, $c_p$ is the specific heat capacity, $k$ is the thermal conductivity and $h$ is the heat transfer coefficient. The wetting rate $\Gamma$ is given by:

$$\Gamma \equiv \frac{\dot{m}}{\pi \cdot d}, \tag{2.5}$$

with $\dot{m}$ being the mass flow rate and $d$ the tube diameter, which can be either the inside or outside diameter depending on where the flow is. For the Nusselt number, L is a characteristic length. Usually, the viscus length scale ($l$) is used as the characteristic length in order to make it independent of the wetting rate and Reynolds number (Schnabel, 2010):

$$l = \left( \frac{(\mu / \rho)^2}{g} \right)^{1/3} . \tag{2.6}$$

## 2.1 Hydrodynamics

The heat transfer in falling film units is predominantly influenced by the hydrodynamics (Dukler, 1976), hence it is important to study the hydrodynamics of the liquid film in detail.

The hydrodynamics of falling films have been extensively studied in the literature (Alekseenko et al., 1994; Kalliadasis et al., 2012) and a number of papers exist using analytical, experimental or numerical methods. Kapitza and Kapitza (1965) were ones of the pioneers in this field and they used shadow photography of the liquid to study the wave development. Since then, several authors have carried out similar studies e.g. Alekseenko et al. (1985); Seikah Ishigai et al. (1972); Nosoko et al. (1994); Patnaik and Perez-Blanco (1996); Plerson and Whitaker (1977); Wasden and Dukler (1989). Density, viscosity, gravity, surface tension and the flow rate were identified as the important factors for the hydrodynamics. These factors are typically expressed as functions of non-dimensional numbers, such as the Reynolds (*Re*) and Kapitza (*Ka*) numbers, in order to distinguish between influences from flowrates and fluid properties and to classify different flow regimes. It should be noted that the viscosity has the single most influence on the value of the Kapitza number.

The average film thickness has been extensively measured and mapped for different running conditions (Brötz, 1954); (Lukach et al., 1972). In addition, as measurement techniques have become increasingly sophisticated, it has become possible to study the flow structures beneath the liquid interface and measure the velocity components with techniques such as Laser Doppler Velocimetry (LDV) (Dietze et al., 2009), Particle Image Velocimetry (PIV) and Particle Tracking Velocimetry (PTV) (Zadrazil et al., 2014).

When it comes to modelling of dynamics of falling films, analytical modelling has been a subject of research for a long time e.g. Brauner (1989). Such studies have often predicted a certain phenomenon that has later been proven experimentally (Kalliadasis et al., 2012). In recent years, it has been possible to directly numerically solve the Navier-Stokes equations for falling films (Gao et al., 2003). Numerical simulations in a two-dimensional (2D) framework have made it possible to study in great detail the hydrodynamics inside a liquid film, which otherwise would be either very difficult or impossible to measure experimentally (Malamataris & Balakotaiah, 2008). Recently, there have also appeared three-dimensional (3D) simulations of falling films (Dietze et al., 2014; Doro, 2012) resolving the spanwise fluid movement.

Several authors, (Al-Sibai, 2005; Seikah Ishigai et al., 1972; Morioka et al., 1993), have studied different flow patterns that emerge for vertical falling films. At the top of a unit, i.e. when the liquid starts to flow downwards, the film is considered flat (Al-Sibai, 2005). As the film travels downwards, the present instabilities, if sufficiently large, will grow into

waves. Afterwards, there is a possible transition from two- to three-dimensional waves (Al-Sibai, 2005).

Many studies argue that, after sufficient length, denoted an entrance region, the flow can be considered *fully developed* (alternatively, the term "*statistically steady*" can be used here, discussed in Chapter 6.1). For hydrodynamics, this means that, after this distance the flow characteristics, such as the film thickness, do not change further downstream. The manifestation of such regimes and the location where the latter regime takes place depend heavily on the operating conditions and no clear definition exists (Seikah Ishigai et al., 1972). Al-Sibai (2005) developed models for *fully developed* regimes under non-evaporative conditions. In that study, the models depend on the Reynolds (*Re*) and Kapitza (*Ka*) numbers and the flow was mapped into five different regimes: Laminar, Sinusoidal, Wavy-Laminar, Transition and Turbulent, see Figure 2-1.

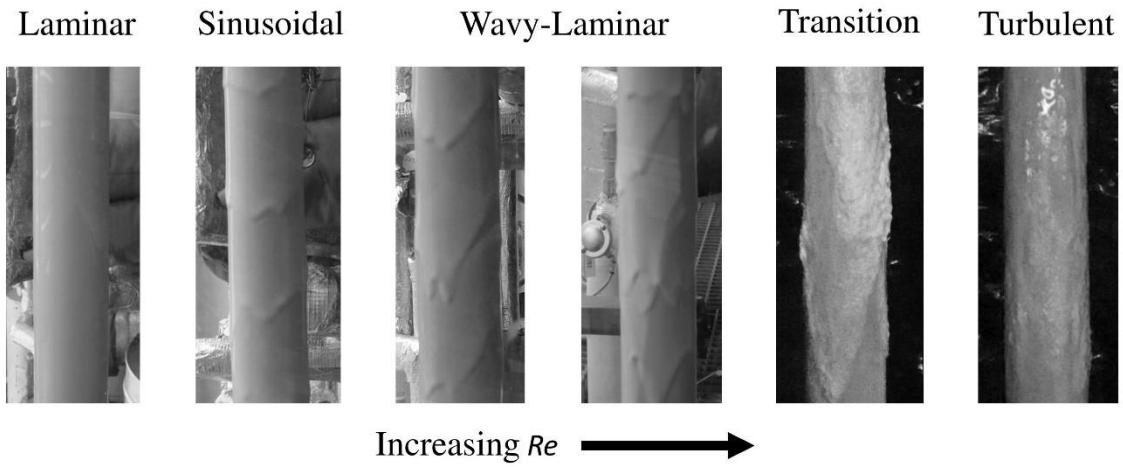


*Figure 2-1: Flow regimes existing in a falling film unit according to Al-Sibai (2005) and illustrated by photos from this work.*

The Laminar regime exists for low *Re* numbers and it is characterised by a calm liquid film without the presence of waves. In this region, the Nusselt analytical solution (Nusselt, 1916) is considered valid. The Sinusoidal regime, also known as the first transition, is characterized by the presence of capillary waves, which may be understood as small ripples at the liquid surface appearing with high frequency and small wavelengths. These waves have almost no influence on the near-wall hydrodynamics (Karimi & Kawaji, 1999).

At higher flowrates the Wavy-Laminar regions come into place, also referred to as the stable Wavy Laminar or inertial Wavy-Laminar regime. Here, the film is partly laminar in the substrate and partly turbulent in the waves (Miller & Keyhani, 2001). Internal recirculation in the liquid, also known as *backflow*, is generated from the wave motions (Seikah Ishigai et al., 1972). In this zone the waves grow larger and so does the wavelength. The waves are sometimes referred to as roll waves or inertial waves driven by gravity.

In the Transition regime, also known as the Turbulent-Laminar or inertial Wavy-Turbulent, the fluid motion gradually changes from being wave-governed to a shear-governed one (Seikah Ishigai et al., 1972). Individual waves can still be seen in this regime, but it is likely that they start to interfere with each other (Miller & Keyhani, 2001). In the Turbulent

regime the flow becomes fully turbulent. The flow is entirely shear-governed and individual waves cannot be detected (Seikah Ishigai et al., 1972).

Due to the characteristics of each flow regime, the resulting flow pattern and film thickness are vastly different. Therefore, the falling film is usually further categorized by describing the film thickness. Numerous studies have attempted to determine the local film thickness of the liquid film in different flow regimes, and a large variety of suggested correlations exist. The film thickness for flat Laminar falling films can be obtained from the Nusselt film theory as (Schnabel & Palen, 1998):

$$\delta_{Laminar} = \left( \frac{3\left(\mu/\rho\right)^2 Re}{g} \right)^{1/3}, \tag{2.7}$$

Lukach et al. (1972) proposed the following correlation for the mean film thickness under Wavy-Laminar conditions:

$$\delta_{Wavy-Laminar} = 1.34 \left( \frac{\left(\mu/\rho\right)^2}{g} \right)^{1/3} \cdot Re^{0.368}, \tag{2.8}$$

and Brötz (1954) proposed the following correlation for turbulent conditions (Re > 600):

$$\delta_{Turbulent} = 0.172 \left( \frac{\left(\mu/\rho\right)^2}{g} \right)^{1/3} \cdot Re^{2/3}. \tag{2.9}$$

Such relations give a good understanding of the local time averaged film thickness in each regime. But since the emerging waves govern much of the underlying flow structures, the wave topology in each regime is also interesting to study (Dietze et al., 2008). Dietze (2016) made a detailed numerical study on the shape of the waves for a large range of Kapitza numbers at small Reynolds numbers. The results of that work showed that a wave in the Wavy-Laminar region consists of a large liquid hump, with small capillary waves in the front. The same study also specified that the topology is very dependent on the *Ka* and *Re* numbers.

The flow structures beneath the interface have been studied both experimentally (by, for example Dietze et al. (2009) and Charogiannis et al. (2015)), but also numerically (Gao et al., 2003). Such numerical studies can provide information that otherwise would be very difficult to attain (Malamataris & Balakotaiah, 2008). These studies revealed the importance of the wave formation at the liquid interface. Curvature of the waves causes a pressure gradient to occur within the liquid film, which, if sufficiently large, leads into an internal recirculation, a phenomenon termed the backflow (Dietze et al., 2008), illustrated

in Figure 2-2. Depending on whether a frame of reference is wave- or wall-fixed, backflow will either occur within the wave or in front of it (Malamataris & Balakotaiah, 2008). The backflow leads to enhanced mixing of the bulk flow (Adomeit et al., 2000),(Kunugi & Kino, 2005).

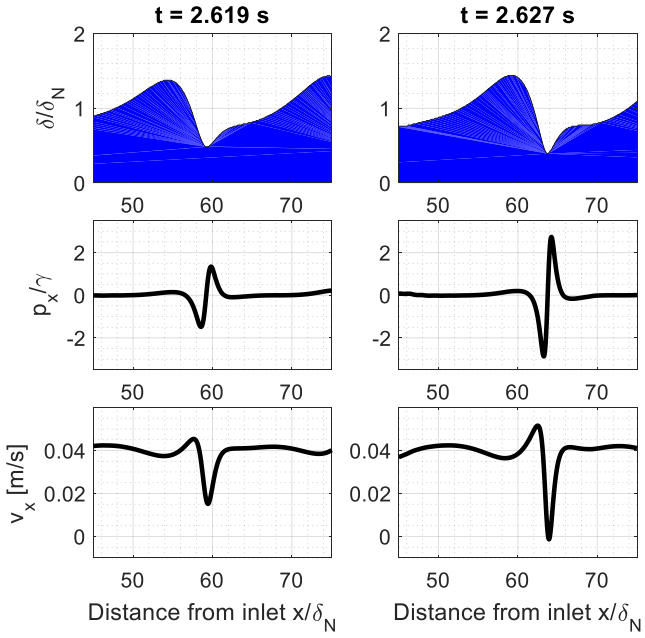


*Figure 2-2. Illustration of backflow as presented in **Paper II**. Normalized film thickness, pressure gradient and streamwise velocity (sampled 40 μm from the wall) at two different time instants (left and right). As the curvature of the wave grows, the pressure gradient grows with it, eventually forcing the fluid within the wave front into internal recirculation, i.e. the backflow (with a negative velocity). The pressure gradient has been normalized with $\gamma=\rho \cdot g$.*

In spite of the fact that extensive work has been carried out in studying the hydrodynamics of falling films, more research is needed before the gained knowledge can be used for the design of new industrial units. For instance, although it is known that the liquid flow is non-symmetrical in the spanwise direction in large-scale units (Al-Sibai, 2005), only a limited number of experimental studies and even less numerical ones address this issue. Recently, Kharlamov et al. (2015) made a thorough investigation of the spanwise liquid redistribution, but were unable to obtain direct experimental evidence for the underlying mechanism causing the shift between predominantly 2D to 3D nature of the flow. In addition, it is yet to be seen up to what extent this transition affects large-scale falling film units. Typical industrial units are large and the surface consists of long plates or tubes, and they are at the moment excessively expensive to simulate numerically (unless the physics of the problem are extensively simplified). More research is thus required concerning what can be achieved with the presently available computational resources, and, additional information is needed on the flow regimes and especially the flow development in such systems.

## 2.2 Heating

Just as the hydrodynamics evolves as the flow moves downwards, so does the heat transfer. The heating causes a temperature gradient to develop within the thin film, resulting in a thermal entry length.

Two definitions of the thermal entry length can be found in the literature: *i)* it is defined as the average distance between the beginning of a heated plate and the point where the thermal boundary layer arrives at the film surface, or *ii)* as the length between the beginning of the heated section and the point from which the heat transfer coefficient (HTC) remains constant for the rest of the flow distance (Lel & Kneer, 2011). The first interpretation was suggested by several authors, e.g. (Mitrovic, 1988), (Lel et al., 2009), (Chinnov & Abdurakipov, 2013). Lel et al. (2009) used thermal cameras to detect a vertical position at the surface when the temperature started to change. The same authors developed correlations that estimate the length of this region to be in the range of 0 to 0.5 *m*. The second interpretation is less straightforward to use, since the heat transfer coefficients need to be measured at multiple locations over a large length. Seikan Ishigai et al. (1974), Wilke (1962), and Mitrovic (1988) made an attempt to determine the length of this zone. However, their results varied significantly, in the range of 0 to 1.5 m. It is interesting to note that Wilke (1962) did not find any significant fluid influence, but instead mainly a dependence on the flow rates. In the same time, the other authors claimed to have observed a pronounced fluid dependence. The relation between the thermal entrance length and hydrodynamics is not discussed in much detail in these publications. In this study, the second definition will be used, as it is more interesting for industrial applications.

Extensive experimental work has been performed in order to map the rate of heat transfer for a subcooled fluid, e.g. (Seikan Ishigai et al., 1974), (Wilke, 1962), (Shmerler & Mudawwar, 1988). These studies were performed on different types of equipment, with respect to size and operating conditions. Local heat transfer measurements in a subcooled system are typically performed by measuring the temperature difference between the wall and the bulk (Wilke, 1962) or the interface (Markides et al., 2016) (Charogiannis et al., 2016).

Correlations for statistically steady conditions were established based on the above-mentioned studies. One commonly used correlation was developed by Schnabel and Schlünder (1980) for non-evaporative conditions under a constant heat flux. Here, the heat transfer coefficient depends on the Reynolds (*Re*) and Prandtl (*Pr*) numbers and can be used to estimate the magnitude of heat transfer in different regimes:

$$Nu_{Heating} = \max \begin{cases} 1.43 \cdot Re^{-1/3} \\ 0.042 \cdot Re^{0.2} \cdot Pr^{0.344} \\ 0.014 \cdot Re^{0.4} \cdot Pr^{0.344} \end{cases}. \tag{2.10}$$

The heat transfer is estimated by taking the largest value from one of the three expressions in (2.10). The authors used a variety of experimental measurements performed using different equipment with different lengths and fluid operating conditions, varying the

Reynolds and Prandtl numbers between 20 and 10,000 and 2 and 210, respectively. Schnabel and Schlünder (1980) estimate the accuracy of the correlation to ±25 %. To compensate for a potentially large temperature gradient in the liquid film, the Nusselt number is sometimes multiplied with a viscosity correction term, $(\mu / \mu_{Wall})^{0.25}$, slightly increasing the value obtained from the correlation.

For the Laminar flow regime, the heat transfer takes place by pure conduction. It is rate-determined by the film thickness and it thus decreases with the Reynolds number. In the Turbulent regime, however, the Nusselt number increases with the Reynolds number (Numrich, 1992) and is also dependent on the Prandtl number. For an intermediate regime (Transition regime), a superposition is often used.

The highest heat transfer is usually achieved in the Laminar regime for very low flow rates due to the thin liquid film, or for very high flow rates in the Turbulent regime, because of the increased fluid mixing. However, large-scale units are often operated in the Transition regime, since low flow rates can lead to wetting problems (Film breakdown, see Chapter 2.6) and high flow rates increase the pressure drop (Evaporation, see Chapter 2.3), give high pumping costs and potential sputtering (Johansson, Vamling, et al., 2009). Even if the value of the heat transfer coefficient can be estimated in the Transition regime, little is known about the flow structure beneath the surface of the film. Also, the transient behaviour for falling film needs to be captured in order to fully understand the system of interest (Markides et al., 2016).

The backflow phenomenon discussed in the previous section, where the liquid is forced into internal recirculation due to a formed pressure gradient, should significantly impact the rate of heat transfer. However, most of these studies only simulated the hydrodynamics and discussed its potential impact on the heat transfer, instead of simulating the latter directly. A limited number of studies that include the heat transfer in the simulations tend to focus on the operating conditions belonging to either the Sinusoidal or Wavy-Laminar regime (Kunugi & Kino, 2005), (Dietze & Kneer, 2011), (Yu et al., 2013),(A. Miyara, 1999),(Akio Miyara, 2001), or on the fully Turbulent regime (Mascarenhas & Mudawar, 2013).

## 2.3 Evaporation

Much knowledge about the evaporative heat transfer comes from correlations developed from experimentally measured data. As previously seen, the liquid film behaves differently in different flow regimes, and therefore evaporative correlations usually weight the Laminar and Turbulent contributions together:

$$Nu_{Evaporation} = \sqrt{Nu_{Laminar}^2 + Nu_{Turbulent}^2} \ . \tag{2.11}$$

Generally, when the Reynolds number is increased, the $Nu_{turb}$ will have a larger effect on the total evaporation rate. Several suggestions exist in the literature and the one we will use in this s work is by Schnabel and Schlünder (1980), who also developed a correlation for heating conditions, that proposes a relation for evaporative conditions :

$$Nu_{Evaporation} = \sqrt{\left(0.90 \cdot Re^{-1/3}\right)^2 + \left(0.00622 \cdot Re^{0.4} \cdot Pr^{0.65}\right)^2} \ . \tag{2.12}$$

The correlation was developed based upon measurements conducted for different fluids with Prandtl numbers in the range of 1.75 – 7 and its accuracy estimated to be ± 20 %. The span of Prandtl numbers for which the correlation was developed is quite narrow and thus has a limited use for industrial fluids. For that reason, Gourdon, Karlsson, et al. (2015) proposed a modified version of the relation:

$$Nu_{Evaporation} = \sqrt{\left(0.90 \cdot Re^{-1/3}\right)^2 + \left(0.011 \cdot Re^{0.2} \cdot Pr^{0.65}\right)^2} \ , \tag{2.13}$$

which was developed for Prandtl numbers in the range of 3 – 800. The authors also compared their correlation to measurement data in the literature and found that the correlation could successfully reproduce the measurements with an accuracy of ± 30-40 %.

To get a deeper understanding of the evaporative heat transfer within the liquid film, attempts have been made to model the turbulence within the liquid film, for example in the work of Mudawwar and El-Masri (1986) or Alhusseini and Chen (2000). The mentioned studies showed a generally good agreement when water was used as a working fluid, but have not been as successful when extrapolated to more viscous fluids, relevant for industrial conditions (Johansson et al., 2008). Doro (2012) has also shown that it is possible to perform numerical simulations of the evaporative falling film at high Prandtl numbers.

Hydrodynamics is relatively similar for evaporative falling films and heated films. However, there are some important differences that will be highlighted in the subsequent subchapters.

### 2.3.1 Boiling point elevation

The addition of soluble material to a liquid changes the boiling characteristics. Boiling Point Elevation (BPE) or Boiling Point Rise (BPR) is the difference in boiling temperature between the solution and the pure solvent when measured at the same pressure. A liquid mixture that contains dissolved organic or inorganic substances will boil at a higher temperature than water at the same pressure. Both fluids used in this work, *Black liquor* and *Dairy product*, represent water with dissolved organic and inorganic substances. The BPE increases with the dry solid content and it also depends on the composition of the dissolved substances (Adams et al., 1997).

Boiling Point Elevation is crucial to the design and performance of an evaporator. The transferred heat in an evaporator is dependent on the temperature difference between the condensing steam and the evaporating fluid, and the BPE can reduce the thermal driving force for the heat transfer. For Black liquor, the BPE increases slowly with the dry solids content up to 50%, but above, it increases rapidly (Adams et al., 1997).

### 2.3.2 Vaporisation mechanism

In a falling film evaporator, the mechanism of heat transfer may either be surface evaporation, nucleate boiling or film boiling. In surface evaporation, vapour is formed only at the liquid-gas interface. The interface is at saturation temperature and the wall is superheated. The degree of superheating is usually small, and therefore also the heat flux, due to the characteristics of the falling film. If the heat flux is increased enough, bubbles start to form at the wall, and nucleate boiling starts. At first, nucleation occurs only spot-wise along the heat transfer surface, and as the heat flux is further increased, more nucleation sites are activated. If the heat flux is increased even further, the bubble formation will eventually be so rapid that the bubbles merge into a gas film, covering the heat transfer surface, and film boiling has been reached (Tong & Tang, 1997).

Because of the low thermal conductivity of the vapour, the heat transfer coefficient for film boiling will be very low. Nucleate boiling gives higher heat transfer coefficients than surface evaporation and is therefore sometimes a preferred mechanism. Due to the bubble formation, nucleate boiling has a strong heat flux dependency, which theoretically should not be the case for surface evaporation. A disadvantage with nucleate boiling is that a larger temperature difference is needed to achieve nucleate boiling, compared with surface evaporation. In addition, for evaporation of liquid mixtures that contain dissolved substances, there is an increased risk of fouling when nucleate boiling is the vaporization mechanism. Today, nucleate boiling is never used deliberately in, for example, the industrial black liquor evaporation plant (Härkönen et al., 1994).

### 2.3.3 Entrainment

Even if nucleate boiling is not intentionally used in the falling film evaporation processes investigated in this work, it is not uncommon to see bubbles within the film. However, rather than originating from nucleate boiling, it is much more likely that they come from

entrainment of vapour in the liquid. The bubbles can, for example, be caused by the presence of surfactants, desorption of volatile dissolved gases and possible wave-breaking (Johansson, Leifer, et al., 2009). Gourdon, Innings, et al. (2015) observed a heat flux dependence for the rate of heat transfer and claimed it was caused by the formation of bubbles altering the flow pattern. The bubbles improve the wettability and make the liquid film thinner, which, for non-turbulent flows, improves the rate of heat transfer. A photo of such bubbles, also known as foam, can be seen in Figure 2-6.

### 2.3.4 Pressure drop and interfacial shear stress

In an evaporator, vapour is produced by the evaporation process. The vapour will cause a gas flow that in turn will give rise to a pressure drop, ΔP. In addition, the entrainment of bubbles discussed in the previous Chapter could contribute to this pressure drop. The pressure drop will affect the local saturation temperature of the product along the surface. Provided that the steam temperature is constant, this will lead to a larger thermal driving force ($\Delta T = T_{steam} - T^*$) at the bottom of the evaporator compared to that at the upper part (see Figure 2-3); thus, it will directly influence the amount of transferred heat. The pressure drop will especially be of importance if the flow runs on the inside of the tube and needs to be considered (Mura & Gourdon, 2017).

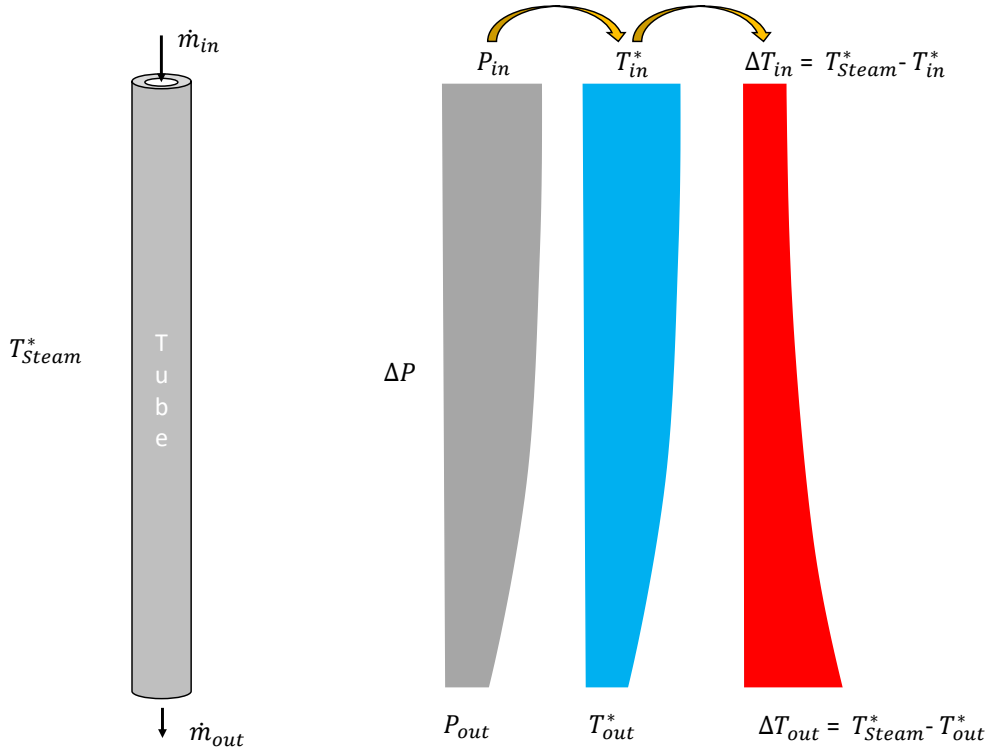


*Figure 2-3. Schematic representation of the effect of the pressure losses (ΔP) on the saturation temperature ($T^*$) and the thermal driving force (ΔT) over a heat transfer tube with the flow on the inside and condensing steam on the outside.*

The vapour flow does not only cause a pressure drop. If large enough, it might also affect the falling film hydrodynamics and, consequently, the heat transfer. In a co-current flow, were the vapour exits at the bottom (as shown in Figure 2-3), the film might be attenuated and accelerated due to friction at the liquid-gas interface. In a counter-current flow, the effect is the opposite. At what vapour flow this occurs is however still debated and depends heavily on the operating conditions (Gourdon & Mura, 2017).

## 2.4 Heating compared to evaporation

The temperature profiles within the liquid film for heating and evaporative conditions for Laminar and Turbulent films respectively, can be described as Figure 2-4 according to Schnabel and Schlünder (1980). For Turbulent film, most of the heat transport resistance lies in the boundary layer close to the wall for both heat transfer modes. For Laminar flow, the temperature profiles within the film are different. For the evaporative case, the temperature profile is a straight line, while for heating it has a more exponential decline indicating a heat transfer resistance throughout the whole film.

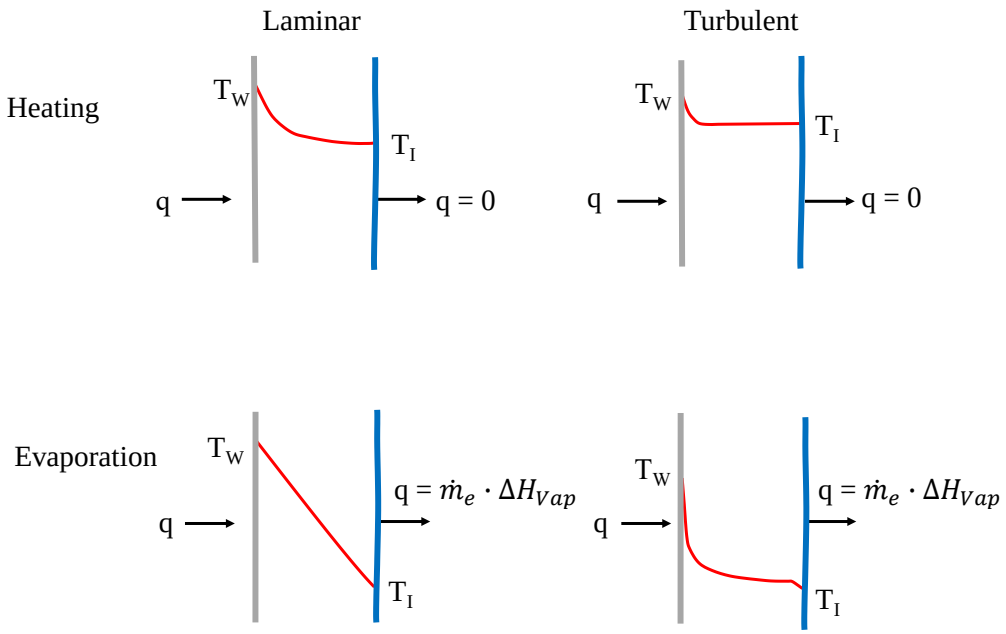


*Figure 2-4. Temperature profiles within a flat film for Laminar and Turbulent flows, depicted both for heated and evaporative conditions according to Schnabel and Schlünder (1980). For surface evaporation, the interface temperature ($T_I$) is equal to the saturation temperature ($T^*$).*

The operating conditions for an industrial falling film unit typically end up in the Wavy-Laminar or Transition regime, where the heat transfer usually is described as mixture between purely Laminar and Turbulent film flow. Therefore, to determine up to what extent heating and evaporation conditions differ, it is a good idea to compare the Nusselt numbers.

Figure 2-5 shows the Nusselt numbers at various wetting rates, obtained from equations (2.10), (2.12) and (2.13) for three different fluids, termed High, Intermediate and Low Viscosity fluid. A full description of the fluid properties is given in Chapter 4.1.3, but the main property of interest here is the viscosity, 6.6, 2.6 and 0.55 mPas for the given fluids, respectively. Before the values are compared, it should be mentioned that the heat transfer coefficient used to obtain the Nusselt numbers are differently defined for heating and evaporative conditions. For heating, the thermal driving force is defined as the difference between wall and bulk temperature, $\Delta T = T_{Wall} - T_{Bulk}$, while for evaporation, defined as the difference between wall and saturation temperature, $\Delta T = T_{Wall} - T^*$.

Generally, it can be said that the predicted value of the Nusselt numbers for heating and evaporative conditions are within each other's uncertainty interval. It is only for the Low Viscosity fluid that the correlation developed by Gourdon, Karlsson, et al. (2015) deviates from the others. But, it should be mentioned that the Prandtl number for that fluid is outside of the validity range of the correlation. The evaporative correlation developed by Schnabel and Schlünder (1980) is not valid for the High and Intermediate Viscosity fluids but here they are still within the same uncertainty as the one developed by Gourdon, Karlsson, et al. (2015). It should also be noted that the inflection point, where the correlations predict a Laminar film, differs for heating and evaporative conditions.

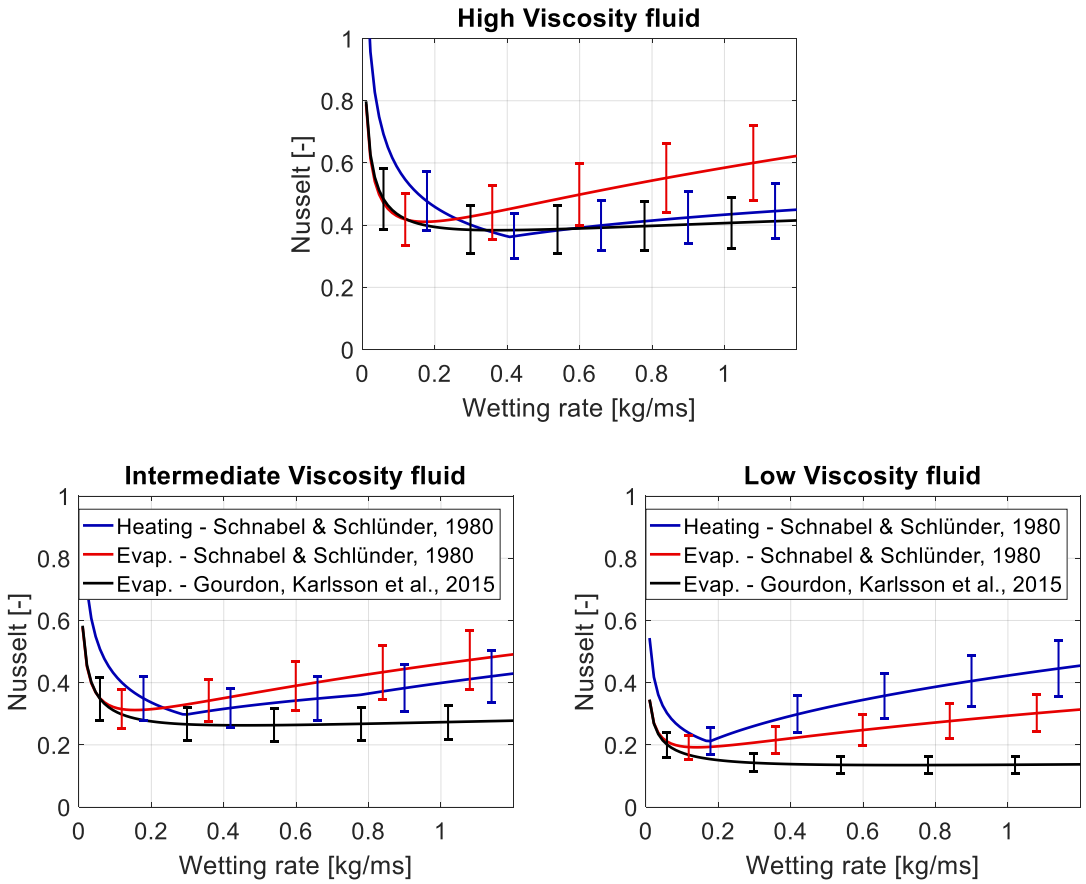


*Figure 2-5. Nusselt numbers at various wetting rates for three fluids investigated in this work, termed High, Intermediate and Low Viscosity fluid. A full description of the fluid properties is given in Chapter 4.1.3, but the main property is the viscosity, which is 6.6, 2.6 and 0.55 mPas respectively. The Nusselt numbers are obtained from heated and evaporative conditions according to Schnabel and Schlünder (1980) and Gourdon, Karlsson, et al. (2015). For all correlations, the viscus length scale is the characteristic length.*

The comparison indicates that knowledge about heat transfer obtained for a heated film can be transferred to an evaporative film. Also, as previously discussed in Chapter 2.3.2, the vaporization mechanism for falling film evaporation is surface evaporation. Therefore, the hydrodynamics of an evaporative film are not significantly altered compared to a heated film, as portrayed in Figure 2-6. In the figure, the entrainment of vapour, as discussed in Chapter 2.3.3, can be seen in the right image.

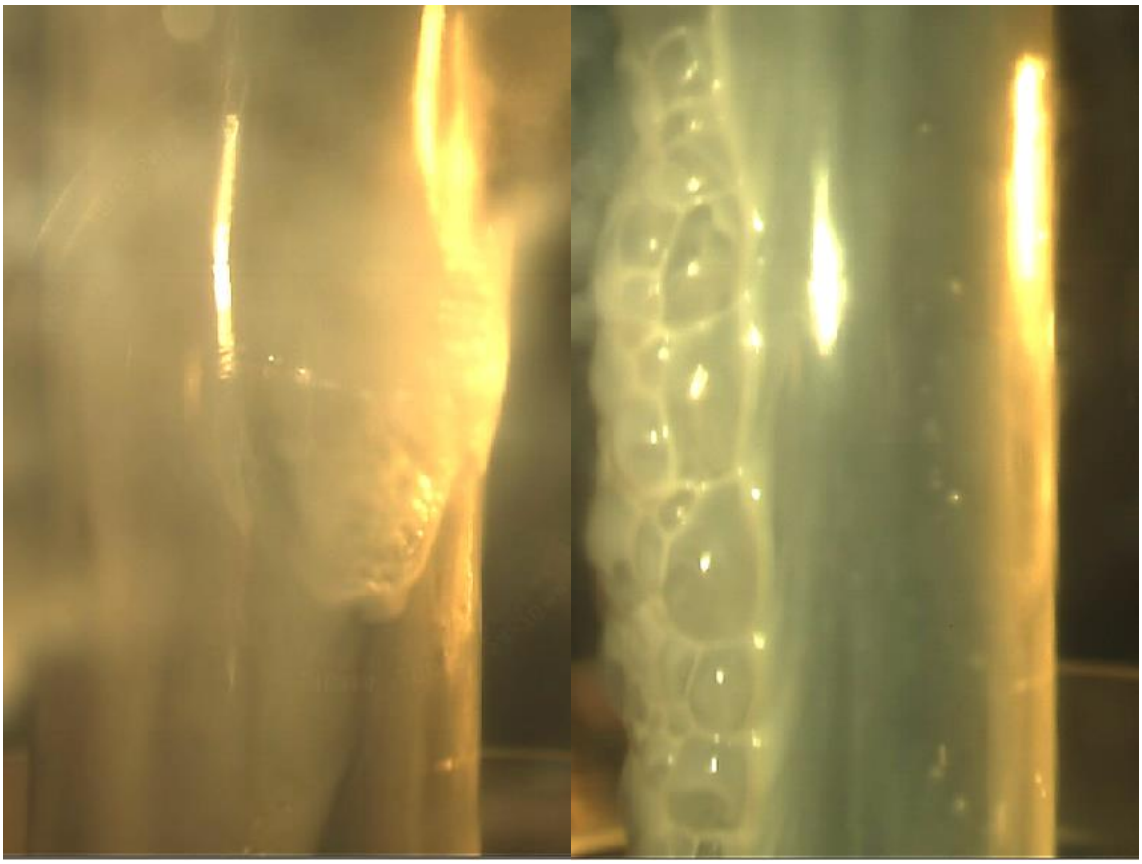

*Figure 2-6. Images of evaporation of dairy product obtained from the pilot evaporator. Left) 11.5 % dry solids and wetting rate 0.16 kg/(m·s), Right) 29 % dry solids and wetting rate 0.34 kg/(m·s).*

## 2.5 Fouling

In heat exchangers there is always a risk of fouling, and vertical falling film units are no exception. Fouling is accumulation of unwanted material on the heat transfer surface that will reduce the rate of heat transfer due to increased conductive resistance caused by the fouling layer. There are several types of fouling and they are all very much dependent upon the operating fluid run in the heat exchangers. The strategies to mitigate the risks for fouling are therefore problem-dependant for each situation and a lot of research has been conducted in this area, for example Gourdon (2009), Hagsten (2016) and Karlsson (2017). Once the heat transfer surfaces become fouled, the heat exchanger needs to be shut down for cleaning, which is both costly and time consuming. Therefore, it is important that, when introducing surface modifications into a heat exchanger, they do not lead to increased fouling problems.

## 2.6 Film breakdown

To maintain a high rate of heat transfer, it is important that the entire heat transfer surface is wetted and covered with a film. The film may be dried out by too extensive heating or too low a wetting rate, but usually a combination of both is the cause. For a heated film, dry patch formation is caused by local surface tension variations, also known as the Marangoni effect. Since the surface tension usually has an inverse temperature dependence (a higher temperature leads to a lower surface tension), breakup can occur if the surface temperature gradient becomes too large. In a wave, the surface temperature of the film is highest at the thinnest part of the film. This means that the surface tension here has its minimum value; the surrounding colder liquid with a higher surface tension will draw liquid from the thinner region, and a dry patch could form (Härkönen et al., 1994).

For an evaporative film, the wetting rate decreases downstream the tube due to the evaporated liquid, increasing the risk of a dry patch. A dry patch does not only cause the significantly lower heat transfer, it could also potentially lead to fouling problems. Surface modifications could potentially add to this problem as the heat transfer surface might be larger. It could also have to opposite effect and stabilising the film by evening out the liquid and rewetting the formed dry patches.

# 3 Methods to improve the rate of heat transfer

There are numerous methods suggested in the literature to improve the rate of heat transfer and they are usually classified as either active or passive. Active methods require external power and examples of such systems are mechanical aids, surface vibration, suction or injection. Passive methods, on the other hand, do not require any external power to operate and examples of such techniques are the use of coated, extended or rough surfaces. Passive methods are most popular in industry as they do not require active maintenance during operation.

In a variety of industrial applications where heat exchangers are involved, extension or modification of the heat transfer surfaces is often used to increase the rate of heat transfer. In such cases, there are three scenarios to enhance the rate of heat transfer: 1) to increase the heat transfer coefficient (HTC) without an appreciable increase of the heat transfer surface, 2): to increase the heat transfer surface without substantially changing the HTC and 3) to combine scenarios 1 and 2 (Webb & Kim, 2005). The first scenario is typically preferred, as the second one can be quite costly if significantly more construction material is required to build the heat exchanger. In addition, an enlarged heat transfer area also introduces a fin efficiency which has to be considered due to the conductive resistance within the introduced surface modification (Webb & Kim, 2005).

To increase the heat transfer coefficient, one needs to consider how the heat exchanger operates. Things such as modes of the heat transfer operation (heating, evaporation, boiling, condensation or cooling), fluid properties and running conditions are vital to consider. Also, spatial orientation of the unit is important as the flow can behave differently if the fluid flows with the help of, against, or perpendicular to gravity. If a surface modification is not carefully designed, the new heat transfer surface could cause unexpected problems and not be worth the investment (Webb & Kim, 2005). To design an effective surface modification, one needs to consider different characteristic surface dimensions such as Height, Length, Pitch and Sharpness of the introduced surface modifications, see Figure 3-1.

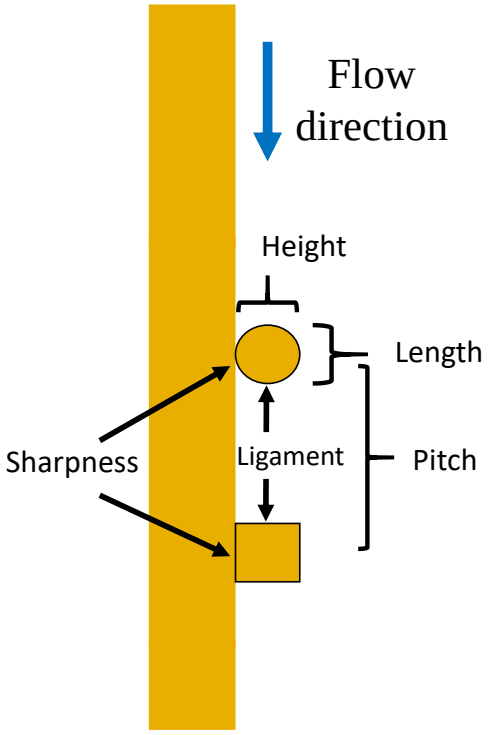


*Figure 3-1. Different characteristic dimensions to be considered when designing the surface modifications for a falling film unit. Difference in the spanwise direction (perpendicular to the image) could also be considered.*

For heat exchangers there exist general design concepts on how to construct an effective modified heat transfer surface (Webb & Kim, 2005). These designs are usually based on decades of research on the flow regimes and characteristics inside these units. For falling film units, much research has been carried out on horizontal tubes, e.g. (W. Li et al., 2011), (Ji et al., 2015), (Fath et al., 2015), (Kabova et al., 2006), (Bender et al., 2018), (Alexeev et al., 2005), (Chamra & Webb, 1996). However, the behaviour of a horizontal tube falling film unit differs significantly from that of with vertical tubes or plates, since gravity influences the liquid flow differently (Kalliadasis et al., 2012). Thus, caution is needed when an attempt is to be made to directly transfer conclusions obtained for one type of falling film unit to another.

For vertical falling film units, no general design suggestions exist (Miriam, 2007). Since this technology is utilized in numerous fields, it is complicated to formulate a universal design concept. Only a handful of studies investigate heat transfer enhancement due to modified surfaces for inclined or vertical falling film. In that manner, T. Gambaryan-Roisman and Stephan (2003) changed the heat transfer mode with initiating micro region evaporation on a grooved surface. Tatiana Gambaryan-Roisman et al. (2011) tried to enhance the heat and mass transfer with introducing microscale surface modifications. Pecherkin et al. (2015) investigated small, diamond-shape knurling textures for pure low viscosity fluids. Changing the heat transfer mode to nucleate boiling is an effective way to

enhance the heat transfer. However, this approach is not suitable for all operating conditions, as the temperature driving force is usually too low to obtain nucleate boiling and microstructures are sensitive to impurities and fouling, see Chapters 2.3.2 and 2.5.

Both H. Li et al. (2018) and Slade et al. (2013) observed that the liquid flow pattern could be significantly altered by the introduction of different types of surface modifications. Wierschem and Aksel (2004) studied the flow field on a sinusoidally-shaped surface at a 45° angle and detected the appearance of recirculation zones in the valleys. Yu et al. (2010) showed that the wall temperature was lower for fluid heating with a grooved surface. Najim et al. (2018) saw significantly enhanced evaporation in their numerical simulations due to the use of a sinusoidally-shaped heat transfer surface.

Raach and Mitrovic (2005) made a numerically study of how wires disturb the flow pattern for water desalination on vertical plates. They found an optimum spacing of Ligament/Height = 18 between the surface modifications. The authors did not provide an explanation to the underlying mechanism, but noted a 100 % increase of the evaporation rate. Salvagnini and Taqueda (2004) applied a wire mesh to the heat transfer surfaces and studied the effects on the heat transfer when water is employed as a working fluid. They found that the evaporation rate could be triplicated.

Broniarz-Press (1997) investigated mass transfer on spirally threaded tubes. The study showed that the rate of mass transfer increased 2-3 times compared to the case with a smooth tube. Shen et al. (1986) saw the same increase for mass and heat transfer on their vertical screw grooved tubes and claimed that such an increase was caused by recirculation zones within the liquid. Zheng and Worek (1996) studied heat transfer on inclined falling films on a modified surface, and also claimed that the observed improvement was caused by recirculation zones within the liquid. Ramadane et al. (1993) looked at the rate of evaporation of a vertical falling film on a surface with large surface fins. The improvement was mainly caused by the increased surface area, with the authors also pointing to a secondary enhancement, due to the non-uniformity of the flow, caused by the fins. Andritz (2018) claim their lamella heating surfaces cause high efficiency and reliability in their units but do not specify how they function.

Goff et al. (1992) and Bandelier (1997) proposed a new concept with large moving spiral fins and found an heat transfer increase of 350 %. The authors claimed that the increase was caused by the radial mixing caused by the fins. Kohrt (2012) studied $CO_2$ absorption into silicon oils on different plate structures in a lab-scale unit. They found that the mass transfer was increased by 30-75 % depending on the fluid viscosity. The same study also noted a three-dimensional flow (3D), but the modified surfaces were also made of 3D structures so this effect is not surprising. Zhao and Cerro (1992) studied the influence of several characteristics for corrugated surfaces for packing material with the thin film flow in a small experimental facility. Miriam (2007) investigated the effect of a vertical grooved surface (longitudinal grooved) and a recorded a heat transfer improvement of around 40 %. Schröder et al. (1979) looked at longitudinal structures for a Na-Cl solution and water respectively, and found an increase in the range of 2-3 times compared to that on a smooth surface. Helbig et al. (2009) investigated the influence on the hydrodynamics caused by the implementation of mini grooves aligned with the main flow direction. Figure 3-2 give examples on how the modified surfaces investigated in literature can look.

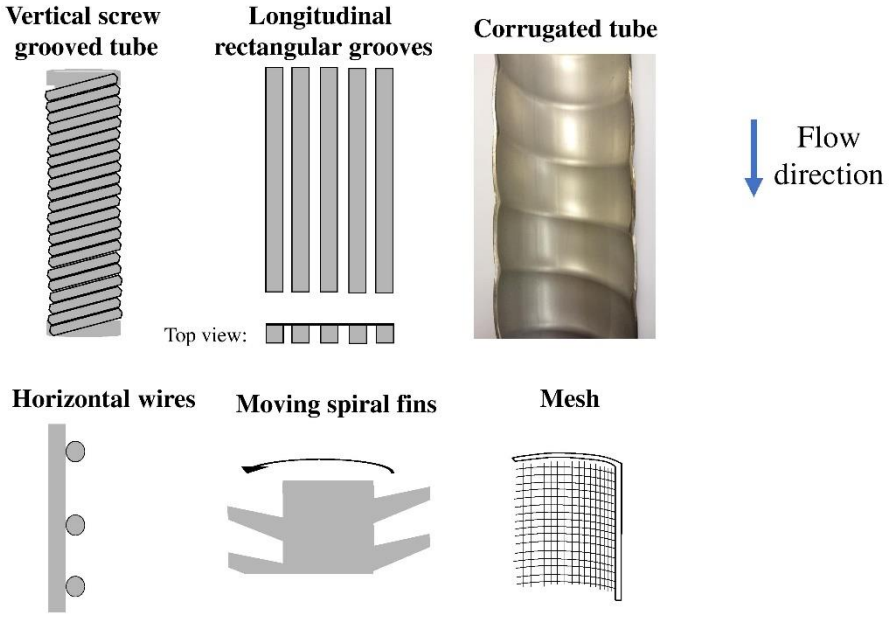


*Figure 3-2. Examples of modified surfaces investigated in the literature for vertical falling films. The flow direction is the same for all modified surfaces, as indicated by the arrow.*

The mentioned studies all show that it is possible to enhance the heat transfer in a vertical falling film unit by introducing surface modifications. Especially modifications perpendicular to the flow are promising as they have been shown to affect the flow pattern of the liquid film (Miriam, 2007). However, additional research is needed on how the flow is affected by the shape of a surface modification for a large span of operating conditions before a design strategy for an industrial unit can be established. In particular, since the viscosity of the working fluid influences the performance of the falling film unit to a great extent, it is important to include into analysis a broad range of fluid properties and operating conditions. The changes in the flow field when modified surfaces are used need to be evaluated in relation to the units operating with smooth surfaces, as that is of vital importance to understand the current limiting mechanisms for achieving higher heat transfer rates and to understand how such surfaces should be designed.

# 4 Experimental

Extensive experimental work has been carried out within this project. Two experimental setups have been used, an atmospheric one and a pilot evaporator. *The atmospheric setup* is constructed to be scalable and accessible. The design facilitates that local film thickness and heat transfer measurements are feasible at multiple vertical positions. In addition, the heat transfer surfaces can easily be replaced, with the inherent limitation of the system to heating conditions. *The pilot evaporator* was built to study falling film evaporation under conditions similar to those in industrial units. In the setup, overall heat transfer and pressure drop measurements under evaporating conditions can be conducted. The heat transfer surfaces can be replaced, but the process is rather costly and time consuming compared to the atmospheric setup. The two setups are located in the same facility, see Figure 4-1, and share several pieces of auxiliary equipment. The following sections will describe the two experimental setups in detail.

*Figure 4-1. Outside view of the facility where the experimental units are located. Everything seen through the glass windows is connected to at least one of the experimental setups.*

## 4.1 Atmospheric setup

The atmospheric setup, used in **Papers I-IV**, was built to be scalable, accessible and to allow for studies of hydrodynamics of falling films over lengths that are industrially relevant. Heating of the film can also be studied, but not evaporation. The heat transfer surfaces can be modified by applying wires.

The setup consists of a 0.8 m long hollow copper tube (inner and outer diameters $d_i$= 0.05 m and $d_o$= 0.06 m, respectively) with an electrical heater mounted inside. Energy is transferred by radiation from the heater surface to the inner tube wall and conducted through the tube wall to the outer surface where the fluid flows. The copper tube can be mounted in two configurations: 1) either directly to the inlet distributor (termed *SHORT tube* here), or, 2) to a 3-m long stainless-steel tube without heating (*LONG tube*), see Figure 4-2. The first configuration makes it possible to simultaneously study the development of the thermal and hydrodynamic profiles. The second setup allows the hydrodynamic profile to reach the statistically steady state already at the beginning of the copper tube, hence enabling studies of only the thermal development region. The system is open to the atmosphere and the product flows on the outside of the tube to facilitate flow observation and heat transfer measurements, see Figure 4-2.

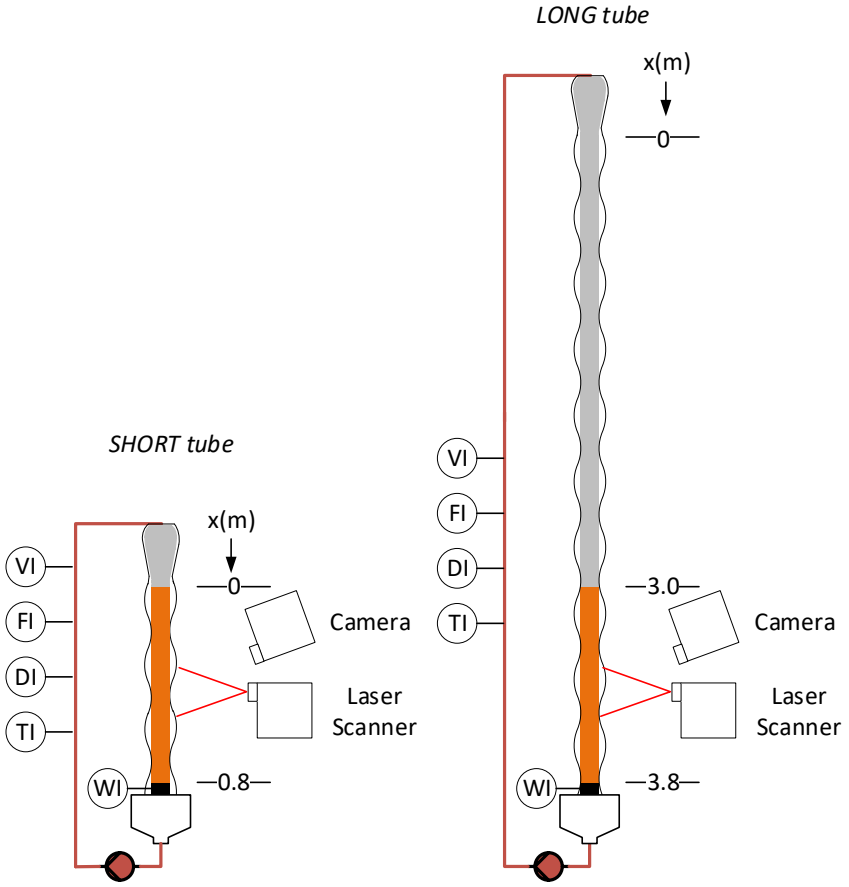


*Figure 4-2 Schematic diagram of the experimental setup used in this work. The heated tube section can be mounted in two different configurations, SHORT or LONG tube (either directly to the distributor or to a 3 m stainless steel pipe in between). DI=Density meter, FI=Flow meter, TI=Temperature meter, VI=viscometer, WI=Power supplied.*

The fluid is circulated with a displacement pump with a variable frequency drive to obtain the desired wetting rate. Note that, in this way, we are not forcing any particular disturbance frequency to the system. The liquid is distributed evenly and smoothly on the tube using a specially designed overflow distributer, shown in detail in **Paper I**. We measure online the temperature, flow rate, density, viscosity and power supplied by the heater and the accuracies of those measurements are presented in Table 4-1. A camera is used to take still images of the flow to get an overall understanding of the flow structure on the tube.

In addition, two novel measuring techniques have been developed in this work to study key features of the falling film. The first one is a laser triangulation scanner that can capture the changes to the flow structures over a 0.1 m long vertical line at high spatial and temporal resolutions. The second approach is a specially designed thermocouple, capable of measuring local time-averaged wall and bulk temperatures. Together with the power provided by the heater, local heat transfer coefficients can be estimated. The accuracy of the measurements can be seen in Table 4-1 and the following subchapters will provide a detailed description of the techniques.

*Table 4-1 Information on the measurement instruments and their accuracy for the Atmospheric setup. UI stands for Uncertainty Interval and is explained in Chapter 4.1.2.1.*

| **Quantity** | **Instrument** | **Accuracy** |
|---|---|---|
| Film thickness | Laser triangulation scanner | ± 0.1 mm |
| Local temperature | Copper-constantan thermocouple | $UI_T$ = ± 1.1 K |
| Local ΔT uncertainty | Copper-constantan thermocouple | $UI_{\Delta T}$ = ± 0.25 K |
| **Online** | | |
| Power | Energy Analyser WM22-DIN, Carlo Gavazzi | $UI_Q$ = ±50 W |
| Temperature | PT-100 H210, ABB | ± 0.2 K |
| Mass flow rate and | PROline promass 80 H, Endress + Hauser | ± 0.15 % of range |
| Density | PROline promass 80 H, Endress + Hauser | 0.5 kg/m3 |
| Viscosity | Viscoscope – Sensor VA-300L, Marimex | ± 1.0 % of value |

### 4.1.1 Laser triangulation scanner

The procedure for measuring the film thickness profiles was developed in **Paper I**. The method uses an optical triangulation scanner (light intersection method) of the model scanCONTROL 2950-100 from Micro-Epsilon. The scanner uses a 20 mW power source to produce a laser beam of the wave length of 658 nm that is enlarged through special lenses to form a static laser line on the target surface. A sensor matrix detects the diffused light and measures the reflected angle at 1280 points along the projected line. The angle is used to calculate the distance *z* to the surface and, with an inbuilt camera, the scanner determines the length *x* of the laser beam that is dependent on the distance *z*, see Figure 4-3. The scanner samples at a frequency of 500 Hz with a spatial resolution of ± $1.2 \cdot 10^{-5}$ m and a nonlinearity, i.e. deviation from true value, of ± 0.16 % based on the full scale output (Micro-Epsilon, 2018).

The scanner is used to continuously measure the distance $z_i(x)$ to the liquid-gas interface along a vertical path. By also measuring the reference distance $z_r(x)$ between the scanner and a clean surface without any flow, the thickness of the liquid film in each point can be calculated as $\delta(x) = z_r(x) - z_i(x)$. In this way and having in mind that the film thickness is small, the influence of the nonlinearity of the scanner is reduced as the thickness only varies slowly with increasing the distance around the true linear value, resulting in a higher measurement accuracy. However, since the measuring of the actual film thickness is carried out in two steps, subtracting $z_i(x)$ from $z_r(x)$, it is of utmost importance that the scanner and the tube are properly fixed and do not move between the measurements.

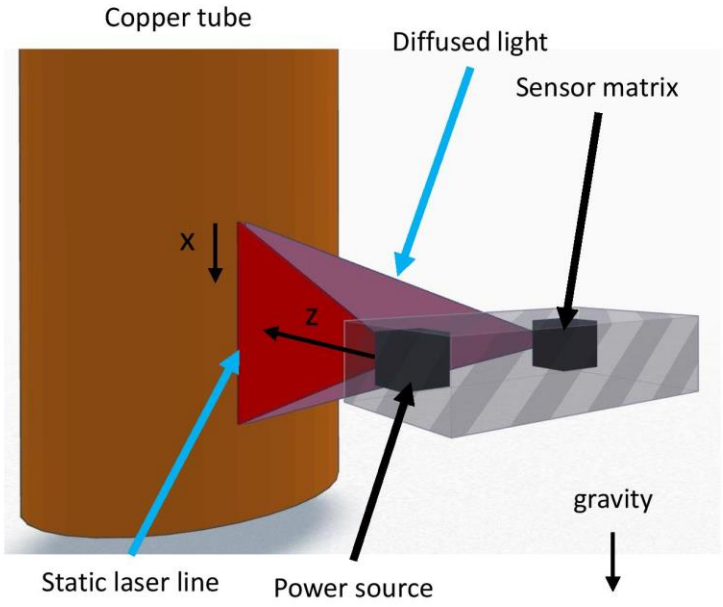


*Figure 4-3: Demonstration of the operating principle of the laser triangulation scanner.*

The measured data are imported into MATLAB and filtered with a standard local regression technique using weighted linear least squares. The goal is to remove unwanted noise, e.g. from occasional falling droplets, which can occur for low viscosity fluids at high wetting rates as a consequence of a turbulent liquid film. From the distances collected, it is possible to quantitatively determine the important film characteristics, such as the wave amplitude, the instantaneous and average film thickness, the wave speed etc.

#### 4.1.1.1 Accuracy of the film thickness measurements

The accuracy and performance of the laser triangulation scanner have been thoroughly examined in **Paper I**. The scanner performs well for several reflecting fluids, like *dairy product*, and captures the flow pattern with high spatial and temporal resolution and the accuracy of the absolute film thickness measurements is at least ± 0.1 mm, also listed in Table 4-1.

### 4.1.2 Local temperature and heat transfer measurements

The procedure to measure local time-averaged wall temperatures profiles was developed in **Paper I**. The method utilizes the principle of a copper-constantan thermocouple. The copper tube in the Atmospheric setup acts as one of the conductors and the junction is created by pressing a constantan needle against the copper tube wall at any desired location. The local wall temperature is thus obtained at the contact point, see Figure 4-4 (Left). An ice bath is used as a reference state and the output voltage is read by a voltmeter. The tube is hollow and there is an electrical heater in its centre. Energy is transferred by radiation from the heater surface to the inner tube wall and conducted through the tube wall to the outer surface where the fluid is supposed to flow. Since most of the energy is transferred by radiation, small temperature variations in the liquid flow have a negligible influence on the energy distribution from the heater. The 5 mm thick copper wall also helps to minimise the impact of unwanted disturbances, such as the fluctuating heat flux from the heater due to fluctuations in the power grid.

*Figure 4-4. Left: Constantan needle measuring the copper tube wall temperature. Right: Beaker used to measure the bulk temperature. The reddish-brown parts are made of copper and the grey part in the front is a rubber cup capable of holding 10 ml, enough to fully submerge the copper plate with liquid. The constantan needle is inserted through a bottom hole in the cylinder handle until it touches the copper plate, closing the circuit of the thermocouple.*

Once the wall temperature is obtained, the needle is inserted into a 10 ml beaker (Figure 4-4 right), through the hole in the plastic cylinder until it touches the copper plate in the front, forming a new junction point. The rubber in the front is pushed against the tube, collecting the flowing liquid, and when the temperature reading stabilizes, the bulk temperature is noted and the beaker is removed from the tube. With the power supplied by the electrical heater, local averaged heat transfer coefficients can be calculated as:

$$\bar{h}_{heating} = \frac{Q}{A_o\left(T_W - T_B\right)}, \tag{4.1}$$

where $Q$ is the supplied power, $A_o$ is the outer surface area and $T_W$ and $T_B$ are wall and bulk temperatures, respectively.

#### 4.1.2.1 Accuracy of the local heat transfer measurements

The accuracy and performance of the temperature measurements have been thoroughly examined in **Paper I**. The thermocouple has a maximum calibration error of ± 0.01 K. However, there are system variations originating from things like the inlet temperature and the flow rate disparities that possibly cause the increase of the actual uncertainty. The system variation for the temperature measurements has been estimated by assuming that $\Delta T = T_{Wall} - T_{Bulk}$ is normally and equally distributed for all measurements. A 95 % Uncertainty Interval (UI) based on all conducted measurements could therefore be calculated as:

$$UI_{\Delta T} = \sqrt{\frac{\sum_i \sum_j \sum_k \left(\Delta T_{ijk} - \overline{\Delta T_{ij}}\right)}{N - M}} \cdot t_d\left(0.025, N - M\right), \tag{4.2}$$

where *i*, *j* and *k* are fluid type, vertical position and individual measurement, respectively. In expression (4.2) $N$ is the total number of measurements, $M$ is the number of averages calculated and $t_d$ is the t-distribution. The value of $UI_{\Delta T}$ has been estimated to ± 0.25 K and together with $UI_Q$, which is ± 50 W, the uncertainty for the heat transfer coefficient for a single measurement in our system can be obtained:

$$\frac{UI_h}{h} = \sqrt{\left(\frac{UI_Q}{Q}\right)^2 + \left(\frac{UI_{\Delta T}}{\Delta T}\right)^2}. \tag{4.3}$$

Since the uncertainty of the heat transfer coefficient depends on the magnitude of $\Delta T$, the error span for individual measurements will be in the range of 4 – 20 % depending on the operating conditions. The large uncertainties occur at higher heat transfer coefficients, due to the small temperature difference. However, the repeated measurements significantly lower the uncertainty. All values presented in this subsection and used to estimate the uncertainty in the temperature measurements are also listed in Table 4-1. $UI_T$ has been obtained in a similar manner as $UI_{\Delta T}$.

### 4.1.3 Experimental procedure

In the Atmospheric setup, the hydrodynamics and heat transfer of a subcooled fluid have been studied on both smooth and modified heat transfer surfaces.

A broad range of fluid properties and operating conditions have been investigated, which has resulted in a wide range of flow regimes. The variation of regimes is achieved by

preparing dairy products of various concentrations by mixing water with different fractions of dairy powder until the mixture becomes a homogenous fluid. Adding dairy powder increases the density and viscosity, which reduces the Reynolds and Kapitza numbers, making it possible to investigate flow regimes from Wavy-Laminar to fully Turbulent.

Just purely hydrodynamic studies were performed in **Paper II** and were carried out on the *Long tube* setup by positioning the laser triangulation scanner at multiple vertical locations. Heat transfer studies combined with hydrodynamic observations were done in **Paper III** and **IV** by measuring the local wall temperature at multiple vertical positions on the copper tube both for the *Short* and *Long tube* configuration (0.20, 0.30, 0.55 m and 3.20 3.30 3.50 m from the inlet respectively). In addition, the inlet and outlet bulk temperatures over the copper tube were also measured to conduct an energy balance to ensure that evaporation could be neglected (the evaporation losses were less than 1 %). Temperature measurements in the tangential direction were also performed to confirm an even heat flux. A heater supplied a constant power of 2.3 kW (15.3 kW/m$^2$). The inlet temperature was maintained at 323 K by external cooling. Table 4-2 specifies the fluid properties for the fluids used in the heat transfer investigation in this work.

*Table 4-2. Operating conditions for the fluids investigated in the Atmospheric setup. All values are either measured or calculated if not explicitly specified. The fluid names are: High Viscosity fluid (HV), Intermediate Viscosity fluid (IV) and Low Viscosity fluid (LV).*

| **Fluid** | **DS** | $\mu$ | $\rho$ | $k$ | $C_p$ | $\sigma$ | $Ka$ | $Pr$ | $Re$ | $\Gamma$ |
|---|---|---|---|---|---|---|---|---|---|---|
| | **%** | **mPas** | **kg/m$^3$** | **W/(m·K)** | **J/(kg·K)** | **N/m** | **-** | **-** | **-** | **kg/(m·s)** |
| **HV** | 31 | 6.6 | 1090 | 0.50[a] | 3500[a] | 0.043[a] | 167 | 46 | 18-170 | 0.12-1.13 |
| **IV** | 20 | 2.6 | 1065 | 0.56[a] | 3800[a] | 0.043[a] | 574 | 18 | 45-423 | 0.19-1.1 |
| **LV** | 0 | 0.55 | 988 | 0.65[b] | 4177[b] | 0.068[b] | 7010 | 3.5 | 132-1854 | 0.07-1.02 |

[a] Value obtained from Madoumier et al. (2015)

[b] Value obtained from NIST (2017)

The influence of surface modification characteristics has been studied by placing differently shaped wires on the copper tube in the *Short tube* configuration, see Figure 4-5. At first, changes to the hydrodynamics were only looked at to screen the influence of different characteristics. Later, heat transfer measurements were also conducted in **Paper IV** for the most promising surfaces designs. The two novel measuring techniques developed in this work were extremely valuable here as the laser triangulation scanner could study the flow pattern over multiple wires and the specially designed thermocouple could measure the wall temperature in between.

*Figure 4-5. Image of a thread applied to the heat transfer surface.*

## 4.2 Pilot evaporator

The pilot evaporator was originally built in 2003 to study falling film evaporation under conditions mimicking those in industrial units and in cooperation with Valmet AB, an industrial supplier of evaporation plants for the pulp and paper industry. The evaporator was designed to be large enough to give industrially relevant results and, in the same time, small enough to be flexible and controllable. Condensing steam is therefore used as the heat supply and approximately 0.050 $m^3$ of product is needed to run the facility. Throughout the years the evaporator has been rebuilt and refitted to suit variable needs and operation modes allowing great flexibility when designing experimental campaigns. However, only the configuration used in this work will be presented here. For the interested reader, further details, from other investigations performed with the pilot evaporator, can be found in the work by Johansson et al. (2005), Gourdon, Karlsson, et al. (2015), Gourdon, Innings, et al. (2015) and Karlsson et al. (2017).

A flowsheet of the pilot evaporator setup can be seen in Figure 4-6. The main component is a 4.125 m long stainless steel tube with an internal diameter ($d_i$) of 48.6 mm, an external diameter ($d_o$) of 51 mm and a total outside heat transfer area ($A_o$) of 0.66 $m^2$. The product flows on the inside and steam condenses on the outside to supply the heat. The tube is enclosed in a shell that is well isolated from the surroundings.

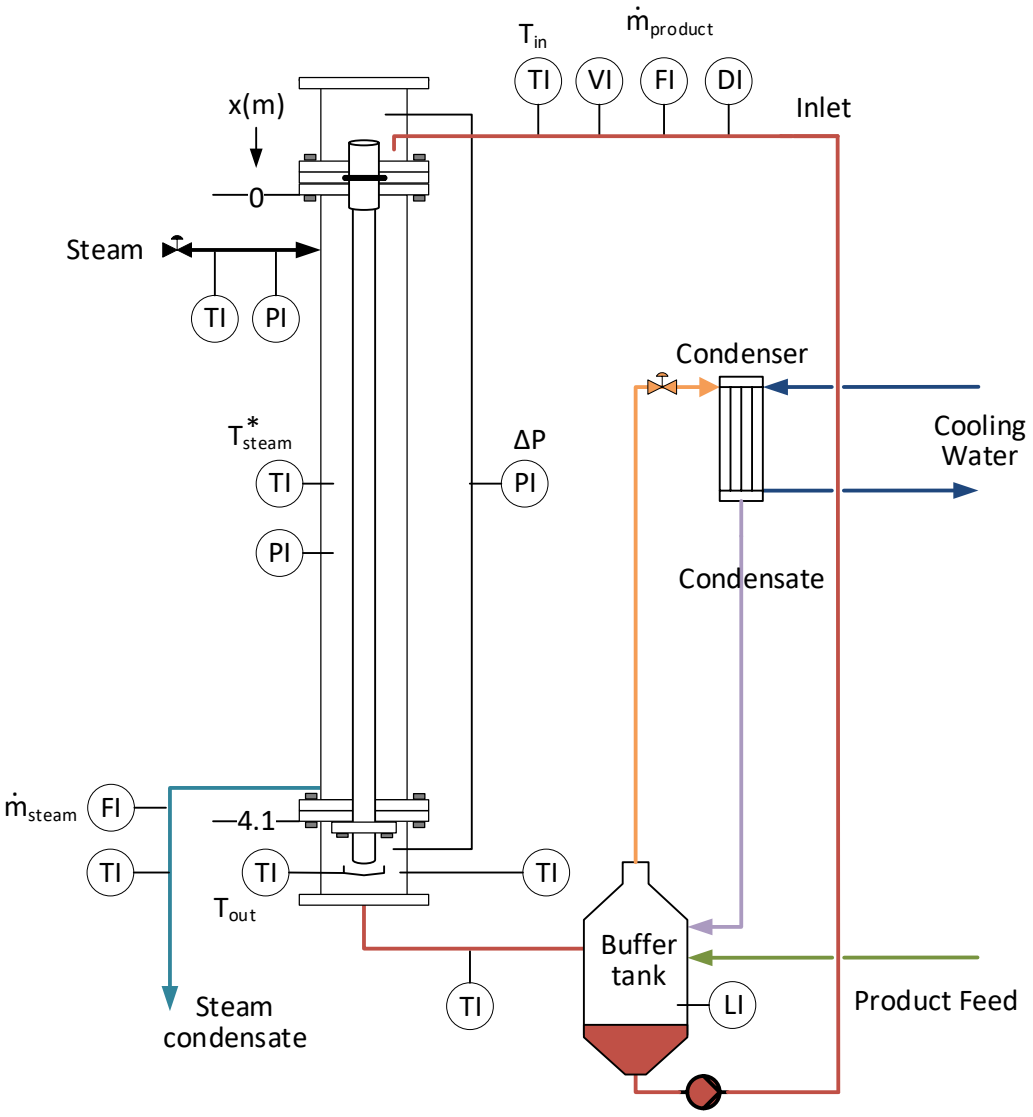


*Figure 4-6. Simplified flowsheet of the pilot evaporator setup. LI = Liquid level indicator, PI= Pressure indicator, DI= Density meter, FI=Flow meter, TI=Temperature meter, VI=Viscometer.*

The product is fed to a buffer tank and then recirculated over the tube by a pump. An overflow distributer on the top guarantees an even distribution of the product under all experimental conditions. The liquid and evaporated vapour exit in the bottom of the tube. The liquid is collected in a cup in order to measure the mixed cup temperature of the product ($T_{out}$). By experience however, the measured mixed cup temperature is closer to the saturation temperature of the outgoing product, $T^*_{out}$, than that of an actual mixed cup. The flow of liquid and gas within the tube results in a pressure drop between the tube inlet and outlet, which is measured by a differential pressure meter. This of course influences the thermal driving force as described in Section 2.3.4. The thermal driving force is controlled by specifying the pressure on the steam side (corresponding to the desired steam saturation temperature, $T^*_{steam}$) and the product outlet temperature. The vapour flows to a condenser where it is condensed and then returned to the buffer tank to maintain constant fluid properties during the experiments.

The evaporator setup comprises a large number of measurement devices, see Figure 4-6. A summary of these devices, together with their accuracy can be seen in Table 4-3.

*Table 4-3. Information on measurement instruments and their accuracy.*

| Quantity | Instrument | Accuracy |
|---|---|---|
| Temperature | TC, Pentronics type K<br>PT-100 H210, ABB H210, H600 | ± 0.05 K after calibration |
| Product mass flow rate | PROline promass 80 H, Endress + Hauser | ± 0.15 % of range |
| Density | PROline promass 80 H, Endress + Hauser | 0.5 kg/m$^3$ |
| Viscosity | Viscoscope – Sensor VA-300L, Marimex | ± 1.0 % of value |
| Pressure | Yokogawa EJA530, EJA510, EJA110 | ± 0.2 of range |
| Volumetric steam condensate | Method: Measure time between two levels with known volume with two VEGASWING 61 vibrating level switches | |

### 4.2.1 Exchangeable heat transfer tube

Considerable effort has in this work been put into rebuilding the evaporator to be capable of replacing the heat transfer surface. The grey bolts seen on the flanges of the evaporator in Figure 4-6 can be untied to remove the heat transfer tube through the bottom of the shell casing. The tube has a flange welded on the bottom part and a cone welded on the top to perfectly seal the steam side from the product side. The cone acts both as a distributor for the liquid to flow smoothly over the top edge, and as smooth surface for the O-ring to seal the steam side from the product side. This construction allows for thermal expansion of the material without damaging the heat transfer tube. The drawback is that each tube has to be individually produced, but since such tubes should already be unique with their surface structures, the process of adding a flange and a cone is relatively cheap and does not yield significant additional construction cost. Instead, the flexibility is increased as different surfaces can be repeatedly tested without the need for rebuilding the evaporator, making the results more trustworthy.

### 4.2.2 Evaluation procedure

The heat transfer is first evaluated by calculating the heat load ($Q_{tot}$) from the steam condensate mass flow ($\dot{m}_{steam}$), the enthalpy of vaporization ($\Delta H_{Vap}$) and the subtraction of losses to the surroundings, measured prior to the experiments ($Q_{losses}(T_{steam})$):

$$Q_{tot} = \dot{m}_{steam}\Delta H_{Vap} - Q_{losses}(T_{steam})\,. \tag{4.4}$$

The losses are of course dependent on the temperature of the steam, but at 80°C, they are approximately 1 kW. The heat load is then used to calculate the overall heat transfer coefficient:

$$U = \frac{Q_{tot}}{A_o(T_{steam} - T_{out})}\,. \tag{4.5}$$

This evaluation method directly indicates how high the rate of heat transfer is without the need for any modelling of, for example, the transport resistance on the steam side. The procedure also includes the effect of the pressure drop since the largest temperature difference is used as the driving force, see Chapter 2.3.4. This is also how a real industrial unit will perform. The procedure works well as an evaluation tool as long as the tube length / heat transfer area is constant, which has been the case for all experiments with the pilot evaporator (neglecting the area increase due to the surface modifications). Our definition of the overall heat transfer coefficient differ slightly from what is normally done in literature for cases with significant pressure drop. It is desirable for the overall HTC to be independent of the tube length and to be comparable with other experimental setups of different sizes. However, in order for us to work which such a definition of *U*, the temperature profile in the evaporator needs to be known. Since we can't measure the temperature profile, large experimental data set would be required to properly estimate the profile (Mura & Gourdon, 2017). Therefore, one can view our definition of the overall heat transfer coefficient for these cases more as a performance indicator.

To compare the results to the correlations presented in Chapter 2.3, or, to the measurements conducted in the Atmospheric setup under heating conditions, modelling of the additional transport resistance needs to be introduced, the following expression has been used:

$$U = \frac{1}{\left(\frac{1}{h_i A_i} + \frac{\delta_w}{k_w A_m} + \frac{1}{h_{cond} A_o}\right) A_o}, \tag{4.6}$$

where $h_i$ is the heat transfer coefficient on the inside (either evaporating or heating), $A_i$ is the heat transfer area on the inside of the tube, $k_w$ is conductivity in the tube wall estimated with the procedure suggested by Assael and Gialou (2003). In expression (4.6) $h_{cond}$ is the heat transfer coefficient of the condensing steam which was estimated using a correlation for condensation on vertical surfaces by Numrich and Müller (2010). $A_m$ is the logarithmic mean area which is calculated in the following way:

$$A_m = \frac{A_o - A_i}{ln\left({A_o}/{A_i}\right)}. \tag{4.7}$$

### 4.2.3 Experimental procedure

Two types of fluids were investigated in the Pilot evaporator, *Water* and *Black liquor* with 30 % dry solids content, both at 70°C. All fluid properties and operating conditions are specified in Table 4-4. The steam temperature was altered in order to change the heat load ($Q_{tot}$).

*Table 4-4. Operating conditions for the fluid investigated in the Pilot evaporator setup. All values are either measured or calculated if not explicitly specified. All experiments were performed at 70°C (Outlet temperature).*

| **Fluid** | **DS** | $\mu$ | $\rho$ | $k$ | $C_p$ | $\sigma$ | $Ka$ | $Pr$ | $Re$ | $\Gamma$ |
|---|---|---|---|---|---|---|---|---|---|---|
| | **%** | **mPas** | **kg/m$^3$** | **W/(m·K)** | **J/(kg·K)** | **N/m** | **-** | **-** | **-** | **kg/(m·s)** |
| **Water** | 0 | 0.40 | 978 | 0.66[c] | 4185[c] | 0.0647[c] | 10053 | 2.5 | 250-2000 | 0.18-1.0 |
| **Black Liquor (BL)** | 30 | 2 | 1167 | 0.58[d] | 3600[d] | 0.025[d] | 480 | 13 | 88-490 | 0.18-1.0 |

[c] Value obtained from NIST (2017)

[d] Value obtained from Adams et al. (1997)

# 5 Numerical Framework

Numerical simulations are an indispensable tool to gain insight into complex structures taking place within the falling liquid film, and to understand how waves form and connect with other fundamental phenomena in the film, in this case the heat transfer. If carried out with sufficient resolution and accuracy, the simulations are of crucial importance here since similar information is not straightforward to obtain from experiments. The following chapter will explain the numerical framework used in this work in **Papers II-IV**.

## 5.1 Governing equations and implementation

In our numerical framework, the film flow is considered two-dimensional, transient and incompressible, and with constant fluid properties. Gravity acts on the film while the latter flows down along a vertical wall with a constant heat flux. Evaporation is not included since the energy balance conducted during the heating experiments, discussed in Chapter 4.1.3, showed that it can be neglected.

The dynamics of the falling film can be described by the Navier-Stokes equations using the single-fluid representation in a wall fixed frame of reference (Dietze et al., 2008). Advection of the volume fraction α is used to distinguish between the two fluids. The Volume of Fluid (VOF) method is used to track the interface. The Bénard-Marangoni effect is not considered since the surface tension coefficient has a weak temperature dependence and only small temperature variations are expected at the liquid interface.

The governing equations involve those for the conservation of momentum, mass and energy, as well as the transport equation for the volume fraction $\alpha$:

$$\frac{\partial}{\partial t}\left(\rho \boldsymbol{v}\right)+\nabla\cdot\left(\rho \boldsymbol{v}\boldsymbol{v}\right)=-\nabla p+\nabla\cdot\left[\mu\left(\nabla \boldsymbol{v}+\nabla \boldsymbol{v}^{T}\right)\right]+\rho \boldsymbol{g}+\boldsymbol{F}_{\sigma}, \tag{5.1}$$

$$\frac{\partial \rho}{\partial t}+\nabla\cdot\left(\rho \boldsymbol{v}\right)=0, \tag{5.2}$$

$$\frac{\partial}{\partial t}\left(\rho c_{p}T\right)+\nabla\cdot\left(\rho \boldsymbol{v}c_{p}T\right)=\nabla\cdot\left(k\nabla T\right), \tag{5.3}$$

$$\frac{\partial \alpha}{\partial t} + \boldsymbol{v} \cdot \nabla \alpha = 0 \,, \tag{5.4}$$

where $\boldsymbol{v}$ is the velocity, $p$ is the pressure, $\boldsymbol{g}$ is the gravitational acceleration, $T$ is the temperature, $\boldsymbol{F}_\sigma$ is the surface tension force that should be active only at the interface and $\alpha$ is the volume fraction. The density $\rho$, the dynamic viscosity μ, the conductivity $k$ and the heat capacity $C_p$ are evaluated in terms of the individual fluid properties and the local volume fraction:

$$X = \alpha \, X_l + \left(1 - \alpha\right) X_g \,, \tag{5.5}$$

where $X$ is the quantity and the subscripts $l$ and $g$ indicate the liquid and gas phases, respectively. The Continuum Surface Force Model (CSF) method proposed by Brackbill et al. (1992) is used to model the surface tension force. The force is expressed as a function of the liquid surface tension coefficient $\sigma$, curvature of the interface $\kappa$ and the gradient of the volume fraction $\alpha$:

$$\boldsymbol{F}_\sigma = \sigma \, \kappa \, \nabla \alpha \,. \tag{5.6}$$

The curvature at the interface is computed from local gradients of the volume fraction:

$$\kappa = \nabla \cdot \left( \frac{\nabla \alpha}{|\nabla \alpha|} \right). \tag{5.7}$$

We use a piecewise-linear geometrical reconstruction scheme for the interface, (Youngs, 1982). In addition, PISO, the least-squares cell-based, PRESTO!, the second-order upwind scheme are used for the pressure-velocity coupling, gradient, pressure and momentum/energy respectively. The interface is tracked with the Euler explicit formulation, and we use the Implicit Body Force formulation, which accounts for the partial equilibrium of the pressure gradient and body forces in the momentum equations.

The time step has been set to $1 \cdot 10^{-5}$ seconds, a factor 2 below the maximum allowable time step requirement proposed by Brackbill et al. (1992) for an explicit treatment of the surface tension. The simulations were done in ANSYS Fluent.

## 5.2 Domain and boundary conditions

As discussed in Chapter 2.1. falling films are typically considered smooth at the inlet, regardless of the operating conditions. For that reason, the numerical simulations are initialized using the analytical solution for the Laminar case derived by Nusselt (1916). Here, the film thickness and the mean velocity are expressed as:

$$\delta_N = \left( \frac{3Re\mu_l^2}{\rho_l^2 g} \right)^{1/3}, \tag{5.8}$$

$$u_N = \left( \frac{Re^2 \mu_l g}{3\rho_l} \right)^{1/3}. \tag{5.9}$$

In the computations, the inlet at $x = 0$ (Figure 5-1) consists of the liquid part, $0 \leq y \leq \delta_N$, and the gas part (air), $\delta_N \leq y \leq 4\delta_N$, both set to 323 K. The streamwise velocity at the inlet in the gas phase is set constant to 1.5 times the Nusselt velocity and in the liquid, the same velocity is specified as a parabolic profile with a fluctuation component to initialize waves in the system:

$$v_x(0, y, t) = \frac{3}{2}\left[ 2\left( \frac{y}{\delta_N} \right) - \left( \frac{y}{\delta_N} \right)^2 \right] \cdot u_N \cdot \left[ 1 + \varepsilon \cdot \sin\left( 2\pi ft \right) \right]. \tag{5.10}$$

In (5.10) $\varepsilon$ is the disturbance amplitude and $f$ is the disturbance frequency. Based on the findings in **Paper II**, they are set to 0.05 and 10 Hz, respectively, in order to quickly reach statistically steady conditions in the computational domain. The remaining boundary conditions are the *pressure outlet* for the outlet, with an *open channel flow* formulation to handle the presence of two interfaces. The wall is specified as *wall* (no-slip) with a constant heat flux of 15.3 kW/m$^2$ (to match the experiments) and the gas boundary, is specified as *symmetry*.

### 5.2.1 Smooth surface domain

The computational domain has been set to 0.8 m in the streamwise direction to match the length of the heated section in the experiments, see Figure 5-1. In the crosswise direction, the domain has been set to $4 \cdot \delta_N$, making it wide enough to neglect interference from the gas boundary. For the smooth surface computational domain, a uniform mesh size of $\triangle$ x=$0.15 \cdot \delta_N$ and $\triangle$ y=$0.060 \cdot \delta_N$ has been used.

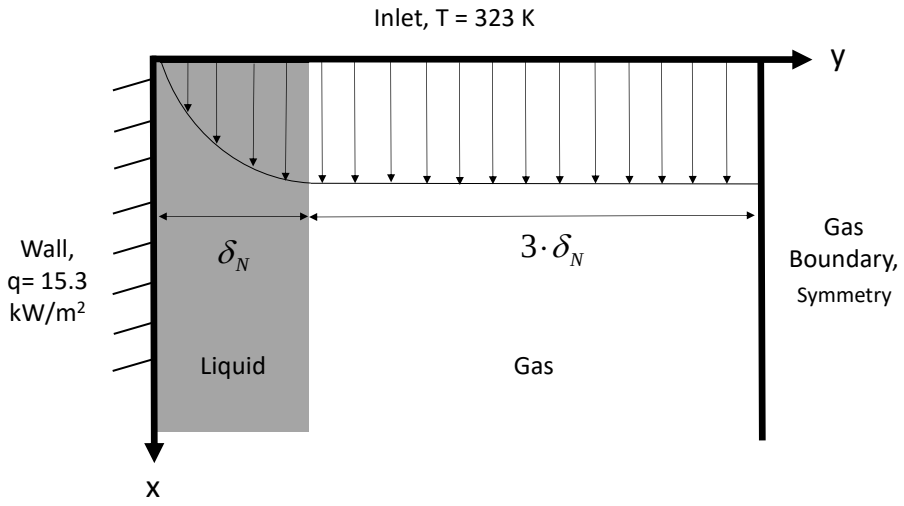


*Figure 5-1. Computational domains used in the present work for smooth surfaces.*

### 5.2.2 Modified surface domain

The computational domain has been set to 0.7 m in the streamwise direction to represent the length of the heated section in the experiments. Modification of the surface is only employed between 0 and 0.5 m in order to also be able to study the flow after the modifications, similar to the way it is done in the experiments. The surfaces are modelled as solid copper. In the crosswise direction, the domain has been set to $7\cdot\delta_N$, making it wide enough to neglect interference from the gas boundary, see Figure 5-2. The use of modified surfaces causes a thicker film thickness, hence the need for a larger computational domain in the crosswise direction as compared to that used for a smooth surface. For the computational domain dealing with modified surfaces, the maximum mesh size has been set to $\triangle$ x=$0.15\cdot\delta_N$ and $\triangle$ y=$0.060\cdot\delta_N$, while being refined around the surface modifications and also including a growth layer at the wall.

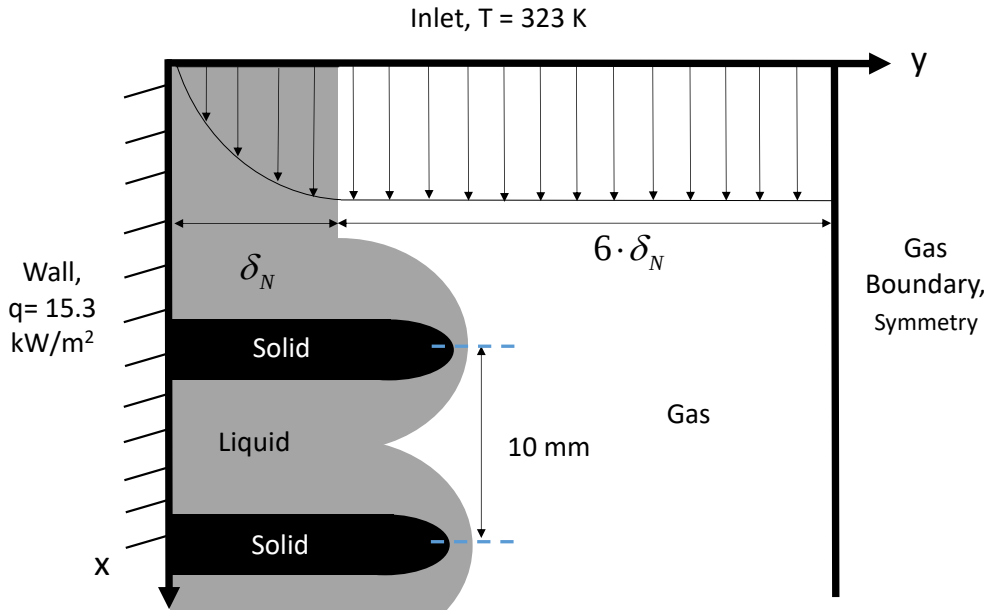


*Figure 5-2. Computational domains used in the present work for the modified surfaces. The modified surfaces cause an increased film thickness, hence the need for a larger computational domain in the crosswise direction. It should be mentioned that the x and y axis have different scales in the figure.*

## 5.3 Post processing

From the simulations, all relevant quantities (volume fraction, temperature, pressure, x-velocity, y-velocity, heat flux and cell volume) at all cell-entre locations and at predefined times steps have been exported from Fluent as ASCII text files. These text files have afterwards been read into MATLAB where the data have been processed.

The location of the liquid-gas interface was calculated based upon the gradient of the volume fraction. The bulk temperature was extracted by weighting the cell temperature with the velocity in the x-direction, averaging the variation in the y-direction for the liquid and time averaged until statistically steady conditions are reached:

$$T_b(x) = \int_{t_1}^{t_2} \left( \int_0^{\delta} v_x(x,y,t) \cdot T(x,y,t) \mathrm{d}y \Big/ \int_0^{\delta} v_x(x,y,t) \mathrm{d}y \right) \mathrm{d}t \,, \tag{5.11}$$

where, $v_x$ is the fluid velocity in the x-direction, $\delta$ is the film thickness and $t$ is the time variable. The wall temperature was also time averaged and extracted at the wall boundary (y=0):

$$T_w(x) = \frac{1}{t_2 - t_1} \int_{t_1}^{t_2} T(x,0,t) \mathrm{d}t \,. \tag{5.12}$$

For those cases where the time variance of these temperatures has been investigated, the time integration has not been performed. The heat flux across the film has been calculated as:

$$q_y(x,y,t) = -k \cdot \frac{\partial T(x,y,t)}{\partial y}. \tag{5.13}$$

## 5.4 Validation of numerical framework

In **Paper III** it was experimentally shown that waves initially grow into a two-dimensional (2D) pattern, which further downstream, disintegrate into a seemingly three-dimensional (3D) structure. However, the flow may appear 3D, but most of the liquid is still seen to clearly move in the streamwise direction. A similar phenomenon has also been observed by Kharlamov et al. (2015) who made a thorough investigation of the spanwise liquid redistribution. The authors noted that the local flow rates could differ significantly in the spanwise direction, but also that the local spanwise flow rates were approximately an order of magnitude smaller than the streamwise flow rates. This justifies the two-dimensional numerical framework as it implies that, even though the flow might appear different in the spanwise direction, this is still rather insignificant compared to what happens in the streamwise direction. (Demekhin et al., 2007). In addition, the modified surface structure investigated in this work, does not vary significantly in the spanwise direction.

The numerical framework has been extensively validated in the papers. **Paper II** validated hydrodynamics on smooth surfaces, **Paper III** heat transfer on smooth surfaces and **Paper IV** hydrodynamics and heat transfer on modified surfaces. The numerical simulations carried out in the three papers were validated against our own experimental measurements and in **Papers II** and **III** we also compared our framework with results from other studies in the field. In addition, **Papers II** and **III** identified how the framework should be formulated in order to yield results relevant to a large-scale pilot unit.

The grid independence has been validated by checking for the presence (i.e. absence) of large temperature jumps between the computational cells and the absence of no significant changes of the temperature lines within a wave as a result of using a finer grid, see Figure 5-3. The finer grid only gives a slightly higher temperature at the wall.

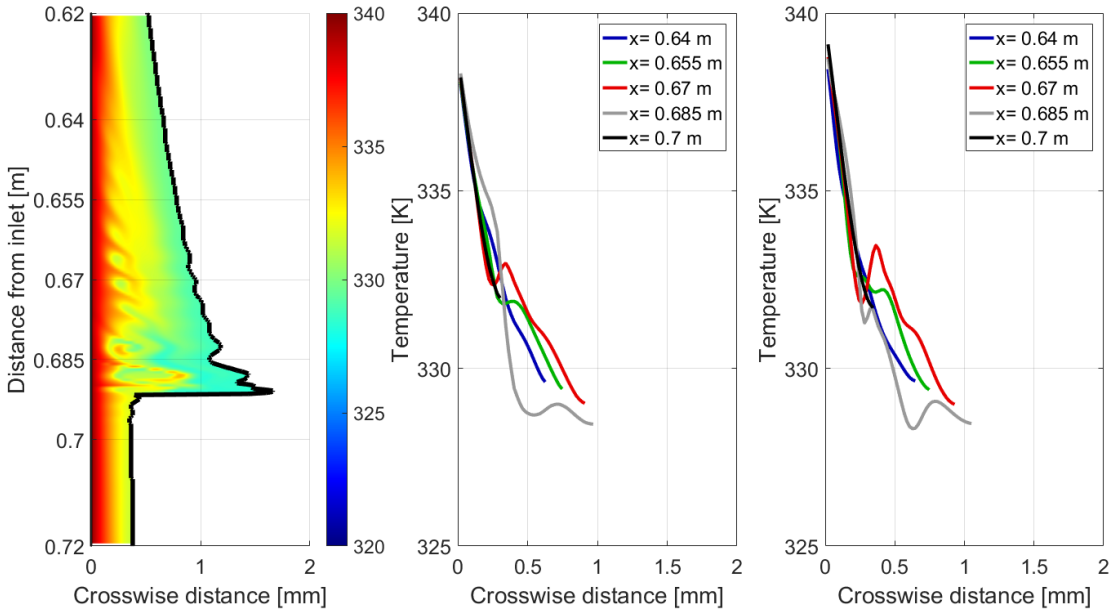


*Figure 5-3. Left) Temperature contour plot of a statistically steady wave for the IV fluid at a wetting rate of 0.47 kg/(m·s). Middle) Temperature profiles at five vertical positions within the liquid film for the Standard grid. Right) A grid with twice as many cells as the standard grid.*

The fluid properties within the numerical framework were chosen to be constant in order to simplify comparison between the different cases invested. When the film is heated as it flows downwards, the temperature changes differently between the cases due to the different wetting rate, film thickness and fluid properties. Since there exist both hydrodynamical and thermal entrance lengths, whose values are unique for each case, knowing the point at which one should compare the cases at *statistically steady* conditions is not trivial. If the fluid properties were temperature dependent as well, it would increase the complexity even further, hence we are assuming here constant fluid properties. To validate this simplification, two simulations for the same case were carried out (Figure 5-4), one with the constant fluid properties (Left) and one with temperature-dependent properties (Right), according to Madoumier et al. (2015). No major difference between the two cases can be seen, and we thus assume our assumption is valid.

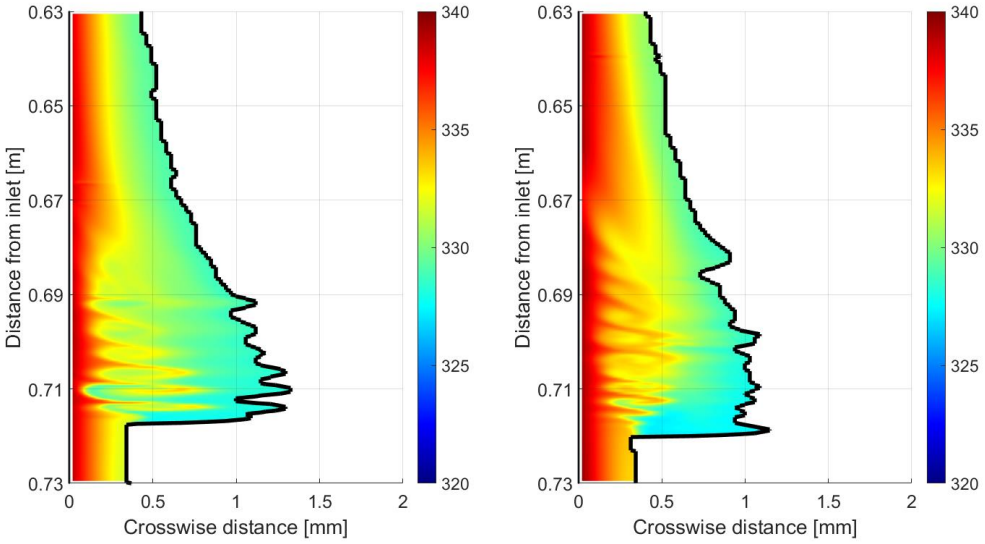


*Figure 5-4. Temperature contour plot of a statistically steady wave for the IV Fluid at a wetting rate of 0.47 kg/(m·s) Left) Constant fluid properties. Right) Temperature dependent fluid properties. Note that there is no major difference between the two cases.*

# 6 Results and Discussion

The results from this work will be presented in five different Chapters. First, the main findings will be presented from **Papers II** and **III** about hydrodynamics and heat transfer of vertical falling films on smooth surfaces. The mechanisms driving the heat transfer will be discussed in more detail than it was done in **Paper III**. In particular, the simulations will be used to provide detailed information on how the heat transfer varies within the liquid film under heating conditions. In Chapter 6.2, the design characteristics of the heat transfer surfaces will be discussed. The knowledge from **Papers III** and **IV** on how heat transfer is affected by the hydrodynamics will be utilized to understand how modification of heat transfer surfaces influences the hydrodynamics. In Chapter 6.3, the use of modified surfaces investigated in **Paper IV** will be discussed and related to the results presented in Chapter 6.1. Also, the knowledge of the transient behaviour of the film will be used to understand the mechanisms that govern the heat transfer within the liquid film. In Chapter 6.4, experimental results for evaporative conditions will be presented. Finally, the difference between the heating and evaporative results will be discussed and their similarities and differences will be addressed in Chapter 6.5. The novel measurement approaches for film thickness profiles and local wall and bulk temperatures and heat transfer coefficients developed in **Paper I** will not be discussed here, as they were presented in Chapters 4.1.1 and 4.1.2.

## 6.1 Hydrodynamics and heat transfer on smooth surfaces

In **Paper II**, hydrodynamics on smooth surfaces were studied both experimentally and numerically. From the experiments it was observed that the liquid-gas interface is flat at the inlet, and, further downstream the present instabilities grows into waves. The waves emerged at different vertical positions, and despite the very different operating conditions, it seemed as the waves stabilized around a frequency of 10 Hz for all investigated conditions. Of course, due to the occasional transition from a 2D to a 3D flow pattern, the wave frequency was not constant, but the identified frequency was the most dominant one in the system. Generally, it could be said that this frequency was obtained after 2 meters.

The dominant frequency found in the experiments was termed the *natural wave frequency* as the results indicated that it was a system frequency. Numerical simulations with various inlet frequencies were also performed. Initially, the waves developed with the inlet frequency, but after a certain downstream distance, which was unique for each case investigated, the waves underwent a transition to the *natural wave frequency*.

In the literature, one often finds the term *fully developed* for flows with formed waves. It may be erroneous to conclude that the waves are indeed *fully developed* just because they cease to develop at a certain location. It can very likely be, as seen in **Paper II**, that the waves will undergo another development of their major features further downstream. Therefore, when a flow reaches the *natural wave frequency*, the flow is instead considered *statistically steady*. This means that, after this distance, the flow characteristics, such as the film thickness and the heat transfer coefficient, do not develop any further but instead are constant, in the time averaged perspective, for the remaining section of the unit, see Figure 6-1.

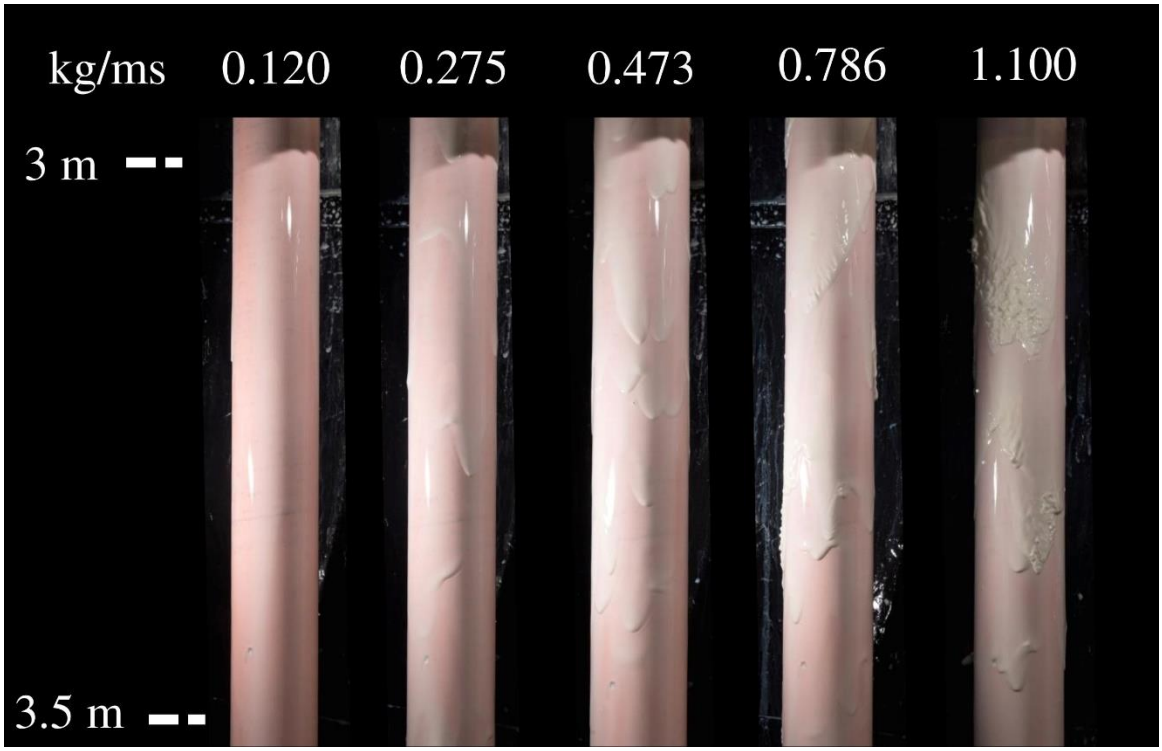


*Figure 6-1. Still images of the Intermediate Viscosity fluid (IV) for different wetting rates at statistically steady conditions, 3 meter from the inlet.*

One could argue that such a position does not exist at all, but that instead an additional transition could happen even further downstream than what was investigated in **Papers II** and **III**. However, if no *statistically steady* value can be extracted, then a question arises on what at all can be said about the conditions in a large-scale unit. We argue here that it is better to have something that is at least approximately correct than not to have anything at all. In addition, the downstream lengths investigated in the papers are seldom seen in the literature, and, also, the distance investigated in our study (4 meters) is very much related to the height of an industrial falling film units, which can be 12-20 meters.

Performing the simulations with the *natural wave frequency* as the inlet frequency resulted in an emergence of a flow pattern early in the computational domain that had a good agreement with the wave shapes measured during the experiments. The simulation domain could therefore be significantly shorter than compared to the flow length in the experiments, as the flow structures quickly reached the natural system frequency. If the

system frequency was unknown, it was also recommended to perform simulations with multiple inlet frequencies in order for the natural system frequency to emerge as quickly as possible in the domain. If the natural system frequency has not been reached, potentially erroneous conclusions can be made about hydrodynamics of a large-scale falling film unit.

With the gained knowledge on how the numerical simulations should be set up to yield flow patterns representative for a large-scale falling film unit, investigations of the heat transfer could be made. In **Paper III**, the heat transfer on smooth surfaces was studied under heating conditions. From the experiments it was found, just as for the hydrodynamics, that there exists an entrance length before the heat transfer coefficient becomes statistically steady. In our unit, that length was found to be approximately one meter. The statically steady heat transfer was found to have a rather good agreement with the existing correlations, such as equation (2.10) developed by Schnabel and Schlünder (1980). However, a transition between different regimes was found to be problematic and not always exact. Also, as the wetting rate is lowered, it becomes more difficult to maintain a stable liquid film, since the latter becomes thinner. Therefore, two scenarios are possible: either one maintains a stable liquid film and has high heat transfer due to the fact that the film is thin, or to face wetting problems and have low heat transfer. If a stable film is maintained, the analytical Nusselt solution is still valid. Also, from **Paper III**, it was concluded that the simulations give the same magnitude of the heat transfer coefficient as the experiments. Three cases were further investigated, each one for a different fluid, but with approximately the same wetting rate. Significant differences were seen between the three investigated fluids, in terms of the magnitude of the heat transfer coefficient and the film thickness, see Figure 6-2.

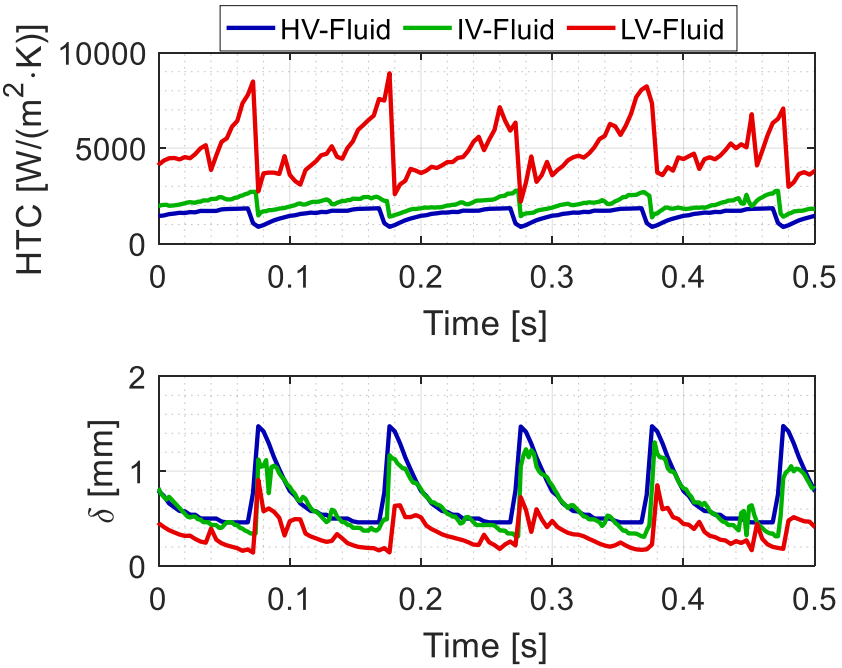


*Figure 6-2. Time variation of the heat transfer coefficient (Top) and the film thickness (Bottom) for the High, Intermediate and Low Viscosity fluids investigated in **Paper III**, all for approximately the same wetting rate, in the range of 0.44-0.48 kg/(m·s).*

**Papers II** and **III** illustrated that the numerical framework developed within this work can accurately represent both the hydrodynamics and the heat transfer in falling films under industrially relevant conditions. Therefore, this framework can be used to 1) better understand what happens within the liquid film, 2) identify the important transport mechanisms and 3) comprehend why there exists such a difference between the three fluids.

To better understand what happens within the liquid film, Figure 6-3 shows the temperature profile in a statistically steady wave for the High Viscosity fluid (HV) at a time instance. Close to the wall, we observe a clear thermal boundary layer and, when moving further out in the film, the temperature drops rapidly. Nearly all temperature profiles are strongly decreasing, however at 0.63 m from the inlet and at the thickness of 0.9 mm, there is a slight temperature increase. This increase is due to bulk mixing, but it is very small and it can be concluded that nearly all the heat transfer is governed by conduction and the thickness of the film. However, it means that the wave slightly enhances the convective transport part, while significantly lowering the conductive part due to the increased film thickness.

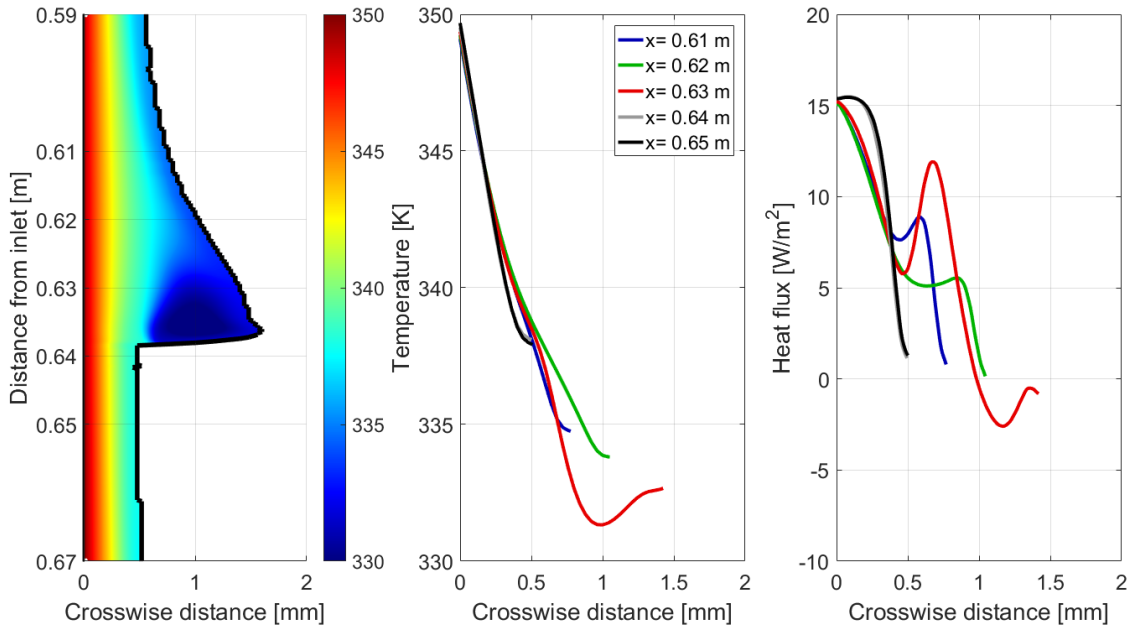


*Figure 6-3. Left) Temperature contour plot of a statistically steady wave for the **High Viscosity fluid (HV)** at a time instance. Middle) Temperature profiles at five vertical positions within the liquid film. Right) Crosswise heat flux variation within the liquid film, calculated from equation (5.13) for the five temperature profiles. Wetting rate 0.48 kg/(m·s), Re 73, Ka 167 and Pr 46.*

For the Intermediate Viscosity fluid (IV), Figure 6-4, it can be observed that the thermal boundary layer close to the wall is slightly thinner than for the HV fluid, and also that some mixing of the layer exists within the wave. This is also shown in the temperature profiles as they initially decrease with the same rate as those with the HV fluid, but already at a thickness of 0.25 mm within the wave their derivative changes. Therefore, the convective contribution to the heat transfer is expected to be slightly higher compared to the case when the HV fluid is used.

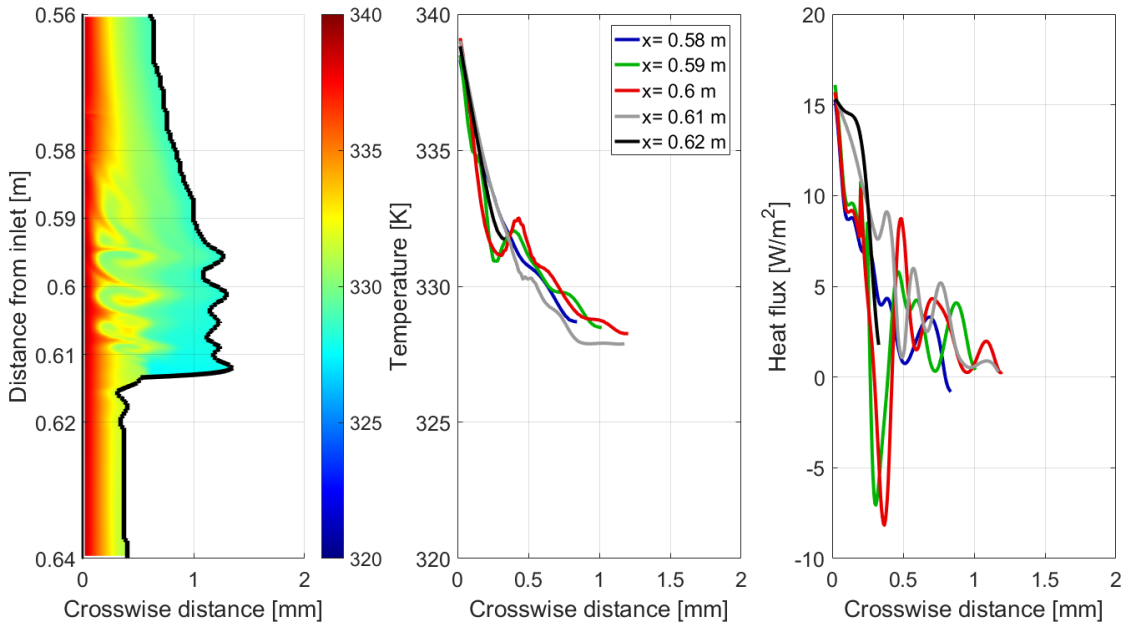


*Figure 6-4. Left) Temperature contour plot of a statistically steady wave for the **Intermediate Viscosity fluid (IV)** at a time instance. Middle) Temperature profiles at five vertical positions within the liquid film. Right) Crosswise heat flux variation within the liquid film, calculated from equation (5.13) for the five temperature profiles. Wetting rate 0.47 kg/(m·s), Re 181, Ka 574 and Pr 18.*

For the Low Viscosity fluid (LV), Figure 6-5, the bulk mixing is significantly stronger, resulting in a much thinner thermal boundary layer. The latter observation is also supported with the temperature profiles as the layer is only very close to the wall, with the temperature profiles rapidly decreasing. Note that the scales differ in Figure 6-3 and Figure 6-4. The convective contribution to the heat transfer is therefore expected to be largest for the LV fluid.

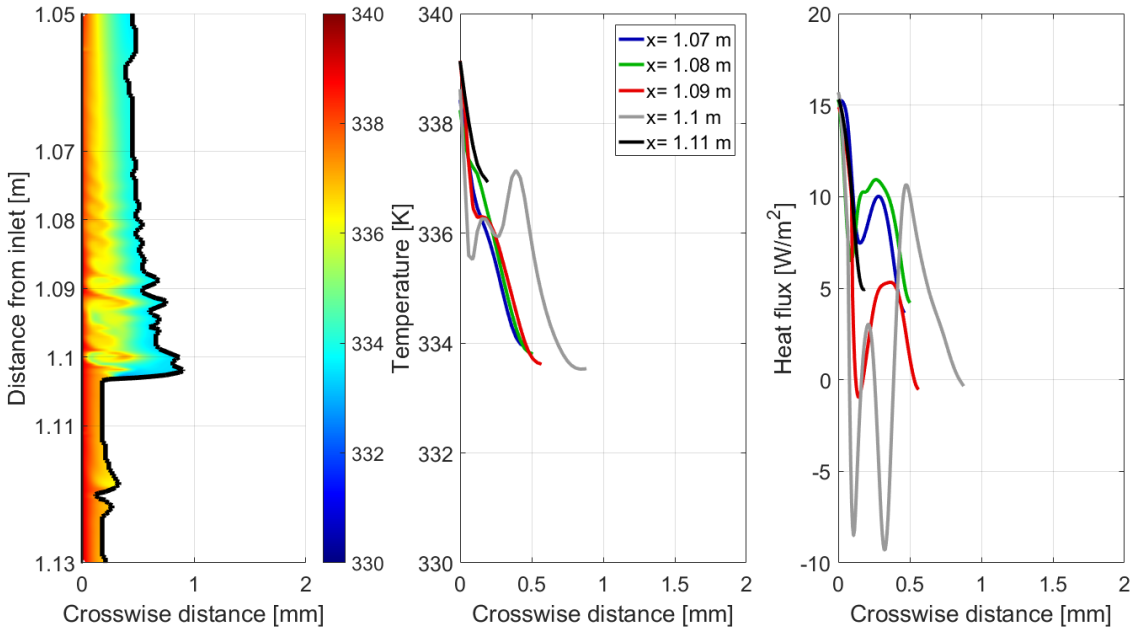


*Figure 6-5. Left) Temperature contour plot of a statistically steady wave for the **Low Viscosity fluid (LV)** at a time instance. Middle) Temperature profiles at five vertical positions within the liquid film. Right) Crosswise heat flux variation within the liquid film, calculated from equation (5.13) for the five temperature profiles. Wetting rate 0.44 kg/(m·s), Re 795, Ka 7010 and Pr 3.5.*

Let us now examine the Nusselt number to better understand the ratio between the convective and conductive heat transfer within the film. For a falling film, the characteristic length (L) for the Nusselt number is often defined as the viscus length scale ($l$), see expression (2.6), to make it independent of the wetting rate (Schnabel, 2010). The time variation for such a definition of the Nusselt number can be seen in Figure 6-6 for the three different fluids. This definition suggests that the conductive transport is slightly more dominant than the convective part and that the latter is significantly lower within a wave. However, that is not in agreement with the temperature profiles seen previously in this chapter. From these profiles it can be clearly concluded that the waves lead to some bulk mixing and that the conductive heat transfer resistance is larger in the wave, since the film is thicker. This definition is thus not a suitable one when looking at the time variation of the heat transfer within the liquid film.

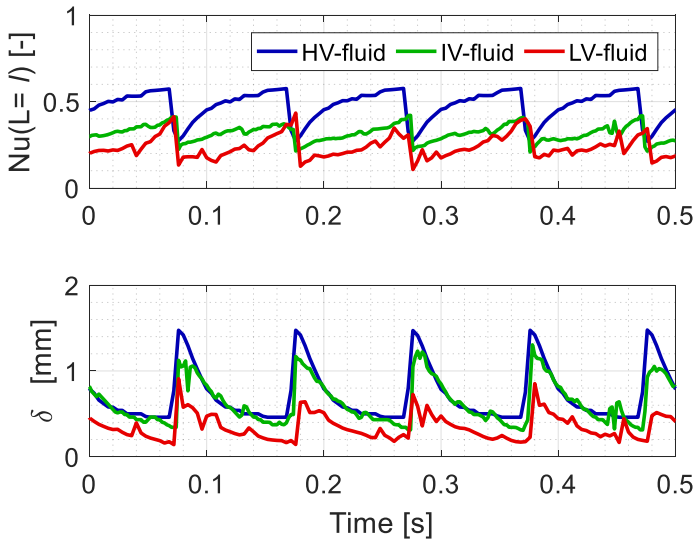


*Figure 6-6. Top) Time variation of the Nusselt number for the High, Intermediate and Low Viscosity fluids. The characteristic length scale is here the viscus length scale (l), see expression (2.6). Bottom) Actual time variation of the film thickness. The wetting rate is approximately the same for all fluids, in the range of 0.44-0.48 kg/(m·s).*

If instead the actual film thickness is used as the characteristic length scale, $L = \delta$ [m], the picture becomes different, see Figure 6-7. Now the convective part is larger than the conductive part and the former also increases within the wave, as it should be according to the temperature profiles. Also, all fluid characteristics seem to be captured, as the same values are shown for all three fluids. The drawback with this approach is that it is difficult to obtain all these values without performing numerical simulations. It should also be pointed out that, regardless of the used definition, the convective and conductive parts are rather equal in size, even if they alternate their respective dominance.

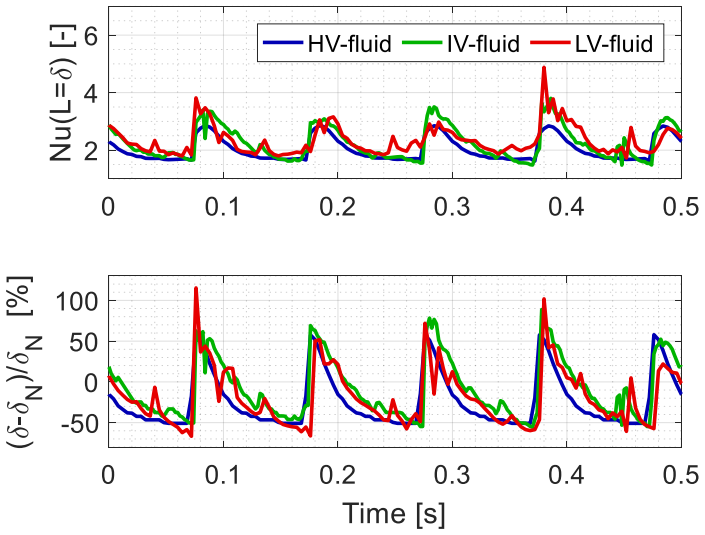


*Figure 6-7. Top) Time variation of the Nusselt number for the High, Intermediate and Low Viscosity fluids. The characteristic length scale is the actual film thickness, $L = \delta$ [m]. Bottom) Actual time variation of the film thickness, scaled with the analytical Laminar solution obtained from (5.8). The wetting rate is approximately the same for all fluids, in the range of 0.44-0.48 kg/(m·s).*

Even if the Nusselt number is the same for all three fluids, there are significant differences in the value of the heat transfer coefficients. The total rate of the heat transfer is highest for the LV fluid. This is partly explained by the fact that the film thicknesses for all three fluids are significantly different (see Figure 6-2), even though the wetting rate is the same. The lower film thickness implies a shorter conduction distance, hence the higher heat transfer as the thermal conductivity is roughly the same for all three fluids. However, since the Nusselt number is the same, that means that the convective term increases to the same extent. This is visualized in Figure 6-8 where the crosswise velocity (y-velocity) within the film is plotted. That velocity is directly related to the convective part as that is the direction where the heat transfer we are interested in takes place. This further highlights the conclusions in **Paper III**, that the film thickness and bulk mixing are fundamentally important for the heat transfer.

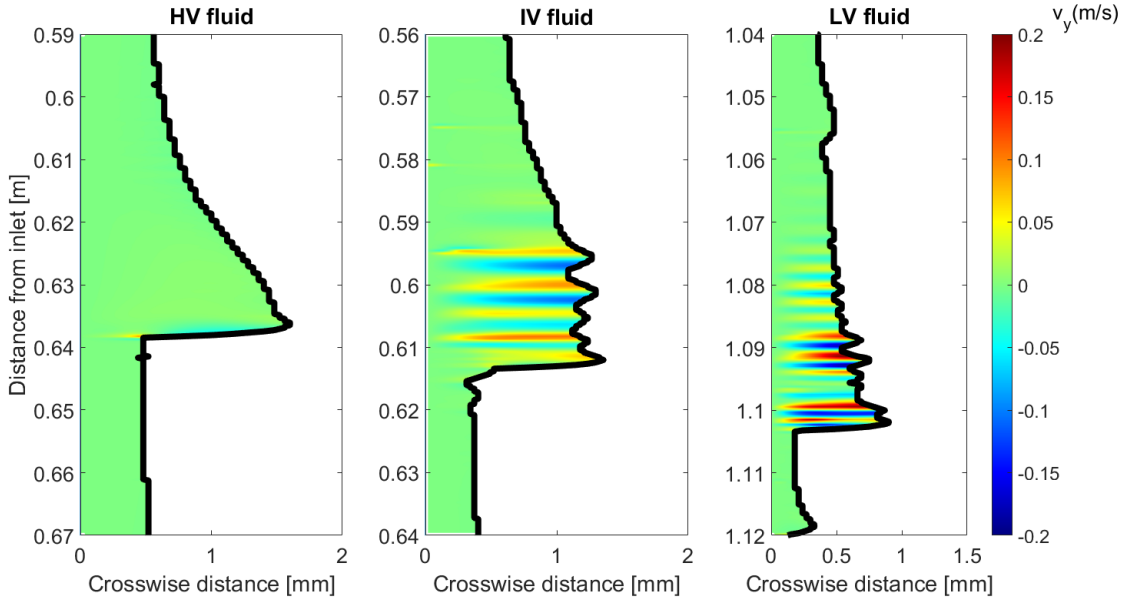


*Figure 6-8. Crosswise velocity within the liquid film for the High, Intermediate and Low Viscosity fluids at approximately the same wetting rate, in the range of 0.44-0.48 kg/(m·s).*

## 6.2 Development of the characteristic dimensions for the surface modifications

The results presented in this Chapter are just a fraction of the experiments performed with modified surfaces, but they highlight the main steps within the development process that led to the choice of surface modifications for the investigations presented in Chapters 6.3 and 6.4.

In **Paper IV** it was shown that the heat transfer is strongly connected to the hydrodynamics and that it can be seen from the flow pattern if the rate of heat transfer is improved with the use of modified surfaces. These findings were discovered quite early in the project and were therefore used to investigate the influence of characteristic surface dimensions of the modified surfaces. Six regimes have been identified: Poor wetting, Wavy, Smooth, Ripples, Pseudo chaotic and Chaotic, see Figure 6-9. Pseudo chaotic and Chaotic flow patterns are expected to significantly increase the rate of heat transfer, whereas Poor wetting or Smooth flow patterns do not have a significant impact. Wavy or Ripple regime might have an impact, but heat transfer measurements are needed to make claims with some degree of certainty.

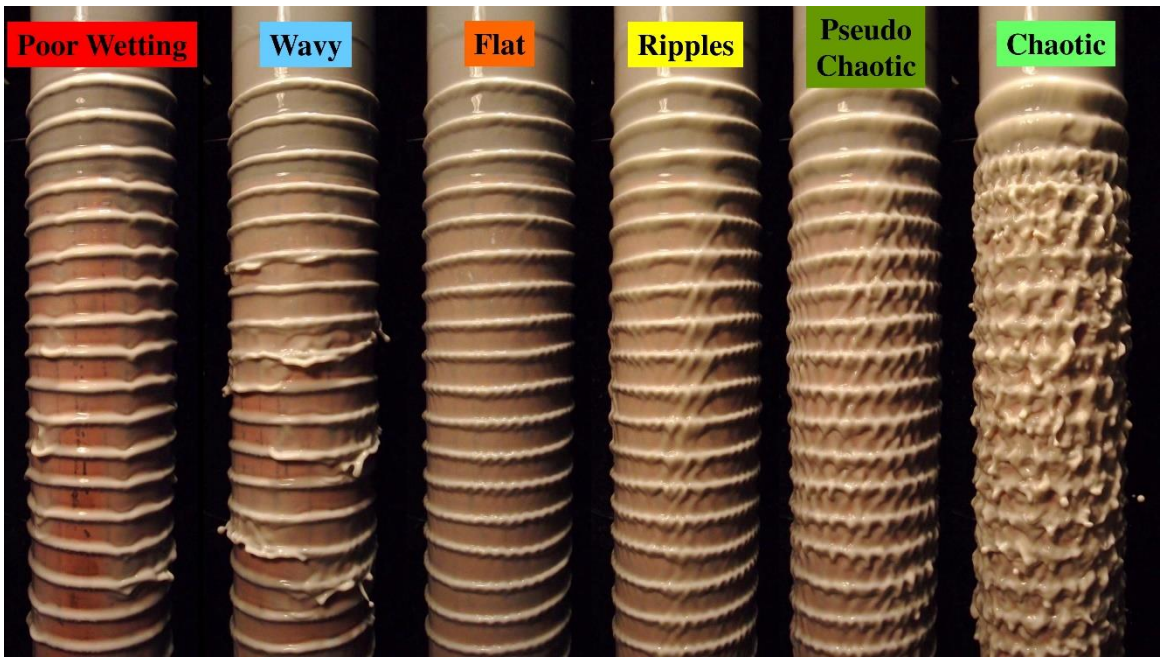


*Figure 6-9. Regimes identified in this work for different surface characteristics at various wetting rates.*

In order to investigate the influence of different surface characteristics, such as Height, Length, Pitch and Sharpness (defined in Figure 3-1), wires were applied to the tube, as described in Chapter 4.1.3, and their impact on the flow patterns was visually inspected for various fluids and wetting rates. The experiments were carried out in two phases. In the first phase, the influence of the characteristics were investigated by using round wires of various sizes, numbers and with different pitch distances applied on to the tube. The number of wires were altered in order to test the effect of different surface modifications lengths. If multiple wires were to be applied, they were applied side by side, almost if as they were

a single wire. The purpose of the first test phase was to get a broad understanding about the general dimensioning of the surface modifications. Therefore, only a single fluid was investigated, with the fluid properties chosen to be in between the High and Intermediate Viscosity fluids. The results from the first test phase are presented in Table 6-1. The results are coloured according to the regime colour code used in Figure 6-9. Operating conditions with large amount of sputtering have also been marked as red and should be considered undesired events.

*Table 6-1. Results from regime investigation with different round wires for a fluid with fluid properties between High and Intermediate Viscosity fluids. d is the wire diameter, pitch is the centre-to-centre distance between the wires and № Wires is the number of wires applied to the tube. The identified regimes are coloured according to Figure 6-9. P = Poor Wetting, W = Wavy, F = Flat, R = Ripples, PC = Pseudo Chaotic, C = Chaotic and S = large amount of Sputtering.*

| **d** | **Pitch** | **№** | **Wetting Rate [ kg/(m·s )]** | | | | | | | |
|---|---|---|---|---|---|---|---|---|---|---|
| **[mm]** | **[mm]** | **Wires** | **0.1** | **0.2** | **0.3** | **0.4** | **0.5** | **0.6** | **0.7** | **0.9** |
| 2 | 10 | 1 | P | W | PC | PC | C | C | S | S |
| 1.6 | 7.5 | 1 | | W | R | C | C | C | C | S |
| 1.6 | 10 | 1 | | W | R | R | C | C | S | S |
| 1.6 | 12.5 | 1 | P | W | R | PC | C | C | S | S |
| 1.25 | 10 | 1 | P | W | R | PC | C | C | C | S |
| 1.25 | 12.5 | 1 | | W | F | R | PC | C | C | S |
| 1 | 7.5 | 1 | | W | PC | PC | C | C | C | C |
| 1 | 10 | 1 | | W | R | PC | C | C | C | C |
| 1 | 10 | 2 | F | W | F | R | R | C | C | C |
| 1 | 10 | 3 | F | W | F | F | R | C | C | C |
| 0.71 | 10 | 1 | | W | F | F | R | PC | C | C |

The conclusion from Table 6-1 is that the surface modifications should probably not be too high in order to avoid large amount of sputtering and the occurrence of flying droplets. Sputtering is generally believed to lead to higher pressure drop, which is undesirable. The modification should also be higher than 0.71 mm in order to have the effect in the preferred operating range. Higher modifications seem to more beneficial at smaller wetting rates. Longer surface modifications are not desirable, indicating that the length should not be longer than necessary. A 10 mm pitch is preferred over a 12.5 mm one.

In the second phase, four differently crafted wires, see Figure 6-10, were investigated for the High and Intermediate Viscosity fluids. The purpose here was to get a more detailed understanding of the influences of different surfaces on the flow pattern and of the importance of the sharpness. The results from those experiments are seen in Table 6-2.

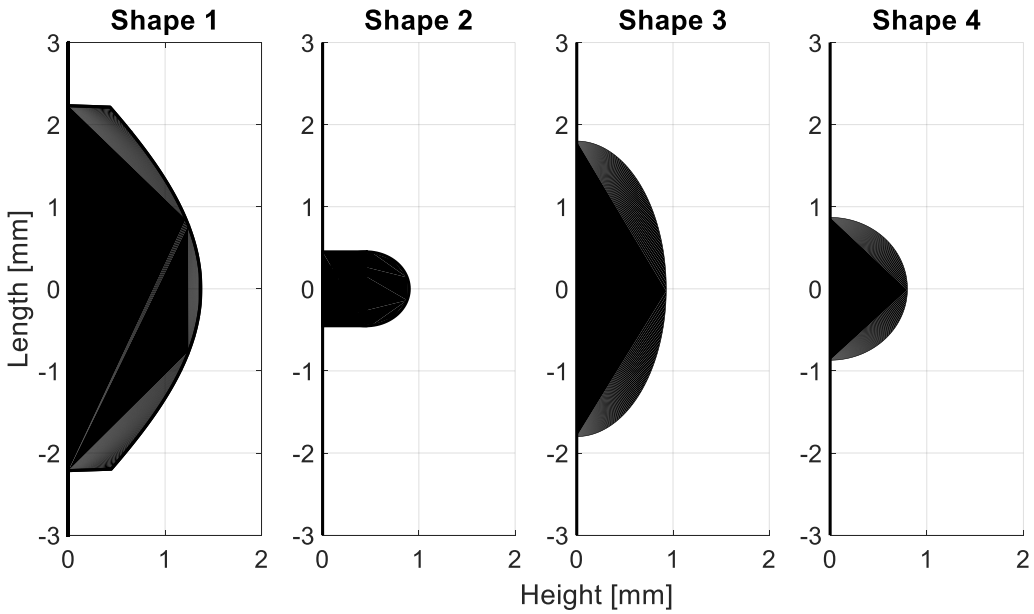


*Figure 6-10. The four crafted wires investigated in this work.*

The conclusions from the results from the second phase test, seen in Table 6-2, are that 10 mm appears to be the most promising pitch and Shapes 1 and 2 perform best for both investigated fluids. They are also significantly different in shape and are therefore of interest to study further in order to understand the heat-transfer enhancing mechanism (see Chapter 6.3). Shape 1T in Table 6-2 is Shape 1, but with a tape put on top in order to smooth out the edges towards the incoming and exiting flow over the structures. Surprisingly, that type of surface still had a significant impact on the flow pattern.

*Table 6-2. Results from regime investigation with the crafted wires seen in Figure 6-10 for the High and Intermediate Viscosity fluid. Shape 1T is Shape 1 but with tape put on top in order to smooth out the edges of the surface modification seen in Figure 6-10. The identified regimes are coloured according to Figure 6-9. W = Wavy, F = Flat, R = Ripples, PC = Pseudo Chaotic and C = Chaotic.*

| **Shape** | **Pitch** | **Wetting Rate [ kg/(m·s )]** | | | | | | | | |
|---|---|---|---|---|---|---|---|---|---|---|
| | **[mm]** | **0.1** | **0.2** | **0.3** | **0.4** | **0.5** | **0.6** | **0.7** | **0.9** | **1.1** |
| **HV fluid** | | | | | | | | | | |
| 1 | 10 | W | R | R | PC | C | C | C | C | C |
| 1 | 15 | W | W | W | W | PC | C | C | C | C |
| 2 | 10 | W | PC | PC | C | C | C | C | C | C |
| 3 | 10 | W | R | R | PC | C | C | C | C | C |
| 4 | 10 | W | F | F | R | PC | C | C | C | C |
| **IV fluid** | | | | | | | | | | |
| 1 | 10 | F | W | W | PC | PC | C | C | C | C |
| 1T | 10 | F | W | W | W | W | W | PC | C | C |
| 1 | 15 | F | W | W | W | W | W | PC | C | C |
| 2 | 10 | F | W | W | C | PC | PC | C | C | F |
| 3 | 10 | F | W | W | W | PC | C | C | C | C |
| 4 | 10 | W | W | W | W | F | F | F | PC | PC |

Unfortunately, the taped surface could not be studied under heating conditions in the atmospheric setup. However, it had a valuable input for the manufacturing of heat transfer surfaces for the pilot evaporator. Since the relatively smooth surfaces had a comparatively large impact on the flow pattern, it was opted to manufacture six different corrugated surfaces. The topology of the corrugated surfaces can be described as six sinusoidal curves, seen in Figure 6-11. An additional surface, with a sharper modification, was also produced by welding wires onto an already existing smooth tube, with the topology also seen in Figure 6-11.

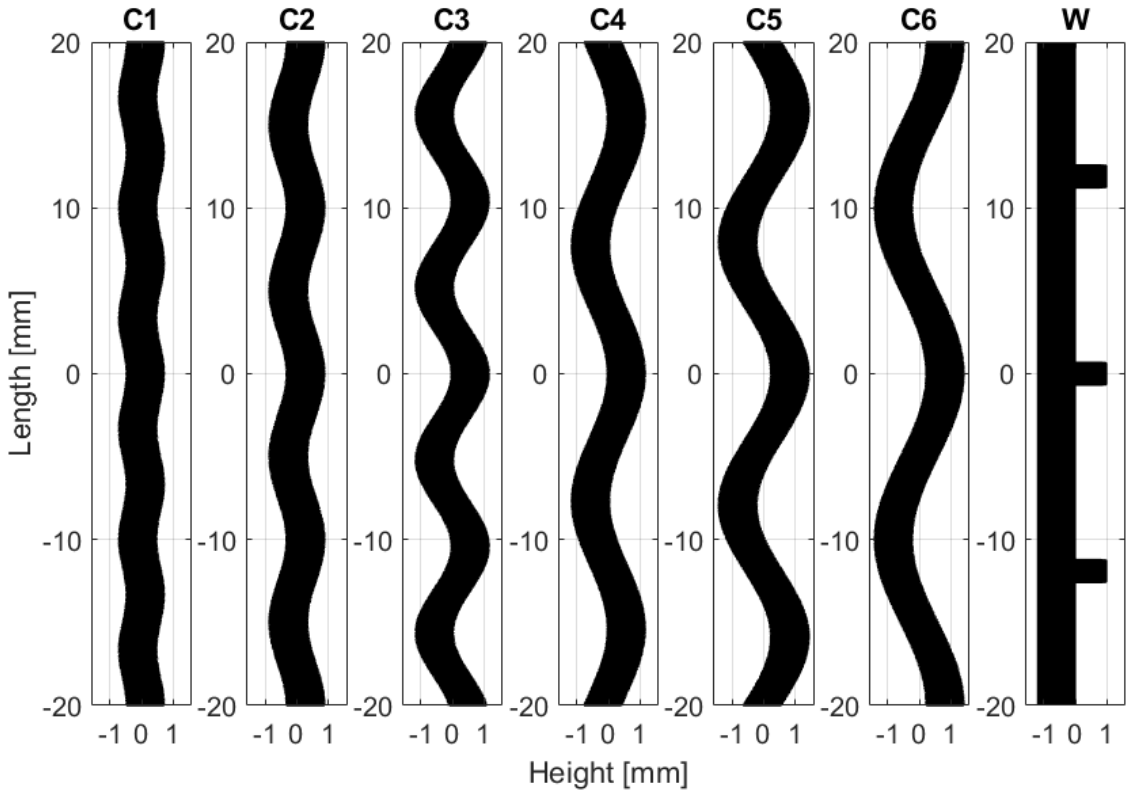


*Figure 6-11. Cross section of the manufactured surfaces investigated in this work. The letter C stands for corrugated and W for welded surfaces, respectively.*

Since the surfaces were intended for installation in the pilot evaporator, the wires were welded onto the inside of the tube, maintaining a smooth outside. On the other hand, the corrugated tubes, due to the manufacturing method, ended up with the same topology on both sides. The resulting flow patterns due to the surface topology for all seven manufactured tubes were investigated by cutting off one small part of the bottom half of the tubes and redirecting that flow, creating a “half shape” tube flow to investigate. The resulting flow patterns for all seven surfaces investigated for the High and Intermediate Viscosity fluid can be seen in Table 6-3.

*Table 6-3. Results from regime investigation with the manufactured surfaces seen in Figure 6-11 for the High and Intermediate Viscosity fluid. The identified regimes are coloured according to Figure 6-9. P = Poor Wetting, W = Wavy, F = Flat, R = Ripples, PC = Pseudo Chaotic and C = Chaotic.*

| **Shape** | **Wetting Rate [ kg/(m·s )]** | | | | | | | |
|---|---|---|---|---|---|---|---|---|
| | **0.1** | **0.2** | **0.35** | **0.5** | **0.7** | **0.9** | **1.1** | **1.2** |
| **HV fluid** | | | | | | | | |
| C1 | F | F | W | W | W | W | W | |
| C2 | F | W | W | W | W | W | W | |
| C3 | F | W | R | PC | PC | PC | PC | W |
| C4 | F | W | W | R | PC | PC | | |
| C5 | F | W | W | R | PC | C | C | |
| C6 | F | F | W | W | R | PC | C | |
| W | | F | R | PC | PC | R | R | |
| **IV fluid** | | | | | | | | |
| C1 | | F | W | W | W | W | W | |
| C2 | F | F | R | C | C | C | C | |
| C3 | | R | PC | C | C | C | C | C |
| C4 | F | F | R | PC | C | C | C | |
| C5 | F | F | R | C | C | C | C | |
| C6 | F | F | W | R | R | PC | C | C |
| W | P | R | C | C | C | C | PC | |

The results in Table 6-3 tell us that nearly all surface shapes have an impact on the flow pattern. The impact is, as expected, generally larger for the Intermediate Viscosity fluid. S1 causes a wavy pattern on the tube surface, which very much resembles the flow structure seen on a smooth tube. As consequence, that structure is probably too small to impact the flow and the rate of heat transfer. Of all the corrugated tubes, C3 is the one that has the most promising effect on the flow pattern. The tube with the welded wires (W) has, of course, an even bigger effect, but that is expected due to a significantly shaper surface modification. It should also be mentioned that C3 and W have a similar topology as Shapes 1 and 2 previously discussed. Therefore, Shapes C3 and W are the most promising ones to be installed in the pilot evaporator, see Chapter 6.4.

## 6.3 Hydrodynamics and heat transfer on modified surfaces

Based on the discussion from the previous chapter on how different surface characteristics influence the flow pattern on the tube, Shapes 1 and 2 were selected for further investigation in **Paper IV**. The two selected heat transfer surfaces differ in terms of height, length and sharpness in the flow direction and they are thus expected to impact the rate of heat transfer differently. The shape and dimensions of the surface modifications can be seen in Figure 6-10. The pitch, i.e. the centre-to-centre distance between the modifications, has been chosen to 0.01 m, based on the pretesting presented in the previous chapter.

The two surfaces were experientially investigated under heating conditions for the HV and IV fluids for a large span of wetting rates. The experiments identify both the cases where the introduction of modified surfaces significantly enhances the heat transfer and conditions where such a measure does not have a significant impact. An improvement ratio factor was introduced,

$$\iota = \frac{h_{\text{modified}}}{h_{\text{smooth}}}, \tag{6.1}$$

in order to highlight the impact the surfaces have on the rate of heat transfer. For the IV fluid, at a wetting rate of 0.47 kg/(m·s) the heat transfer was enhanced by a factor 2 on Shape 1 and 2.5 on Shape 2. The flow pattern on the tube was significantly altered by the applied wires and one could observe here a seemingly chaotic pattern. However, according to the recorded high-speed videos, most of the flow still moved in the streamwise direction, just as seen and discussed for the smooth surfaces in **Paper III**. Numerical simulations were carried out for the selected cases, and the temperature profile for each modified surface, presented in the same way as for the smooth surface in Chapter 6.1, can be seen in Figure 6-12 and Figure 6-13.

Figure 6-12 shows the temperature profile under statistically steady conditions for the Intermediate Viscosity fluid (IV) at a time instance for the wetting rate of 0.47 kg/(m·s) using Shape 1. The thermal boundary layer is very thin here in comparison to that on a smooth surface and there is significant bulk mixing occurring within the film that results in an improvement factor of at least 2.

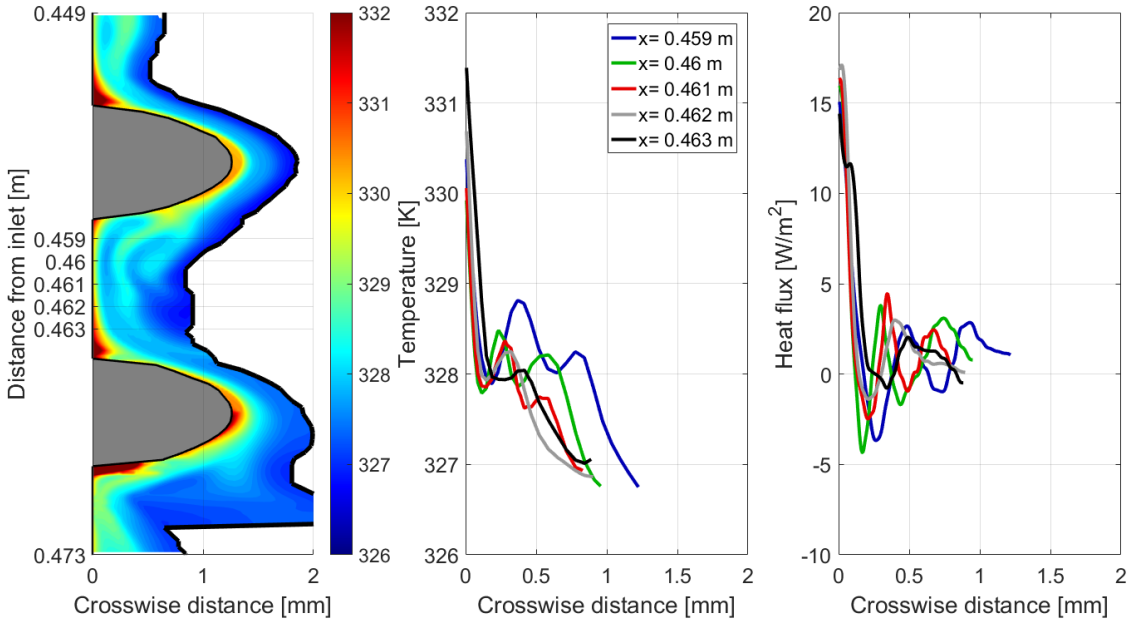


*Figure 6-12. Left) Temperature contour plot at a time instance under statistically steady conditions for the Intermediate Viscosity fluid using Shape 1. Middle) Temperature profiles at five vertical positions within the liquid film. Right) Crosswise heat flux variation within the liquid film, calculated from equation (5.13) for the five temperature profiles. Wetting rate 0.47 kg/(m·s), Re 181, Ka 574 and Pr 18.*

On Shape 2 for the same fluid, see Figure 6-13, there is even more bulk mixing taking place and the thermal boundary layer is even smaller. The stronger bulk mixing is of course the reason why the improvement factor is higher with a value of 2.5.

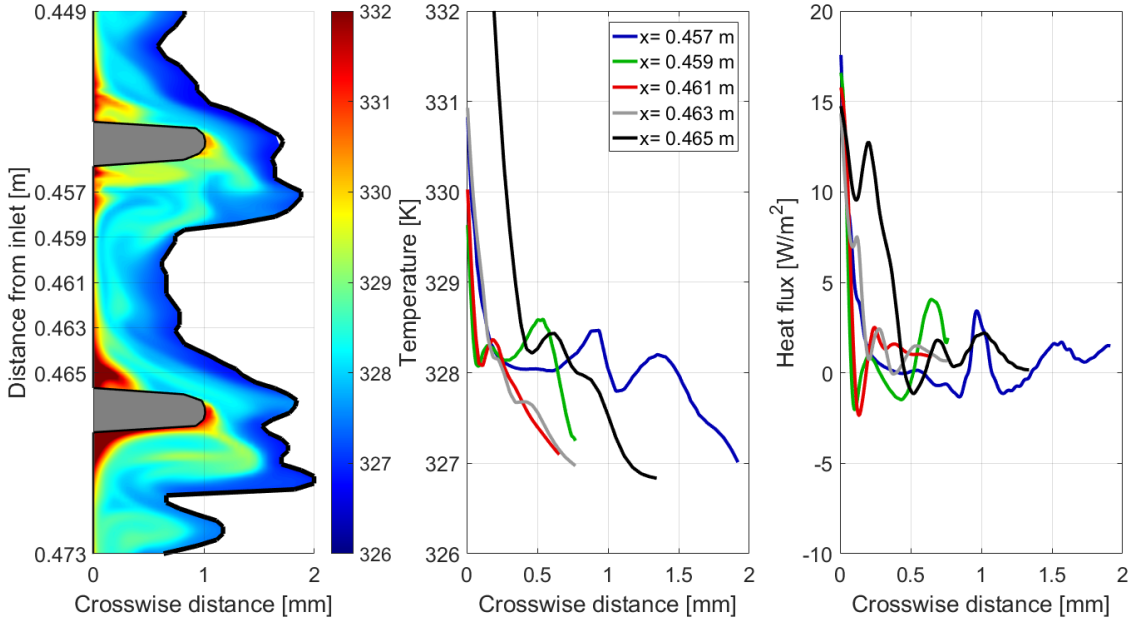


*Figure 6-13. Left) Temperature contour plot at a time instance under statistically steady conditions for the Intermediate Viscosity fluid on Shape 2. Middle) Temperature profiles at five vertical positions within the liquid film. Right) Crosswise heat flux variation within the liquid film, calculated from equation (5.13) for the five temperature profiles. Wetting rate 0.47 kg/(m·s), Re 181, Ka 574 and Pr 18.*

The heat transfer improvements seen on the different surfaces are obviously linked to surface modifications. If the surface modifications are removed, the rate of heat transfer will decline rapidly. That decline is clearly seen in Figure 6-14, which shows the improvement factor slightly before and after the last surface modification in the computational domain. After the latter modification located at 0.5 meter from the inlet, the improvement factor is rapidly decreasing and already at 0.55 meters from the inlet the factor is close to 1, which corresponds to the rate of heat transfer seen on a smooth surface. The results show how important the pitch distance is for the heat transfer improvement. In addition, it also indicates that the chosen pitch distance is fairly optimal, as the improvement factor has dropped below 1.5 already after two pitch distances from the last surface modification.

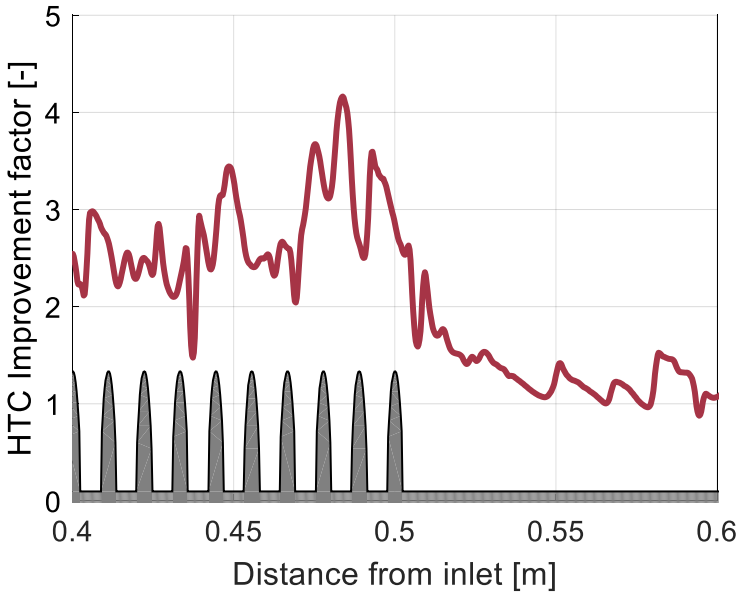


*Figure 6-14. Snapshot of the rate of decline of the heat transfer improvement occurring after the last surface modification for the IV fluid on Shape 1. Wetting rate 0.47 kg/(m·s), Re 181, Ka 574 and Pr 18.*

Since there is significantly more bulk mixing occurring on the modified surface, the convective part of the heat transfer should be significantly larger than that on a smooth surface. Figure 6-15 shows the Nusselt number with $L = \delta \ [m]$ as the characteristic length, discussed in Chapter 6.1, for all three fluids using Shape 1. The figure shows that the Nusselt number is significantly higher for the modified surface compared to the results seen for the same fluid on a smooth surface in Figure 6-7. Also note that the Nusselt number is not the same for all three fluids, as it was on the smooth surface. This indicates that the convective heat transfer is different for the different fluids on the modified surfaces, which was shown in **Paper IV**. Nevertheless, the large Nusselt number indicates that convection is the most important mechanism that contributes to the high heat transfer rate on the modified surfaces.

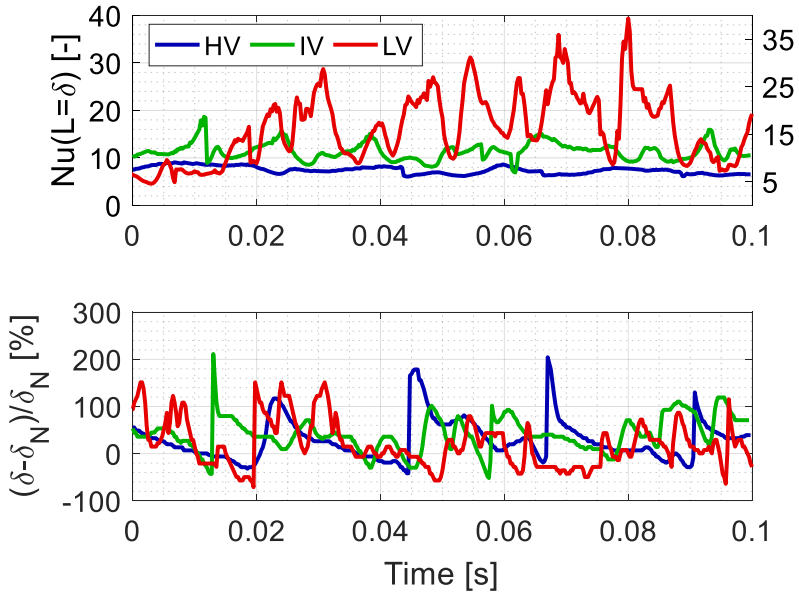


*Figure 6-15. The Nusselt number (Top) for the High, Intermediate and Low Viscosity fluids on Shape 1. The Nusselt number is significantly higher here than compared to the smooth counterpart seen in Figure 6-7. The improvement is due to the increased convective transport, since the film is slightly thicker than that on a smooth surface, where it fluctuates around the Nusselt solution (Bottom).*

In **Paper IV**, it was shown that the increased heat transfer was caused by time-dependent recirculation zones occurring behind the surface modifications. We have also shown that these zones were caused by the build-up of the pressure gradient within the film, occurring 0.75 ms prior to the flow reversal. This process is greatly similar to the way that waves on a smooth surface cause backflow in the wave front. In this way, the bulk mixing is enhanced, and at a larger extent for the modified surfaces. The pressure gradient within the film for smooth surfaces originates from the curvature of the waves that is, in turn, related to the local wetting rate. Therefore, it is reasonable to assume that the local mass flow has something to do with the improvement of the heat transfer for the modified surfaces.

Figure 6-16 shows a cross correlation between the local mass flow on the top of the surface modification and the negative streamwise velocity 1 mm after the surface modification (and 40 µm from the wall) for the Intermediate Viscosity fluid using Shape 1. The two properties are 0.8 anti-correlated with a time lag of 5.25 ms. This means that, when a large amount of liquid flows over the surface modification it results in the occurrence of recirculation zones. This is not only similar to how backflow within a wave behaves, but it also resembles the classical phenomenon of the flow around a sphere or cylinder, where the size of the wake behind the object is related to the Reynolds number.

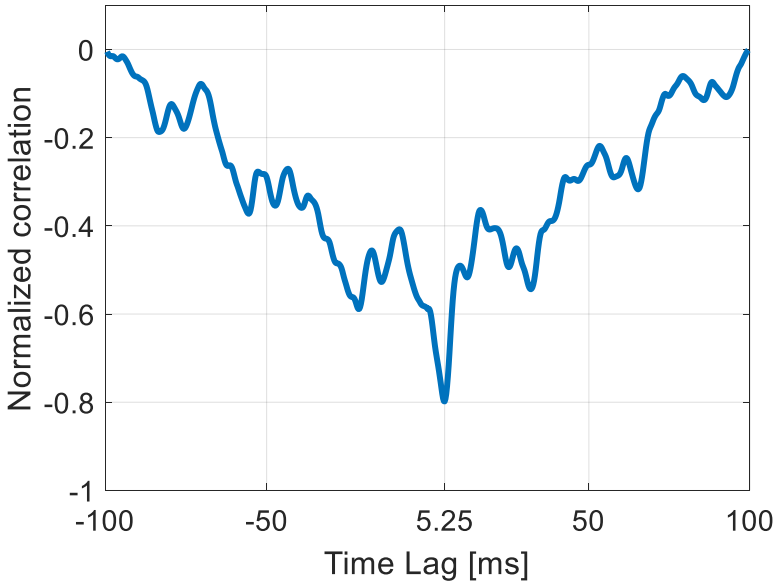


*Figure 6-16. Cross correlation between the local mass flow on top of the surface modification and the negative streamwise velocity 1 mm after the surface modification (and 40 µm from the wall) for IV fluid on Shape 1 at a wetting rate of 0.47 kg/(m·s). The two properties are 0.8 anti-correlated with a time lag 5.25 ms, meaning that the high local mass flow leads to a recirculation zone.*

If the time-fluctuating mass flow is the reason behind the improved heat transfer, one may suspect that the heat transfer improvement is related to the inlet perturbation frequency, which introduces a disturbance to the mass flow. The disturbance is needed on smooth surfaces to initialize waves in the computational domain. A frequency of 10 Hz was shown to be representable for the flow pattern on smooth surfaces in **Paper II**. Figure 6-17 shows the wall and bulk temperatures for the simulations performed with different inlet frequencies of 0, 10 or 30 Hz on the modified surface (Shape 1) for the Intermediate Viscosity fluid at a wetting rate of 0.47 kg/(m·s). The wall temperature for a smooth surface is also added as a reference. Interestingly, a frequency of 0 Hz still results in the same wall temperature as seen in **Paper IV**, it just takes a somewhat longer flow distance for the instabilities in the flow to grow, compared to the 10 Hz case, as previously used. If instead a frequency of 30 Hz is used, the heat transfer improvement is detected much earlier in the computational domain, compared to the 0 or 10 Hz cases. This is a reasonable result, since more pronounced fluctuations at the inlet should lead to more bulk mixing. Nevertheless, the results clearly indicate that the observed heat transfer improvement is not related to the inlet perturbation frequency, but instead is initialized solely by the introduction of surface modifications in the domain. After 0.5 meter from the inlet, when the surface modifications in the domain ends, the wall temperature rises just as on a smooth surface at the inlet.

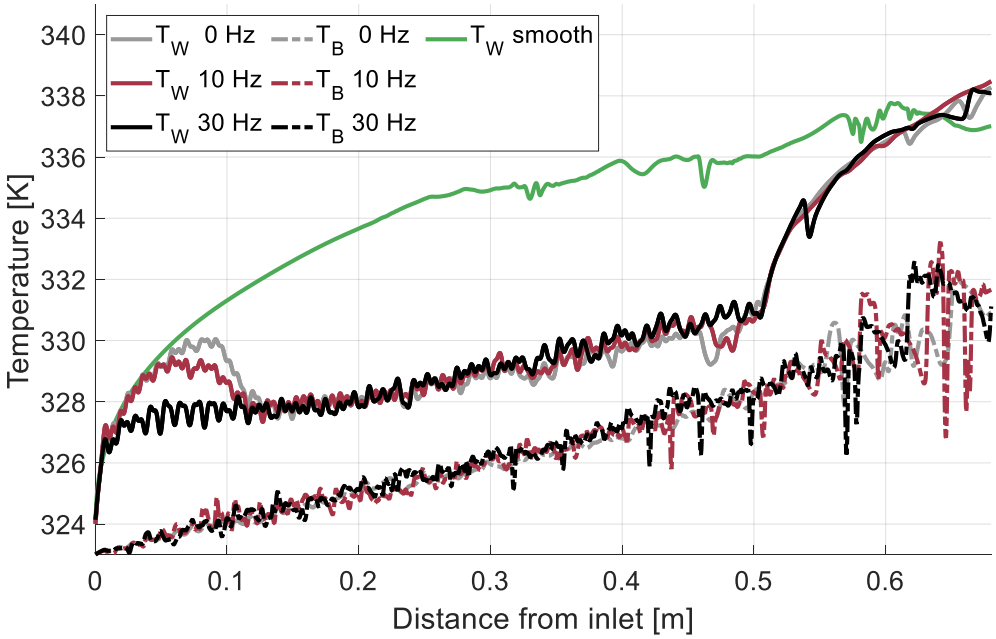


*Figure 6-17. Snapshot of the wall and bulk temperatures extracted from three different simulations performed with a different inlet frequency (f) on Shape 1 for IV fluid on Shape 1 at a wetting rate of 0.47 kg/(m·s). The surface modifications in the domain ends after 0.5 m, hence the rise in the wall temperature. The wall temperature for a smooth surface is also added as a reference.*

In summary, surface modifications enhance the rate of heat transfer by a time-fluctuating mass flow in the way that a high local flow rate causes a pressure gradient, which then leads to creation of a recirculation zone. Such a sequence of events produces bulk mixing and results in higher heat transfer. To some extent, this confirms the initial observation that the heat transfer improvement can be related to the visual appearance of the liquid film discussed in Chapter 6.2. It also agrees with the fact that no significant heat transfer improvement was seen at low wetting rates, neither in the experiments nor in the simulations in **Paper IV**.

## 6.4 Evaporation on smooth and modified surfaces

From the discussion in Chapter 6.2, surfaces C3 and W presented in Figure 6-11 were selected for further investigation in the pilot evaporator. The surfaces are similar to Shapes 1 and 2 discussed in the previous Chapter. The surfaces were tested for two different fluids, *Black liquor* at a dry solids content of 30 % and *Water*. The fluid properties are described in detail in Chapter 4.2.3, and they bear a close resemblance with the IV and LV fluids previously discussed. The overall heat transfer coefficients, calculated from equation (4.5), for the two investigated fluids, at $\Delta T_{out}$ = 10 K and various wetting rates for the investigated surfaces can be seen in Figure 6-18. The correlations developed by Gourdon, Karlsson, et al. (2015) and Schnabel and Schlünder (1980) (Evaporation) for smooth surfaces are also included as a reference and their resulting overall heat transfer coefficients have been calculated from equation (4.6).

Both correlations are here used for both fluids, even though the correlation proposed by Gourdon, Karlsson, et al. (2015), due to the dependence on Prandtl number, is only valid for *Black liquor* and the one by Schnabel and Schlünder (1980) only for *Water*. The correlation by Gourdon, Karlsson, et al. (2015) is considered valid for Prandtl numbers in the range of 3 - 800 and for *Water* that value is 2.5, which is not far off. It is therefore interesting that the two correlations predict so different results for *Water* on a smooth surface, indicating that there are uncertainties present when comparing the measurements with the existing correlations.

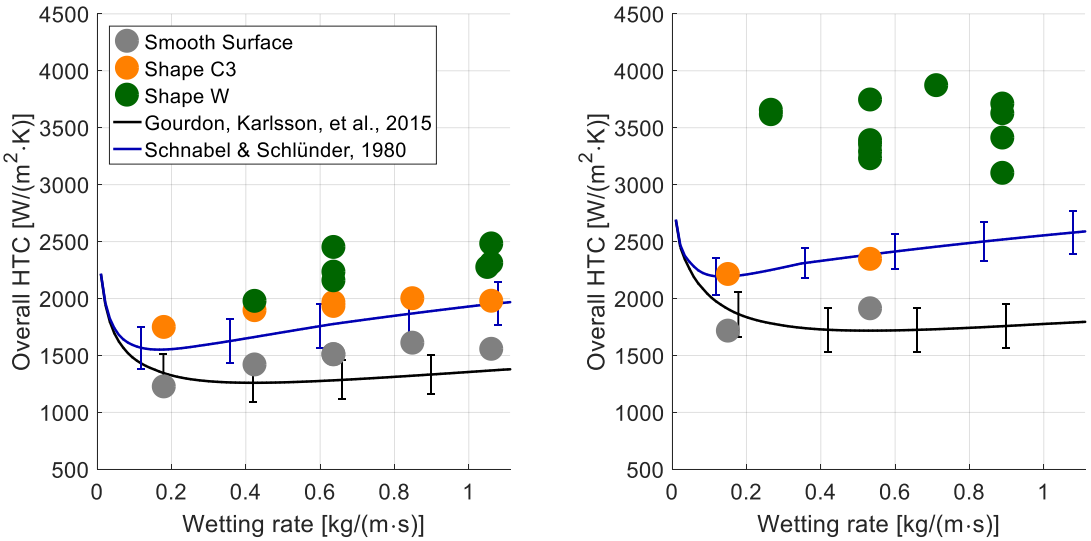


*Figure 6-18. Overall heat transfer coefficient for the three different heat transfer surfaces experimentally investigated in the pilot evaporator for various wetting rates and at $\Delta T_{out}$ = 10 K. Left) Black liquor at 30 % DS, Right) Water.*

Even if there are uncertainties regarding the absolute overall HTC values for the smooth surface, it is clear from the measurements that there is an improvement to the rate of heat transfer by using modified surfaces. From Figure 6-18 it can be seen that the rate of heat

transfer is increased for all wettings rates for both fluids on both modified surfaces. For *Black liquor*, the improvement is around 30 % for Shape C3, and 40 % for Shape W. For *Water*, the corresponding numbers are 25 % and 75 %. Since the rate of heat transfer is higher for all the modified surfaces compared to the smooth one, the heat load on the evaporator will be higher. The higher heat load implies more liquid evaporated, causing a higher vapour flow, resulting in a larger pressure drop and lower temperature driving force, or, potentially leading to shear thinning of the film. In addition, for *Black liquor*, the fluid properties will change at a higher rate if more vapour is evaporated, since the dry solids content of the outgoing fluid will be higher. Therefore, a more straightforward evaluation of the improvement rate is to compare measurements at the same evaporator load, see Figure 6-19.

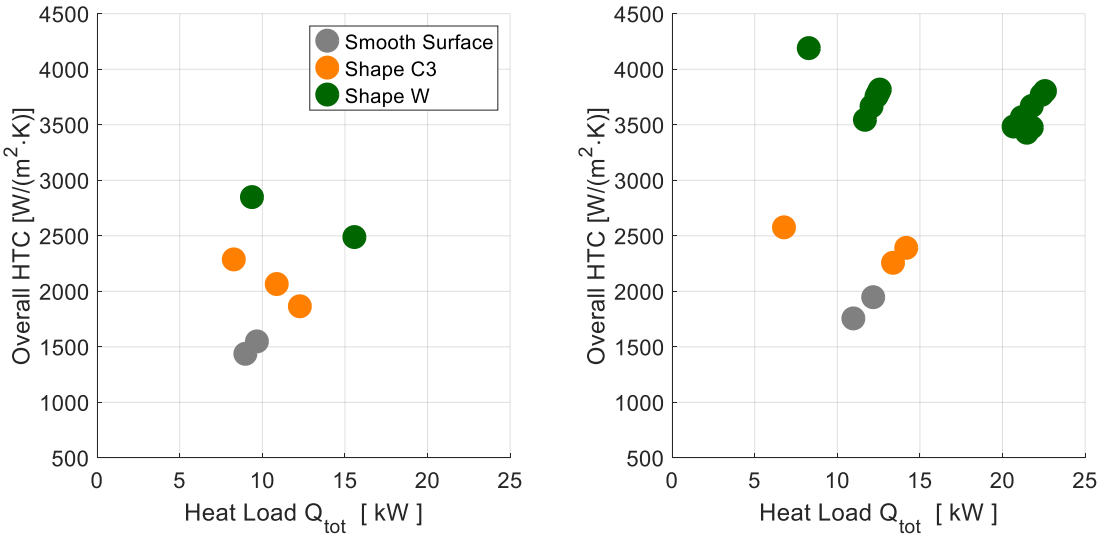


*Figure 6-19. Overall heat transfer coefficient for the three different heat transfer surfaces experimentally investigated in the pilot evaporator for various evaporator loads, controlled by changing $\Delta T_{out}$, more specifically $T_{steam}$. Left) Black liquor at 30 % dry solids. Right) Water. The volume flow is 300 l/h for all measurements, which corresponds to a wetting rate of 0.63 and 0.53 kg/(m·s) for the fluids respectively.*

The evaporator load in Figure 6-19 was controlled by changing the thermal driving force, $\Delta T_{out}$, or more specifically $T_{steam}$. Since the $\Delta T_{out}$ is only varied between 2.5 and 10 K it only has small effects on the fluid properties close to the wall for the product. All measurements are conducted at the same volume flow rate of 300 l/h and here an even larger heat transfer improvement for the modified surfaces can be seen. For *Black liquor*, the improvement is around 50 % for Shape C3, and 100 % for Shape W if one compare at approximately the same heat load. For *Water*, the same numbers are 30 % and 90 %, respectively. The values for the modified surfaces are high and seem to increase for lower heat loads. It should be noted that $Q_{losses}$, which is used to account for the losses in the evaporator, is around 1 kW, and therefore, the lower the heat load, the larger the uncertainties. However, that does not explain the trend seen in the data points and further methods of evaluating the results are needed.

The area increase due to the modification of the surface is relatively minor compared to the total heat transfer improvement. For Shape C3 it is approximately 3 % on both in- and outside and for Shape W approximately 16 % on the inside only. Also, especially in the

latter, it is questionable how much of an improvement it is due to a probable fin efficiency in the surface modifications. If the area increase is neglected, the thermal driving force at the outlet ($\Delta T_{out} = T_{steam} - T_{out}$) can be visualized as straight lines in the heat load graph.

Since the pressure drop causes the thermal driving force to vary along the length of the tube, there is an uncertainty related to the averaged $\Delta T$. Vertical error bars, with the maximum value equal to the overall heat transfer coefficient calculated from the inlet temperature difference ($\Delta T_{in} = T_{steam} - T_{in}^{*}$), can highlight this uncertainty. The overall HTC will of course never be as high as the error bar, but it gives a representative understanding of how important the pressure drop is. The longer the error bar, the higher the pressure drop.

Equation (4.6) can be used to visualize the size of the evaporative heat transfer coefficient, by calculating overall heat transfer coefficients for various values for the evaporative HTC. Since the heat transfer resistances for the wall and for the condensing steam are temperature dependent, two curves, representing the minimum (70°C) and maximum (80°C) values of $T_{steam}$, for each evaporative heat transfer coefficient should be calculated. In addition, an infinite evaporative HTC represents a theoretical maximum value for the overall heat transfer coefficient, assuming that the correlations used to estimate the heat transfer resistance for the wall and the condensing steam are correct.

Figure 6-20 shows all of the above visual representations added to the results presented in Figure 6-19 for *Water*. Now it becomes clear that the previously seen heat load dependence is strongly connected to the heat transfer resistance caused by the wall and the condensing steam. The measurements, dependent upon which modified surface is used, follow either the 5 000 or the 20 000 $W/(m^2K)$ curve for the evaporative heat transfer coefficient. The values for Shape W are extremely high. Therefore, as can be seen in the figure, multiple repetitions with the same outcome have been performed. Even the error bars slightly extend above the theoretical limit. It should be mentioned that the pilot evaporator was never designed to measure such high heat fluxes and there are thus reservations related to the obtained value. In addition, slight changes to the estimation of the heat transfer resistance from the wall and the condensing steam have an enormous impact on the evaporative heat transfer coefficient. Therefore, one should regard the heat transfer for *Water* on Shape W as high, but interpret its exact value with caution.

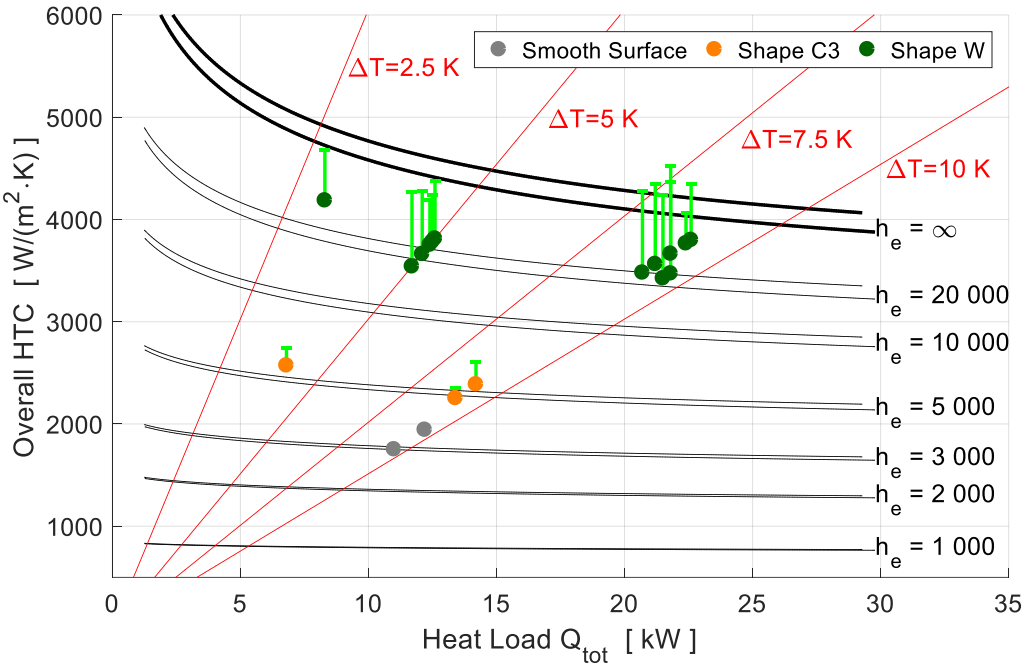


*Figure 6-20. Overall heat transfer coefficient for water as seen in Figure 6-19. The thermal driving force, $\Delta T_{out}$, and multiple evaporative heat transfer coefficient, calculated with equation (4.6), at steam temperatures of 70 and 80°C has been added to the figure.*

Figure 6-21 shows the same results but for *Black liquor*. For *Black liquor* the heat load dependence is stronger than for *Water* and it cannot solely be explained by the added resistance from the condensing steam and the wall. Unfortunately, experimental measurements for different evaporation loads on a smooth surface were not performed in this study. Therefore it is difficult to conclude if this is just a phenomenon seen on the modified surfaces or if it generally occurs. Gourdon, Innings, et al. (2015) found a heat flux dependence on smooth surfaces for dairy product which they linked to the formation of bubbles. They observed a lower HTC at smaller heat loads, the dependence opposite to what is seen on the modified surfaces. Also, their evaporative heat transfer coefficient varied between 2 200 and 3 200 $W/(m^2K)$ for loads between 2.5 and 10 kW, a variation smaller than the one seen here. Further studies are thus needed to determine the precise cause to the heat load dependence for *Black liquor*.

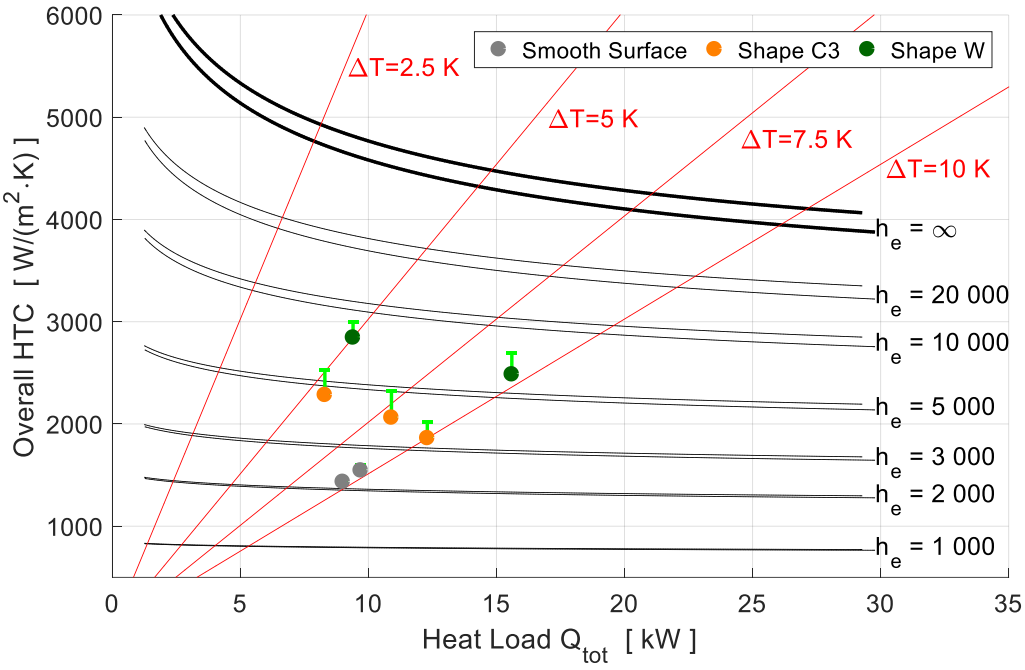


*Figure 6-21. Overall heat transfer coefficient for black liquor as seen in Figure 6-19. The thermal driving force, $\Delta T_{out}$, and multiple evaporative heat transfer coefficient, calculated with equation (4.6), at steam temperatures of 70 and 80°C has been added to the figure.*

## 6.5 Difference between heating and evaporation on modified surfaces

So far in the thesis, the results from heating and evaporation on smooth and modified surfaces have been presented separately. For both heat transfer modes, a significant increase in the rate of heat transfer has been observed. In this Chapter, we will compare how they relate, and then discuss similarities and speculate about the cause of possible differences.

Figure 6-22 shows the evaporation results for *Black liquor* from Figure 6-18 together with the heating results for the *Intermediate Viscosity* fluid as presented in **Paper IV**. The heat transfer coefficient for heating results obtained in the atmospheric setup have been translated to an overall HTC via equation (4.6) by using the same heat transfer resistance for the wall and the condensing steam as during the evaporative experiments. The correlations from Gourdon, Karlsson, et al. (2015) (Evaporation) and Schnabel and Schlünder (1980) (Heating) are added as a reference for the respective fluids. Even if the shape of the modified surfaces and the fluid properties are not quite the same (e.g. Ka is 480 and 547 respectively), both the absolute HTC values and trends are for most conditions similar for the two modes of heat transfer. For both cases, a sharper surface modification yields a larger rate of heat transfer and, regardless of the shape, the latter is significantly higher than compared to the one a smooth surface. The improvement is smaller at higher wetting rates due to an increased rate of heat transfer on the smooth surface and a relatively low wetting rate dependence for the modified surfaces in that end. The only major difference between the heat transfer modes is seen at low wetting rates. The measurements under heating conditions show no clear heat transfer improvement, while the results for evaporative conditions do.

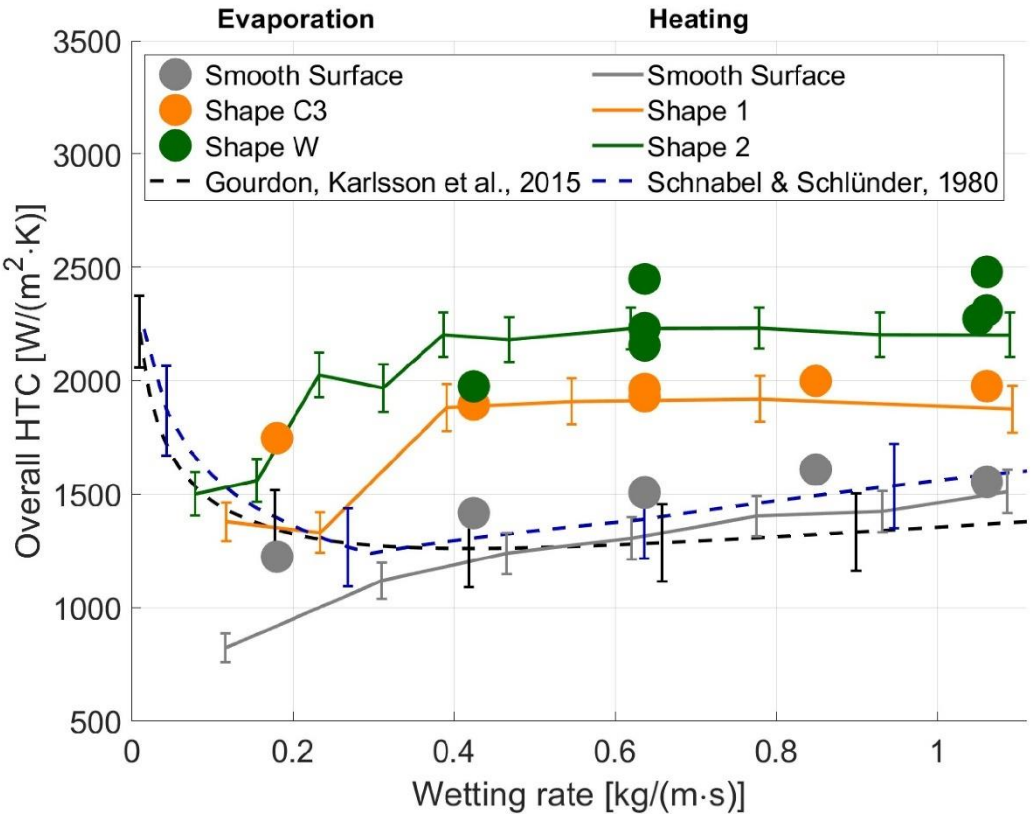


*Figure 6-22. Overall heat transfer coefficient at various wetting rates on smooth and modified heat transfer surfaces, obtained for evaporation of Black liquor and heating of the Intermediate Viscosity fluid. The correlations from Gourdon, Karlsson, et al. (2015) (Evaporation) and Schnabel and Schlünder (1980) (Heating) are included as a reference.*

As discussed in **Paper IV**, accurate measurements at low wetting rates are challenging due to the risk for film breakdown. In the atmospheric setup, the film is heated by an electrical heater, and in the pilot evaporator from condensing steam. The former method is more likely to experience problems with dry patches. A formed dry patch causes a higher wall temperature, and due to the constant heat flux (constant power supplied), the temperature will continue to rise further escalating the problem. When heat is supplied by condensing steam, the circumstances are reversed as the higher wall temperature will lead to a lower condensation rate, and to a lower heat flux due to the locally smaller thermal driving force. Therefore, this could be a possible explanation for the observed difference at low wetting rates between the results obtained for the different heat transfer modes. For the evaporative case, it is also possible that entrainment of vapour (discussed in Chapter 2.3.3), improves the wettability due to the formation of bubbles and sequentially causes a thinner liquid film, which would improve the rate of heat transfer. Furthermore, as reported in **Paper IV**, wetting problems for heating conditions for Shape 2 were observed at low wetting rates.

The above argumentation holds for the difference between heating and evaporation measurements for experimental results. The numerical framework, however, is constructed in such a way that wetting problems are far less likely to occur. In **Paper IV**, the numerical simulations showed that the heat transfer coefficient was not increased at low wetting rates for the modified surface. However, the same simulation revealed that the film was

significantly thicker on the modified surfaces, as compared to the smooth surface case. Therefore, the surface modifications must affect the temperature gradient inside the liquid film, otherwise, the HTC would not be approximately the same as on the smooth surface. This is exactly what can be observed in Figure 6-23, which shows the Intermediate Viscosity fluid at a wetting rate of 0.12 kg/(m·s) on Shape 1. The left image shows a flat liquid on the tube at a time instance, but a few milliseconds later, much like on a smooth surface, a wave passes and stirs up the bulk (right), affecting the temperature gradient. This behaviour was observed in Chapter 6.2 and termed a wavy flow pattern. Therefore, it is much likely that, if the liquid film flow is somehow increased, the heat transfer can potentially be higher.

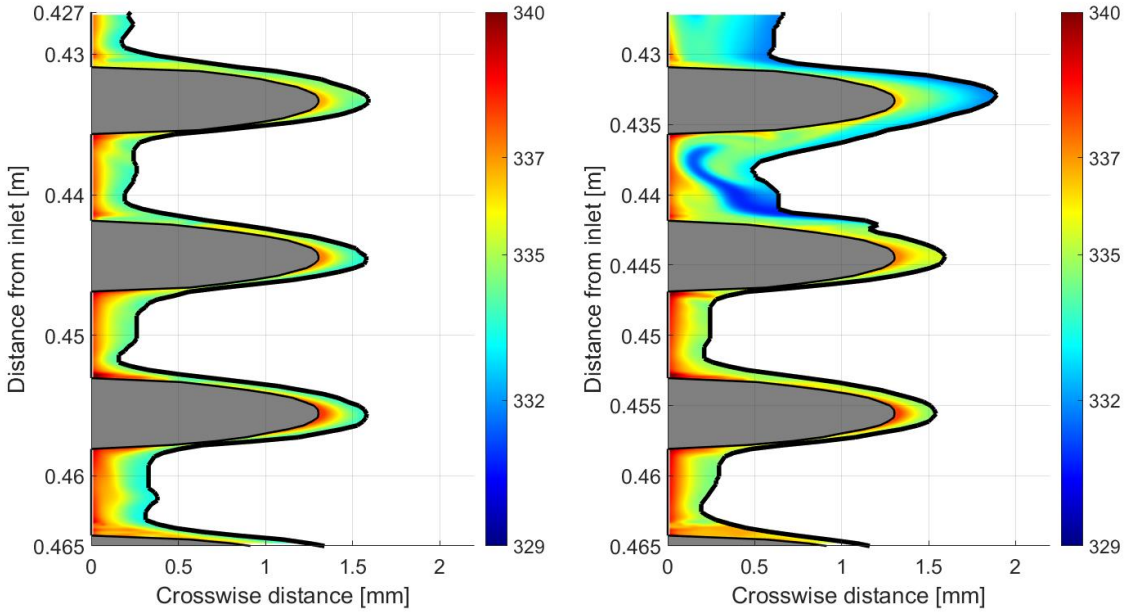


*Figure 6-23. Temperature contour plot at a two different time instance under statistically steady conditions for the Intermediate Viscosity fluid at the wetting rate of 0.12 kg/(m·s) using Shape 1. Re 45, Ka 574 and Pr 18.*

For the experiments in the pilot evaporator, there is a high co-current vapour flow, and outlet vapour velocities above 20 m/s were not uncommon during the experiments. The heat transfer improvement for the modified surfaces, under evaporative conditions and at low wetting rates, could therefore be caused by the high vapour flow generated in the pilot evaporator. In that manner, Dietze and Ruyer-Quil (2013) argue that the gas flow can affect the heat transfer. Zadrazil and Markides (2014) performed measurements on a vertical falling film with co-current gas and they clearly showed that the liquid streamwise velocity could be significantly accelerated by a higher co-vapour flow, therefore presenting a compelling piece of evidence for this theory.

# 7 Conclusions

In this work, hydrodynamics and heat transfer of vertical falling films are investigated. To measure local characteristics of the flow under heating conditions, novel measurement techniques are developed for film thickness profiles and local temperature measurements. The film thickness profiles are measured with an accuracy of at least ±0.1 mm, which resolves the flow pattern with a high spatial and temporal resolution. The accuracy of the individual temperature measurements is ±1.1 K and the accuracy of the variation $\Delta T = T_{Wall} - T_{Bulk}$ is ±0.25 K. The latter can be used to estimate the local heat transfer coefficient with an accuracy in the range of 5-20 %.

The developed experimental techniques have been used to distinguish between entrance effects and statically steady conditions, which is of importance for an industrial unit. The statically steady conditions, are reached typically 1 - 2 meters downstream the inlet. The film thickness profiles, along with local heat transfer coefficients, are measured in order to categorize and understand the variation between different operating conditions for industrially relevant fluids.

The techniques are also used to establish and validate a numerical framework for simulations of falling films in an industrial unit. The framework directly solves the Navier-stokes equations in two dimensions, using the Volume of Fluid method. The numerical framework is used to study the complex flow structures inside the thin liquid film and to differentiate between the convective and conductive mechanisms governing the rate of heat transfer. It is shown that both mechanisms are of importance for the heat transfer, which is very much governed by the waves.

The knowledge acquired on the film flow behaviour on the smooth heat transfer surfaces used today is used to propose new heat transfer surfaces for falling films of industrial use. Various surface modifications are investigated experimentally in order to determine the optimal surface characteristics, such as height, length, sharpness and pitch. It is shown that the height should be at least larger than the Nusselt film thickness, preferably 1 mm high. The pitch should be around 10 mm, and the sharpness has a significant impact as well. A number of surfaces with different sharpness are chosen for further studies.

Both the experimental measurements and the numerical framework show that it is possible to enhance the rate of heat transfer by up to 150 %, dependent upon how sharp the new modified surfaces are constructed. The modified surfaces enhance the rate of heat transfer by initializing more bulk mixing. Irregularities in the flow cause a pressure gradient that, in turn, leads to time-fluctuating recirculation zones behind the surface modifications, which results in a significant increase of the convective heat transfer.

The measurements carried out under evaporative conditions agree with the ones obtained during heating conditions. Potentially, the rate of the heat transfer on the modified surfaces is even higher during evaporate conditions due to a contribution from the co-current vapour flow. However, further studies are needed to confirm this hypothesis.

# 8 Future research

The research presented in this thesis has broadened the understanding of hydrodynamics and heat transfer in vertical falling film units, operating under industrially relevant conditions. The obtained knowledge has also been exploited to introduce modifications of the heat transfer surfaces. Before such surfaces can indeed be used in industry, there are a couple of matters that should be further investigated:

- To investigate a broader range of fluid properties to obtain more detailed information on the conditions/applications for which the new surface modifications are most beneficial.

- To study the effect of the pressure drop in more detail to provide a basis for optimal design of evaporators using the modified surfaces, especially with regard to different levels of temperature/pressure and coflowing vapour. Such an analysis includes comparison and probably further development of models for friction factors and heat transfer coefficients.

- To investigate whether entrainment of vapour in the liquid film has any influence on the heat transfer results for the modified surfaces.

- To explore different modes of fouling that could be a problem for industrial implementations of the new surfaces.

- To use the developed numerical framework to further optimize the design of the heat transfer surface. An investigation is needed on alternative pitch, height and length distances.

- To include evaporation in the numerical framework with the aim of understanding the observed difference between the experimental heating and evaporation results.

- To examine the importance of irregular flow patterns and structures (e.g. capillary waves) by performing full 3D simulations.

# Acknowledgements

The financial support of **Valmet AB, Tetra Pak**, **Energimyndigheten** (Swedish Energy Agency), **Troëdssons forskningsfond**, **Bo Rydins stiftelse**, **Chalmers Energy Initiative** and the computational resources provided by **Chalmers Centre for Computational Science and Engineering** (C3SE) together with the **Swedish National Infrastructure for Computing** made this work possible and is gratefully acknowledged.

Firstly, I would like to thank you, **Mathias Gourdon,** for all the work you put into helping me in my research and for securing funding for the project. You have thought me a lot over all the years that we have worked together.

**Srdjan Sasic**, thank you for your never-ending support and all your valuable contribution. I am indebted to you for your support during hard and stressful times, and, for teaching me how to become a good researcher.

Thank you, **Lennart Vamling,** for all the good discussions we had, and for allowing me to take on responsibility in order to grow as a researcher. Thanks to **Lars Olausson** for being the original inventor of the idea to modify the heat transfer surfaces. Thanks also to **Fredrik Innings** and **Olle Wennberg** for all your input and discussions, your industrial perspective has really improved my research.

Special thanks are extended to the Master students whom I supervised, and for the great contributions their thesis projects have made to my research: **Christoph Karl Ambros**, **Carl Liljenzin** and **Magnus Walander**. Good luck to you all in the future!

Thanks to all the people that has contributed with administrative, economic and maintenance support. Special thanks to **Erik Larsson** and the people at the **Workshop** for their invaluable help with maintaining the experimental equipment.

My sincerest thanks go to my **former colleagues** at Värmeteknik och Maskinlära (Heat and Power Technology) and my **new colleagues** at Kemiteknik (Chemical Engineering) at Chalmers, thank you for creating a friendly work environment. **Tor Sewring**: Thanks for all the dinner company. **Erik Karlsson**: Thank you for being a valuable friend and co-worker, and for all your help and support.

To all my friends, thank you for being in my life. It does not matter how we meet, you all bring me a lot of joy and happiness which I am very grateful for.

Last, but not least, I would also like to thank my family, for always supporting me in my decisions and for being there when I need you. I could not wish for a better family. **Mum** and **Dad**, you are the best parents. **Lars** and **Madeleine**, you mean a lot to me and are the best siblings in the world. I love you all!

# Nomenclature

### Abbreviations

| | |
|---|---|
| 2D | Two-dimensional |
| 3D | Three-dimensional |
| BL | Black liquor |
| BPE | Boiling point elevation |
| CSF | Surface Force Model |
| DI | Density meter |
| FI | Flow meter |
| HTC | Heat transfer coefficient |
| HV | High Viscosity |
| IV | Intermediate Viscosity |
| *Ka* | Kapitza number |
| LI | Liquid level indicator |
| LV | Low Viscosity |
| *Nu* | Nusselt number |
| PI | Pressure indicator |
| *Pr* | Prandtl number |
| *Re* | Reynolds number |
| TI | Temperature meter |
| UI | Uncertainty interval |
| VI | Viscometer |
| VOF | Volume of Fluid |
| WI | Power supplied |

**Symbols**

| | |
|---|---|
| $A$ | Area [$m^2$] |
| $C_p$ | Heat capacity [J/(kg·K)] |
| $DS$ | Dry solids content [kg/kg] |
| $d$ | Diameter [m] |
| $F_\sigma$ | Surface tension force [$N/m^3$] |
| f | Disturbance frequency [Hz] |
| $g$ | Gravitational acceleration [$m^2/s$] |
| | |
| $h$ | Heat transfer coefficient [$W/(m^2 \cdot K)$] |
| $\bar{h}$ | Time averaged heat transfer coefficient [$W/(m^2 \cdot K)$] |
| $k$ | Thermal conductivity [W/(m·K)] |
| $L$ | Characteristic Length [m] |
| $l$ | Viscous length scale [m] |
| $m$ | Mass [kg] |
| $\dot{m}$ | Mass flow rate [kg/s] |
| p | Pressure [Pa] |
| $Q$ | Heat load, Power supplied [W] |
| q | Heat flux [$W/m^2$] |
| $T$ | Temperature [K] |
| $t$ | Time [s] |
| $t_d$ | t-distribution |
| $U$ | Overall heat transfer coefficient [$W/(m^2 \cdot K)$] |
| $u_N$ | Nusselt film velocity [m/s] |
| $v$ | Velocity [m/s] |
| $x$ | Streamwise direction (coordinate) [m] |
| $y$ | Crosswise direction (coordinate) [m] |
| $z$ | Distance to laser triangulation scanner (coordinate) [m] |
| | |
| α | Volume fraction |
| Γ | Wetting rate, mass flow rate per unit with [kg/(m·s)] |
| $\Delta H_{Vap}$ | Enthalpy of vaporization [kJ/kg] |
| $\Delta T$ | Temperature difference [K] |

| | |
|---|---|
| $\delta$ | Film thickness [m] |
| ε | Disturbance amplitude |
| $\theta$ | Spanwise direction (coordinate) [m] |
| ι | Improvement ratio factor |
| κ | Curvature of the interface |
| $\mu$ | Dynamic viscosity [Pa·s] |
| π | Pi |
| $\rho$ | Density [kg/m$^3$] |
| σ | Surface tension [N/m] |

**Subscripts**

| | |
|---|---|
| *0* | Initial conditions |
| *B* | Bulk |
| *e* | Evaporation |
| *g* | Gas |
| *I* | Interface |
| *i* | Inner |
| *l* | Liquid |
| *m* | Logarithmic mean |
| *N* | Nusselt |
| *o* | Outer |
| *tot* | Total |
| *W* | Wall |
| *Modified* | Modified surface |
| *Smooth* | Smooth surface |

**Superscripts**

| | |
|---|---|
| * | Saturated |

# References


Adams, T. N., Frederick, W. J., Grace, T. M., Hupa, M., Lisa, K., Jones, A. K., & Tran, H. (1997). *Kraft recovery boilers*. American Forest & Paper Association, New York:381.

Adomeit, P., Leefken, A., & Renz, U. (2000). *Experimental and numerical investigations on wavy films*. Paper presented at the 3rd European Thermal Sciences Conf, Stuttgart, Germany.

Al-Sibai, F. (2005). *Experimentelle Untersuchung der Strömungscharakteristik und des Wärmeübergangs bei welligen Rieselfilmen.* RWTH Aachen, Aachen.

Alekseenko, S. V., Nakoryakov, V. E., & Pokusaev, B. G. (1985). Wave formation on vertical falling liquid films. *International Journal of Multiphase Flow, 11*(5), 607-627.

Alekseenko, S. V., Nakoryakov, V. E., & Pokusaev, B. G. (1994). *Wave Flow of Liquid Films*: Begell.

Alexeev, A., Gambaryan-Roisman, T., & Stephan, P. (2005). Marangoni convection and heat transfer in thin liquid films on heated walls with topography: Experiments and numerical study. *Physics of Fluids, 17*(6), 062106.

Alhusseini, A. A., & Chen, J. C. (2000). Transport Phenomena in Turbulent Falling Films. *Industrial & Engineering Chemistry Research, 39*(6), 2091-2100.

Andritz. (2018). Multiple-effect evaporator and concentrator. *Multiple-effect evaporator and concentrator*. 2018-10-10. Retrieved from https://www.andritz.com/products-en/group/pulp-and-paper/pulp-production/kraft-pulp/evaporation-plants/multi-effect-evaporators-concentrators

Assael, M. J., & Gialou, K. (2003). Measurement of the Thermal Conductivity of Stainless Steel AISI 304L up to 550 K.

Bandelier, P. (1997). Improvement of multifunctional heat exchangers applied in industrial processes. *Applied Thermal Engineering, 17*, 777-788.

Bender, A., Stephan, P., & Gambaryan-Roisman, T. (2018). Numerical investigation of the evolution and breakup of an evaporating liquid film on a structured wall. *International Journal of Heat and Fluid Flow, 70*, 104-113.

Brackbill, J. U., Kothe, D. B., & Zemach, C. (1992). A continuum method for modeling surface tension. *Journal of Computational Physics, 100*(2), 335-354.

Brauner, N. (1989). Modelling of wavy flow in turbulent free falling film. *International Journal of Multiphase Flow, 15*(4), 505-520.

Broniarz-Press, L. (1997). Enhancement of mass transfer coefficients in spiral films. *International Journal of Heat and Mass Transfer, 40*, 4197-4208.

Brötz, W. (1954). Predetermination of absorption rate of gases in flowing liquid layers (Über die Vorausberechnung der Absorptionsgeschwindigkeit von Gasen in strömenden Flüssigkeitsschichten). *Chemie-Ingenieur-Technik, 26*(8-9), 470-478.

Chamra, L. M., & Webb, R. L. (1996). Advanced micro-fin tubes for evaporation. *International Journal of Heat and Mass Transfer, 39*(9), 1827-1838.

Charogiannis, A., An, J. S., & Markides, C. N. (2015). A simultaneous planar laser-induced fluorescence, particle image velocimetry and particle tracking velocimetry technique for the investigation of thin liquid-film flows. *Experimental Thermal and Fluid Science, 68*, 516-536.

Charogiannis, A., Zadrazil, I., & Markides, C. N. (2016). Thermographic particle velocimetry (TPV) for simultaneous interfacial temperature and velocity measurements. *International Journal of Heat and Mass Transfer, 97*, 589-595.

Chinnov, E. A., & Abdurakipov, S. S. (2013). Thermal entry length in falling liquid films at high Reynolds numbers. *International Journal of Heat and Mass Transfer, 56*(1-2), 775-786.

Demekhin, E. A., Kalaidin, E. N., Kalliadasis, S., & Vlaskin, S. Y. (2007). Three-dimensional localized coherent structures of surface turbulence. I. Scenarios of two-dimensional–three-dimensional transition. *Physics of Fluids, 19*(11), 114103.

Dietze, G. F. (2016). On the Kapitza instability and the generation of capillary waves. *Journal of Fluid Mechanics, 789*, 368-401.

Dietze, G. F., Al-Sibai, F., & Kneer, R. (2009). Experimental study of flow separation in laminar falling liquid films. *Journal of Fluid Mechanics, 637*, 73.

Dietze, G. F., & Kneer, R. (2011). Flow Separation in Falling Liquid Films. *Frontiers in Heat and Mass Transfer, 2*(3).

Dietze, G. F., Leefken, A., & Kneer, R. (2008). Investigation of the backflow phenomenon in falling liquid films. *Journal of Fluid Mechanics, 595*, 435-459.

Dietze, G. F., Rohlfs, W., Nährich, K., Kneer, R., & Scheid, B. (2014). Three-dimensional flow structures in laminar falling liquid films. *Journal of Fluid Mechanics, 743*, 75-123.

Dietze, G. F., & Ruyer-Quil, C. (2013). Wavy liquid films in interaction with a confined laminar gas flow. *Journal of Fluid Mechanics, 722*, 348-393.

Doro, E. O. (2012). *Computational modeling of falling liquid film free surface evaporation.* Georgia Institute of Technology, Mechanical Engineering.

Dukler, A. E. (1976). The role of waves in two-phase flow: some new understanding. *Chemical Engineering Education*(XI), 108–138.

Fath, A., Horn, T., Gambaryan-Roisman, T., Stephan, P., & Bothe, D. (2015). Numerical and experimental analysis of short-scale Marangoni convection on heated structured surfaces. *International Journal of Heat and Mass Transfer, 86*, 764-779.

Gambaryan-Roisman, T., & Stephan, P. (2003). Analysis of falling film evaporation on grooved surfaces. *Journal of Enhanced Heat Transfer, 10*(4), 445-457.

Gambaryan-Roisman, T., Yu, H., Löffler, K., & Stephan, P. (2011). Long-Wave and Integral Boundary Layer Analysis of Falling Film Flow on Walls With Three-Dimensional Periodic Structures. *Heat Transfer Engineering, 32*(7-8), 705-713.

Gao, D., Morley, N. B., & Dhir, V. (2003). Numerical simulation of wavy falling film flow using VOF method. *Journal of Computational Physics, 192*(2), 624-642.

Goff, H. L., Soetrisnanto, A., Schwarzer, B., & Goff, P. L. (1992). A new falling film evaporator with spiral fins. *The Chemical Engineering Journal, 50*, 169-171.

Gourdon, M. (2009). *Sodium Salt Scaling in Black Liquor Evaporators*: Chalmers University of Technology.

Gourdon, M., Innings, F., Jongsma, A., & Vamling, L. (2015). Qualitative investigation of the flow behaviour during falling film evaporation of a dairy product. *Experimental Thermal and Fluid Science, 60*, 9-19.

Gourdon, M., Karlsson, E., Innings, F., Jongsma, A., & Vamling, L. (2015). Heat transfer for falling film evaporation of industrially relevant fluids up to very high Prandtl numbers. *Heat and Mass Transfer, 52*(2), 379-391.

Gourdon, M., & Mura, E. (2017). Performance evaluation of falling film evaporators in the dairy industry. *Food and Bioproducts Processing, 101*, 22-31.

Gullichsen, J., & Fogelholm, C.-J. (2000). *Papermaking Science and Technology - Chemical Pulping 6B*. Helsinke, Finland.

Hagsten, C. (2016). *Cleaning of ultra-high temperature milk fouling Structural and compositional changes*: Physical Chemistry, Faculty Of Science, Lund University.

Helbig, K., Nasarek, R., Gambaryan-Roisman, T., & Stephan, P. (2009). Effect of Longitudinal Minigrooves on Flow Stability and Wave Characteristics of Falling Liquid Films. *Journal of Heat Transfer-Transactions of the Asme, 131*(1).

Härkönen, M., Aula, A., & Aittomäki, A. (1994). *Heat transfer and hydrodynamics of falling liquid films*. Tampere University of Technology: The Finnish Academy of Technology.

Ishigai, S., Nakanisi, S., Koizumi, T., & Oyabu, Z. (1972). Hydrodynamics and Heat Transfer of Vertical Falling Liquid Films: Part 1, Classification of Flow Regimes. *The Japan Society of Mechanical Engineers, 15*(83), 594-602.

Ishigai, S., Nakanisi, S., Takehara, M., & Oyabu, Z. (1974). Hydrodynamics and Heat Transfer of Vertical Falling Liquid Films : Part 2. Analysis by Using Heat Transfer Data. *Bulletin of JSME, 17*(103), 106-114.

Ji, W.-T., Numata, M., He, Y.-L., & Tao, W.-Q. (2015). Nucleate pool boiling and filmwise condensation heat transfer of R134a on the same horizontal tubes. *International Journal of Heat and Mass Transfer, 86*, 744-754.

Johansson, M., Leifer, I., Vamling, L., & Olausson, L. (2009). Falling film hydrodynamics of black liquor under evaporative conditions. *International Journal of Heat and Mass Transfer, 52*(11), 2769-2778.

Johansson, M., Olausson, L., & Vamling, L. (2005). *A new test facility for black liquor evaporation.* Paper presented at the Heat transfer in components and systems for sustainable energy technologies.

Johansson, M., Vamling, L., & Olausson, L. (2008). Turbulence models for falling film hydrodynamics and heat transfer compared with experimental values for black liquor *Nordic Pulp & Paper Research Journal* (Vol. 23, pp. 256).

Johansson, M., Vamling, L., & Olausson, L. (2009). Heat transfer in evaporating black liquor falling film. *International Journal of Heat and Mass Transfer, 52*(11-12), 2759-2768.

Kabova, Y. O., Alexeev, A., Gambaryan-Roisman, T., & Stephan, P. (2006). Marangoni-induced deformation and rupture of a liquid film on a heated microstructured wall. *Physics of Fluids, 18*(1), 012104.

Kalliadasis, S., Ruyer-Quil, C., Scheid, B., & Velarde, M. G. (2012). *Falling Liquid Films* (Vol. 176). Springer: Applied Mathematical Sciences.

Kapitza, P. L., & Kapitza, S. P. (1965). Wave flow of thin layers of a viscous fluid. In D. T. Haar (Ed.), *Collected Papers of P.L. Kapitza* (pp. 662-709): Pergamon.

Karimi, G., & Kawaji, M. (1999). Flow characteristics and circulatory motion in wavy falling films with and without counter-current gas flow. *International Journal of Multiphase Flow, 25*(6-7), 1305-1319.

Karlsson, E. (2017). *The formation and dissolution of sodium salt scales in black liquor evaporators*: Göteborg : Chalmers University of Technology, 2017.

Karlsson, E., Gourdon, M., & Vamling, L. (2017). The Effect of Bulk Crystals on Sodium Salt Scaling in Black Liquor Evaporators. *Nordic Pulp and Paper Research Journal, 32*(02), 299-308.

Kharlamov, S. M., Guzanov, V. V., Bobylev, A. V., Alekseenko, S. V., & Markovich, D. M. (2015). The transition from two-dimensional to three-dimensional waves in falling liquid films: Wave patterns and transverse redistribution of local flow rates. *Physics of Fluids, 27*(11), 114106.

Kohrt, M. (2012). *Experimentelle Untersuchung von Stofftransport und Fluiddynamik bei Rieselfilmströmungen auf mikrostrukturierten Oberflächen.* (Doktor der Ingenieurwissenschaften), Technischen Universität Berlin, Berlin.

Kunugi, T., & Kino, C. (2005). DNS of falling film structure and heat transfer via MARS method. *Computers & Structures, 83*(6-7), 455-462.

Lel, V. V., Al-Sibai, F., & Kneer, R. (2009). Thermal Entry Length and Heat Transfer Phenomena in Laminar Wavy Falling Films. *Microgravity Science and Technology, 21*(S1), 215-220.

Lel, V. V., & Kneer, R. (2011). Heat Transfer Phenomena in Laminar Wavy Falling Films: Thermal Entry Length, Thermal-Capillary Metastable Structures, Thermal-Capillary Breakdown.

Li, H., Yi, F., Li, X., Pavlenko, A. N., & Gao, X. (2018). Numerical Simulation for Falling Film Flow Characteristics of Refrigerant on the Smooth and Structured Surfaces. *Journal of Engineering Thermophysics, 27*(1), 1-19.

Li, W., Wu, X.-Y., Luo, Z., & Webb, R. L. (2011). Falling water film evaporation on newly-designed enhanced tube bundles. *International Journal of Heat and Mass Transfer, 54*(13-14), 2990-2997.

Lukach, Y. Y., Radchenko, L. B., & Tananayiko, Y. M. (1972). Determination of the average thickness of a film of water during gravitation of flow along the exterior surface of vertical polymeric pipes. *International Chemical Engineering*(12), 517-519.

Madoumier, M., Azzaro-Pantel, C., Tanguy, G., & Gésan-Guiziou, G. (2015). Modelling the properties of liquid foods for use of process flowsheeting simulators: Application to milk concentration. *Journal of Food Engineering, 164*, 70-89.

Malamataris, N. A., & Balakotaiah, V. (2008). Flow structure underneath the large amplitude waves of a vertically falling film. *AIChE Journal, 54*(7), 1725-1740.

Markides, C. N., Mathie, R., & Charogiannis, A. (2016). An experimental study of spatiotemporally resolved heat transfer in thin liquid-film flows falling over an inclined heated foil. *International Journal of Heat and Mass Transfer, 93*, 872-888.

Mascarenhas, N., & Mudawar, I. (2013). Study of the influence of interfacial waves on heat transfer in turbulent falling films. *International Journal of Heat and Mass Transfer, 67*, 1106-1121.

Micro-Epsilon. (2018). Manual - Laser Triangulation Scanner *scanCONTROL 29xx*. 2018-07-09. Retrieved from http://www.micro-epsilon.com/download/manuals/man--scanCONTROL-29xx--en.pdf

Miller, W. A., & Keyhani, M. (2001). The effect of roll waves on the hydrodynamics of falling films observed in vertical column absorbers. http://digital.library.unt.edu/ark:/67531/metadc718324/

Miriam, L. A. (2007). *Experiments on falling film evaporation of a water-ethylene glycol mixture on a surface with longitudinal grooves.* (Doktor der Ingenieurwissenschaften), Technischen Universität Berlin, Berlin.

Mitrovic, J. (1988). Der Wäermeaustausch am Berieselungsküehler. *Wärmeübertrager, 40*(6), 243-249.

Miyara, A. (1999). Numerical analysis on flow dynamics and heat transfer of falling liquid films with interfacial waves. *Heat and Mass Transfer, 39*(4), 298-306.

Miyara, A. (2001). Flow Dynamics and Heat Transfer of Wavy Condensate Film. *Journal of Heat Transfer, 123*(3), 492.

Morioka, I., Kiyota, M., & Nakao, R. (1993). Absorption of Water Vapor into a Film of Aqueous Solution of LiBr Falling along a Vertical Pipe. *International Journal Series B Fluids and Thermal Engineering, 36*(2), 351-356.

Mudawwar, I. A., & El-Masri, M. A. (1986). Momentum and heat transfer across freely-falling turbulent liquid films. *International Journal of Multiphase Flow, 12*(5), 771-790.

Mura, E., & Gourdon, M. (2017). Pressure drop in dairy evaporators: Experimental study and friction factor modelling. *Journal of Food Engineering, 195*, 128-136.

Najim, M., Feddaoui, M. b., Nait Alla, A., & Charef, A. (2018). Computational Study of Liquid Film Evaporation along a Wavy Wall of a Vertical Channel. *Mathematical Problems in Engineering, 2018*, 1-11.

NIST. (2017). NIST Chemistry WebBook. *NIST Chemistry WebBook*. 2017-10-26. Retrieved from http://webbook.nist.gov/cgi/cbook.cgi?Name=water&Units=SI

Nosoko, T., Yoshimura, P. N., Nagata, T., & Oyakawa, K. (1994). Characteristics of two-dimensional on a falling liquid film. *Chemical Engineering Science, 51*(5), 725-732.

Numrich, R. (1992). Heat transfer for falling film evaporation. *Wärmeübergang bei der Fallfilmverdampfung, 27*(5), 331-335.

Numrich, R., & Müller, J. (2010). Filmwise Condensation of Pure Vapors *In VDI-GVC (ED.)*. VDI Heat Atlas: Berlin: Springer.

Nusselt, W. (1916). Die oberflachenkondensation des wasserdampfes. *Zeitschrift des Vereins Deutscher Ingenieure, 60*, 541-546.

OECD-FAO. (2018). OECD-FAO Agricultural Outlook. *OECD Statistics*. 2018-10-10. Retrieved from https://stats.oecd.org/

Patnaik, V., & Perez-Blanco, H. (1996). Roll waves in falling films: an approximate treatment of the velocity field. *International Journal of Heat and Fluid Flow, 17*(1), 63-70.

Pecherkin, N., Pavlenko, A., & Volodin, O. (2015). Heat Transfer and Crisis Phenomena at the Film Flows of Freon Mixture over Vertical Structured Surfaces. *Heat Transfer Engineering*, 1-12.

Plerson, F. W., & Whitaker, S. (1977). Some Theoretical and Experimental Observations of the Wave Structure of Falling Liquid Films. *Industrial & Engineering Chemistry Fundamentals, 16*(4), 401-408.

Raach, H., & Mitrovic, J. (2005). Seawater falling film evaporation on vertical plates with turbulence wires. *Desalination, 183*(1-3), 307-316.

Ramadane, A., Goff, P. L., & Liu, B. (1993). The enhancement of heat transfer in falling film evaporators by a non-uniform flow rate. *Energy Efficiency in Process Technology*.

Salvagnini, W. M., & Taqueda, M. E. S. (2004). A Falling-Film Evaporator with Film Promoters. *Ind. Eng. Chem. Res., 43*(21).

Schnabel, G. (2010). Heat Transfer to Falling Films at Vertical Surfaces. In VDI-GVC (Ed.), *VDI Heat Atlas* (2nd ed., Vol. 2nd ed.). Berlin: Springer.

Schnabel, G., & Palen, J. W. (1998). Wärmeubergang an senkrechten berieselten Flächen. *VDI Wärmeatlas, 8th Edition, Springer-Verlag Berlin, Sect. Md*.

Schnabel, G., & Schlünder, E. U. (1980). Wärmeübergang von senkrechten Wänden an nichtsiedende und siedende Rieselfilme. "Heat Transfer from Vertical Walls to Falling Liquid Films with or Without Evaporation." *Verfahrenstechnik, 14*(2), 79-83.

Schröder, J. J., Fast, P., & Sander-Beuermann, W. (1979). Hydrodynamics and heat transfer on vertically finned surfaces in falling film evaporators. *Desalination, 31*, 19-34.

SEA. (2017). *Energiläget i siffror / Energy in Sweden Facts and figures 2017 (Swedish Energy Agency)*.

Shen, Z. Q., C.H., L., & F., L. (1986). *Effect of systematic grooved surface on the rate of heat and mass transfer in a falling liquid film*. Paper presented at the 8th International Heat Transfer Conference, San Francisco, USA.

Shmerler, J. A., & Mudawwar, I. (1988). Local heat transfer coefficient in wavy free-falling turbulent liquid films undergoing uniform sensible heating. *International Journal of Heat and Mass Transfer, 31*(1), 67-77.

Slade, D., Veremieiev, S., Lee, Y. C., & Gaskell, P. H. (2013). Gravity-driven thin film flow: The influence of topography and surface tension gradient on rivulet formation. *Chemical Engineering and Processing: Process Intensification, 68*, 7-12.

Tong, L. S., & Tang, Y. S. (1997). *Boiling Heat Transfer And Two-Phase Flow* (Second ed.). Washington DC: Taylor & Francis.

Valmet. (2018). High-Performance Evaporation Systems. *EVAPs Brochure*. 2018-10-29. Retrieved from https://www.valmet.com/pulp/chemical-recovery/services/new-technology/evaporation-plants-rebuild/

Wasden, F. K., & Dukler, A. E. (1989). Insights into the Hydrodynamics of Free Falling Wavy Films. *AIChE Journal, 35*(2), 187-195.

Webb, R. L., & Kim, N.-H. (2005). *Principles of Enhanced Heat Transfer* (Second ed.). Great Britain: Taylor & Francis.

Wierschem, A., & Aksel, N. (2004). Influence of inertia on eddies created in films creeping over strongly undulated substrates. *Physics of Fluids, 16*(12), 4566-4574.

Wilke, W. (1962). Wärmeübergang an Rieselfilme. *VDI-Forschungsheft, 490*(28).

Youngs, D. L. (1982). Time-Dependent Multi-Material Flow with Large Fluid Distortion. *Numerical Methods for Fluid Dynamics, 24*(2), 273–285.

Yu, H., Gambaryan-Roisman, T., & Stephan, P. (2013). Numerical Simulations of Hydrodynamics and Heat Transfer in Wavy Falling Liquid Films on Vertical and Inclined Walls. *Journal of Heat Transfer, 135*(10), 1010101 - 1010109.

Yu, H., Löffler, K., Gambaryan-Roisman, T., & Stephan, P. (2010). Heat transfer in thin liquid films flowing down heated inclined grooved plates. *Computational Thermal Sciences, 2*(5), 455-468.

Zadrazil, I., & Markides, C. N. (2014). An experimental characterization of liquid films in downwards co-current gas–liquid annular flow by particle image and tracking velocimetry. *International Journal of Multiphase Flow, 67*, 42-53.

Zadrazil, I., Matar, O. K., & Markides, C. N. (2014). An experimental characterization of downwards gas–liquid annular flow by laser-induced fluorescence: Flow regimes and film statistics. *International Journal of Multiphase Flow, 60*, 87-102.

Zhao, L., & Cerro, R. L. (1992). Experimental characterization of viscous film flows over complex surfaces. *International Journal of Multiphase Flow, 18*, 496-516.

Zheng, G. S., & Worek, W. M. (1996). Method of heat and mass transfer enhancement in film evaporation. *International Journal of Heat and Mass Transfer, 39*, 97-108.